2021-01-25

Heterogeneous Catalytic H2S Oxidation within Supercritical CO2 for a New Sulfur Recovery Process

Lee, Seungwook

UNIVERSITY OF CALGARY

Heterogeneous Catalytic H_2S Oxidation within Supercritical CO_2 for a New Sulfur Recovery Process

by

Seungwook (Tommy) Lee

A THESIS

SUBMITTED TO THE FACULTY OF GRADUATE STUDIES

IN PARTIAL FULFILMENT OF THE REQUIREMENTS FOR THE

DEGREE OF DOCTOR OF PHILOSOPHY

GRADUATE PROGRAM IN CHEMISTRY

CALGARY, ALBERTA

January, 2021

Abstract

Many natural gas sources can have small amounts of acid gases (H_2S and CO_2). These acid gases are removed from the natural gas for the consumers due to toxicity and low heating value. Conventionally, acid gas is removed by absorption into aqueous amine solutions. This separated acid gas can then be injected into reservoirs for sequestration or can be further processed to convert the H_2S to S_8 by sulfur recovery. For low-quality acid gases (< 1% H_2S in CO_2), available methods to remove H_2S results in waste rather than marketable sulfur. The remaining CO_2 is at near atmospheric pressure, often being released to the environment due to high recompression costs.

In this thesis, an alternative sulfur recovery process is investigated to produce marketable sulfur and high-pressure CO_2 using post cryogenic separation of low-quality acid gases. Cryogenic distillation for acid gas separation is beneficial, resulting in a high-pressure liquid form of acid gas that does not require recompression. However, currently available low-pressure methods to convert H_2S to S_8 do not take the advantage of this high-pressure. Heterogeneous catalysis was utilized to convert H_2S to S_8 within the high-pressure CO_2 in this thesis. For the high-pressure sulfur recovery process to be viable, several studies were completed in order to provide the best conditions to carry out the heterogeneous catalysis in high-pressure CO_2.

Sulfur solubility within high-pressure CO_2 was initially studied to define the process conditions to maintain a single-phase product and subsequent separation of produced sulfur and CO_2. The sulfur solubility study also allowed for the modelling of the sulfur fugacity coefficient within high-pressure CO_2, which was utilized in a high-pressure Gibbs Free Energy Minimization routine to calculate the theoretical equilibrium

conversion limit of H_2S to S_8. Heterogeneous H_2S oxidation catalyses were experimentally carried out to verify calculated high-pressure thermodynamic conversion limits by the Gibbs Free Energy Minimization routine. Kinetic limitations were found at lower temperatures and higher pressures in pursuit of improving the thermodynamic conversion limit. The kinetics of the high-pressure heterogeneous H_2S oxidation catalysis were studied to model the kinetic limitations of the reaction within the high-pressure CO_2.

The three models developed allow for high-pressure calculations of S_8/CO_2 solubility conditions, thermodynamic H_2S equilibrium conversion limits, and minimum residence times required for the equilibrium conversion limits to establish. These models therefore enable practical industrial condition optimization to carry out the heterogeneous catalytic oxidation of H_2S within high-pressure CO_2.

Acknowledgments

I would like to thank my supervisor, Dr. Marriott for all his guidance and support throughout my time at the University of Calgary. Dr. Marriott's curiosity and enthusiasm have encouraged and always will encourage me to learn more and pursue my own curiosity. I am forever in debt for the amazing opportunity.

I would also like to thank my committee members, Dr. Birss and Dr. Kusalik, for providing valuable feedback throughout this research.

Thank you to the members of the Marriott research group and Alberta Sulphur Research Ltd, both past and present, for helping me and making my time in Calgary so enjoyable.

I also would like to thank Ms. Janice Crawford and the rest of the graduate program support staff.

This thesis was funded by Dr. Marriott's NSERC Discovery Grant and the University of Calgary.

My appreciation goes out to all my family and friends for supporting me and providing times to relax and enjoy life outside of school.

Lastly, I would like to thank my wife, Alison, who has been more support than I could have ever imagined. It has been an extraordinary time for Alison and me to experience the graduate student life together, and I am very proud of our achievement together.

Dedication

To my parents, Jungsuk and Hyung

Table of Contents

List of Tables

List of Figures and Illustrations

List of Symbols, Abbreviations and Nomenclature

Symbol	Definition
AGI	Acid gas injection
AQ	Anthraquinone
EOR	Enhanced oil recovery
ER	Eley-Rideal
FID	Flame ionization detector
FPD	Flame photometric detector
GC	Gas chromatography
GEM	Gibbs Free Energy Minimization
HP	High-pressure
HPLC	High performance liquid chromatography
IC	Ion chromatography
JANAF	Joint Army Navy Air Force
k	Rate constant
LH	Langmuir-Hinshelwood
NIST	National institute of standards and technology
PFPD	Pulsed flame photometric detector
R^2	Correlation coefficient
REFPROP	Reference fluid thermodynamic and transport properties
SSE	Sum squared error
t	Time
TCD	Thermal conductivity detector
TGA	Thermal gravimetric analysis
THC	Tetrahydrocannabinol
TLV	Threshold limit value

Chapter 1: Introduction

1.1 Motivation

Lean natural gas is primarily composed of methane (CH_4), although it can also contain various concentrations of hydrogen sulfide (H_2S) and carbon dioxide (CO_2). Shale gas is an example of a lean natural gas that contains a low-level of H_2S (< 0.1%) and larger amounts of CO_2 (*ca.* 10%).[1,2] Both acid gas components (H_2S and CO_2) must be removed before the CH_4 is transported to consumers, because CO_2 has no heating value and H_2S is toxic.[3,4] Table 1-1 shows examples of gas quality specifications according to TransCanada pipelines and Alliance USA.[4]

Table 1-1. Gas quality specifications

	TransCanada Pipelines	**US Pipelines**
Specs	**Canadian Mainline**	**Alliance USA**
Hydrogen Sulphide	Max. 16 ppmv	Max. 16 ppmv
Total Sulfur	Max. 11 ppmv	Max. 11 ppmv
Carbon Dioxide	Max. 2% by volume	Max. 2% by volume
Oxygen	Max. 0.4% by volume	Max. 0.4% by volume
Temperature	Max. 323.15 K	Max. 323.15 K
Heating Value	Min. 36 MJ/m^3 Max 41.34 MJ/m^3	Min. 36 MJ/m^3
Water	Max. 84 ppmv	Max. 84 ppmv
Hydrocarbon Dewpoint	Max. 263.15 K at 5500kPa absolute	Max. 268.15 K at opt. pres.

Removed acid gas fluid (H_2S and CO_2) can be injected into storage/disposal reservoirs, a process called acid gas injection (AGI). CO_2 can be cleaned up for subsurface injection (CO_2 injection) or for sale as a secondary value-added product for enhanced oil recovery (EOR),[5,6] as a fine chemical for reaction material, or an alternative solvent to conventional organic solvents.[7] If the H_2S component of an acid gas is converted to elemental sulfur (S_8) by partial oxidation, a process called sulfur recovery, then there can be another valuable material that can be sold for sulfuric acid production which is used in the manufacturing of fertiliser. Normally, when recovering sulfur, the remaining CO_2 is released into the atmosphere.

For many natural gas sources, acid gases are separated from the high-pressure production stream using alkanolamines, which discharges the separated acid gas at near-atmospheric pressure. The low-pressure separated acid gas requires recompression back to high-pressure in order to overcome the wellhead injection pressure if acid gas injection is the intended disposal process. Another option for this separated acid gas could be cleaning up CO_2 for sale by sulfur recovery which converts the H_2S into another valuable material S_8. Existing sulfur recovery processes for low-quality acid gas produce low-quality sulfur with unwanted by-product formed from reactions with sulfur for sulfuric acid production.[8] Here produced sulfur can be an environmental liability rather than a marketable product.

An alternative method for acid gas separation is by cryogenic distillation, which distills CH_4 from carefully frozen/liquified acid gas mixtures.[9-11] Cryogenic distillation discharges the separated acid gas as a high-pressure fluid, thereby reducing energy requirements by eliminating/minimizing recompression steps and removing the reliance on the alkanolamine solvents. Utilizing cryogenic separation of acid gas is advantageous in

terms of preserving high-pressure. However, there is no current technology for removing low-levels of H_2S (< 1 % H_2S) from high-pressure CO_2, if the cleaned-up CO_2 stream is being sold for other uses. Exploring the option to convert the H_2S to S_8 within the high-pressure CO_2 is the goal of this thesis, in order to minimize post-recovery compression requirements as well as forming high-quality marketable S_8. The suggested process of high-pressure acid gas separation and oxidation of H_2S within high-pressure CO_2 is shown in the Figure 1-1.

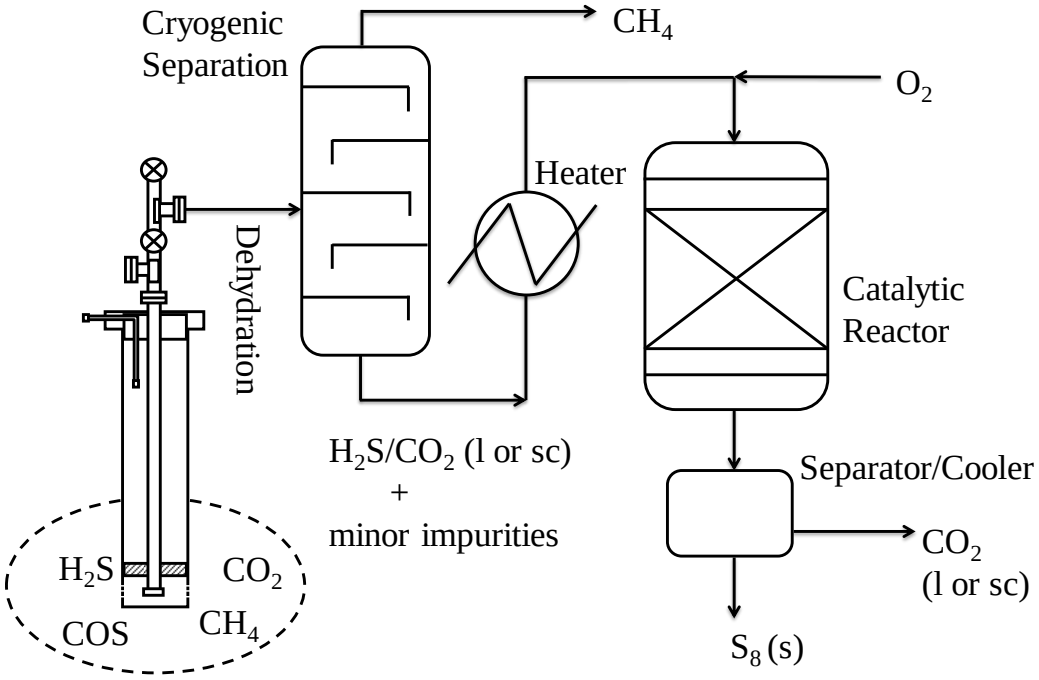

Figure 1-1. Simplified schematic of the proposed sulfur recovery process in high-pressure CO_2.

1.2 Structure of the thesis

This is a manuscript-based thesis and has been organized into six chapters, of which Chapters 3, 4, and 5 presents experimental results of which Chapter 3 and 4 have been

published and Chapter 5 is aimed at publication. Chapter one describes the motivation for the presented research and a detailed introduction. The introduction contains currently available and commonly practiced methods to separate acid gas and remove H_2S in the industry and the current limitations when handling low-quality acid gas. An alternative method to process low-quality acid gas is introduced, along with the questions required to provide the best operating conditions for such a process. The manuscript-based chapters are presented as submitted in the corresponding journals and have been modified and formatted according to the faculty of graduate studies guidelines to be consistent and to improve the flow of the thesis.

Chapter 2 presents the relevant literature review for this thesis. Typical sources for the potential products (S_8 and CO_2) of the proposed process are discussed. The physical and chemical properties of products are reviewed, and how the products can be used are presented in this chapter. Processes utilizing high-pressure CO_2 are reviewed with its advantages. Heterogeneous catalysis is discussed with literature reviews of H_2S conversion to S_8.

In Chapter 3, the vapour-liquid equilibrium between S_8 and high-pressure CO_2 is discussed. The solubilities of S_8 within high-pressure CO_2 were experimentally obtained over an applicable range of temperature and pressure, and a semi-empirical Fluctuation Solution Theory was fit to the experimental solubilities in order to calculate the fugacity coefficient of S_8 within high-pressure CO_2. The manuscript was published as " Lee, S.; Marriott, R. A., Solubility of Elemental Sulfur in Dense Phase Carbon Dioxide from T = 324 to 424 K and p = 10 and 20 MPa. *J. Natural Gas Eng*. 2018, 3 (1), 62-73".[12]

Chapter 4 contains a discussion of the high-pressure heterogenous catalysis of H_2S to S_8 within CO_2 and the limiting equilibria. A previously existing in-house Gibbs Energy Minimization (GEM) routine was modified to more accurately calculate the equilibrium H_2S oxidation reaction at high-pressure by incorporating the fugacity coefficients of many chemical species involved within high-pressure CO_2. The calculated equilibrium H_2S conversion limits at high-pressure were supported by experimental tests involving well known Claus catalysts. The contents of this chapter were published as "Lee, S.; Deering, C. E.; Stashick, M. J.; Chou, N.; Marriott, R. A., Experimental high-pressure hydrogen sulfide partial oxidation and equilibrium calculation by Gibbs Energy Minimization. *Ind. Eng. Chem. Res.* **2020**, 59 (45), 19890-19896".[13]

In Chapter 5, the kinetics of high-pressure heterogeneous catalysis are discussed due to the observance of kinetic limitations while lowering the experimental temperature to improve the thermodynamic equilibrium conversion limit of H_2S to S_8. Based on the experimentally measured reaction rates, a model was developed to calculate the minimum residence time required to establish the calculated equilibrium by the updated GEM calculation. The contents of this chapter are intended to be submitted to a refereed journal in the future.

Finally, Chapter 6 summarizes all the significant findings from each chapter and highlights the best operating conditions to convert H_2S to S_8 within high-pressure CO_2. Potential future research directions are also presented.

Co-author contributions are spelled out in the Appendix at the end of the thesis in A1.

1.3 Conventional aqueous amine separation and unconventional cryogenic separation

Any natural gas that contains significant amounts of H_2S (> 16 ppmv) is called sour gas.[4] The primary sources of H_2S in natural gas can be aquathermolysis of oil, microbial sulfate reduction, and thermochemical sulfate reduction of organosulfur species or metal sulfide. In all these mechanisms, CO_2 is always a by-product, and therefore sour gas often contains CO_2.[2] The removal of the acid gas components (H_2S and CO_2) from the sour natural gas is called gas sweetening or treatment, which is necessary for safety and product quality purposes. The separated acid gas components can be injected into a reservoir for disposal/storage or can go through a sulfur recovery process where H_2S is converted to S_8 as a salable product. In the sweetening process of the sour natural gas, several aqueous amines can be used to absorb the acid gas within a solution. The regeneration of the rich amine solution, containing absorbed acid gas, is separated into a lean amine solution and the acid gas. The alkanolamine separation processes discharge the separated acid gas near atmospheric pressure, which may not be the most energy efficient because significant extra energy is required for recompression if acid gas injection is chosen. More recently, cryogenic separation has been utilized to distill CH_4 out of the raw natural gas, which results in a liquid state of acid gas. The high-pressure liquid acid gas out of cryogenic separation is beneficial, because it requires little to no recompression before transportation.

1.3.1 Absorption into solvents

Separating acid gases from the sour natural gas could be completed in several ways,[14-17] the more common alkanolamine absorption process is described here.

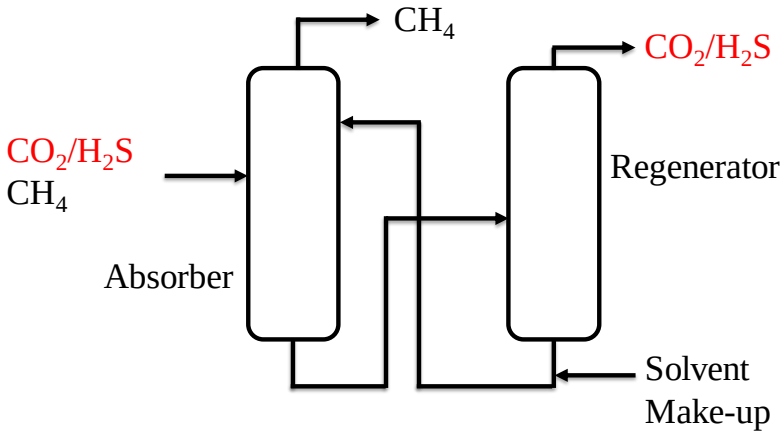

Figure 1-2. Simplified schematic of alkanolamine absorption process

Sour gas is passed through various amines such as monoethanolamine (MEA), diethanolamine (DEA), and methyldiethanolamine (MDEA) in an absorber, where H_2S and CO_2 can be selectively absorbed in the amine solution.[14]

$$R_xNH_{3-x} + H_2S \rightleftharpoons R_xNH_{4-x}^{+} + SH^{-} \quad (1\text{-}1)$$

$$2\ R_xNH_{3-x} + CO_2 \rightleftharpoons RNH_{4-x}^{+} + R_xNHCOO^{-} \quad (1\text{-}2)$$

$$R_3N + CO_2 + H_2O \rightleftharpoons R_3NH^{+} + (OH)COO^{-} \quad (1\text{-}3)$$

There are two pathways for CO_2 absorption, one is a formation of carbamate species (Equation 1-2) and the other is a formation of carbonate ions (Equation 1-3). Labile proton on central amino N atom is required for CO_2 to form the carbamate ion. Therefore, sterically hindered tertiary amine can be used to selectively absorb H_2S because the formation of the carbonate is kinetically much slower than the formation of the carbamate in the presence of primary or secondary amine.[18] The acid gas absorbed aqueous amine solutions are regenerated by heating at T = 373 to 413 K in a regenerator to produce acid gas at low-pressure (~ 0.2 MPa).[14] The regenerated aqueous amine solution is then

circulated back to the absorber to continue sweetening more of the sour gas.[14] The general cost of amine separation is 60 dollars per ton of CO_2.[19]

The low-pressure acid gas can continue to a sulfur recovery process, where the H_2S is oxidized to S_8. In the cases of low-quality acid gases (< 20 mol% H_2S), the low-concentrations of H_2S cannot sustain a flame required in a thermal reactor of modified Claus sulfur recovery plant, and often go through alternative low-H_2S recovery processes. Acid gas mixtures can be reinjected for storage, production reservoir pressure maintenance or enhanced oil recovery (mostly for pure CO_2). If H_2S can be removed from low-quality acid gases, the remaining CO_2 is released to the atmosphere if not recompressed for other purposes such as enhanced oil recovery. Because the amine separated acid gas is discharged at low-pressure, significant cost of 12 dollars per ton of CO_2 is associated to recompress the low-pressure acid gas back to a high-pressure.[20,21] Thus, processes that can avoid this recompression step are desirable.

1.3.2 Cryogenic separation

Cryogenic distillation processes are an alternative method to the use of aqueous amine processes for the separation of acid gas from raw sour natural gas. Unlike amine absorption, cryogenic separation does not necessarily require solvent. With cryogenic separation, fewer processing steps, less equipment, and less energy is required.[9] While cryogenic separation is not as common as amine absorption, many companies offer cryogenic separation processes such as Controlled Freeze Zone (CFZ™) by ExxonMobil,[9] Special Pre-Extraction (SPREX®) by the Institut Français du Pétrole (IFP), TOTAL and AXENS solutions,[10] and Cryocap™ by Air Liquide Global E&C Solutions.[11]

Cryogenic separation processes work by distillation of CH_4 from carefully frozen or liquefied CO_2 and H_2S in specially designed distillation towers. These processes are taking advantage of the big difference in volatility between acid gases and CH_4, as shown in Table 1-2 and Figure 1-3.

Table 1-2. Boiling points and melting points of acid gases and CH_4.

	H_2S	CO_2	CH_4
T_{vap} (0.1 MPa)/ K	212.85	194.65[a]	110.95
T_{melt} (0.1 MPa) / K	190.85	216.55[b]	91.15

[a] Sublimation point of CO_2. [b]Triple point of CO_2 at 0.52 MPa[22]

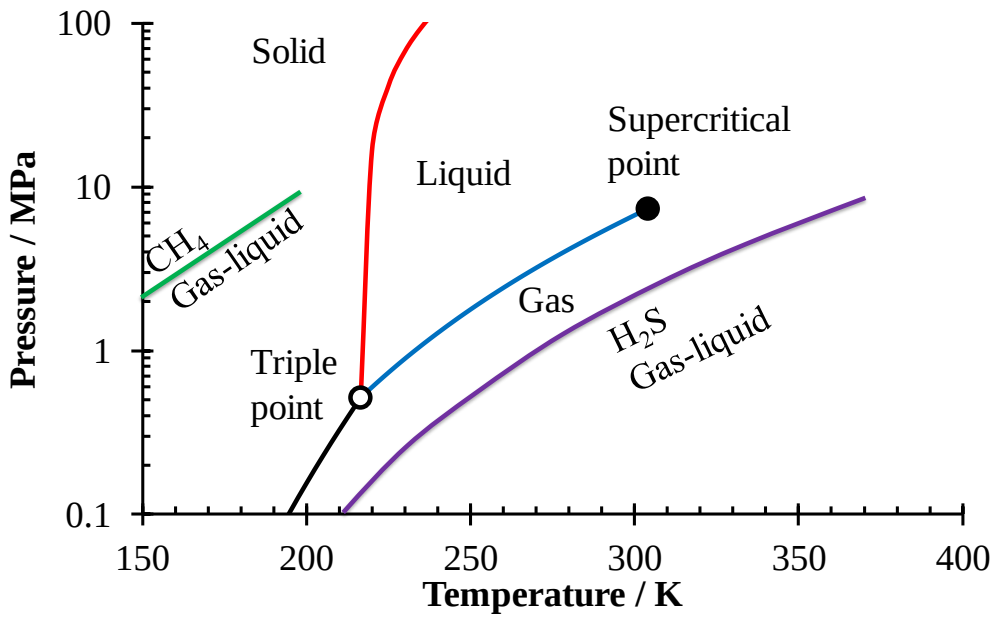

Figure 1-3. Phase behaviour of CH_4 and H_2S on the pure CO_2 phase diagram.

The resulting separated acid gas from these cryogenic distillation processes is discharged as a high-pressure liquid that can be injected into reservoirs for acid gas injection without any further compression. No need for recompression gives economical benefit in addition to already estimated 30 % energy and cost-efficient cryogenic separation compared to the

amine separation.[23] If the recompression required for the amine separated acid gas is taken into the economical estimation, the cost saving can increase to about 40 % when using the cryogenic separation. While this reduces the CO_2 emission, acid gas injection also prevents the production of sulfur, which could be undesirable if a market is readily accessible. In addition, some high-pressure acid gases could be a great source of CO_2 as a fine chemical or as a fluid for enhanced oil recovery, but only if the small amount of H_2S can be removed without dropping the CO_2 pressure below the supercritical region. Further distillation to remove the H_2S is costly and complicated, due to the relative volatilities of CO_2 and H_2S being similar.[24] There are currently no commercial methods to oxidize low-level H_2S to S_8 in the high-pressure CO_2 fluid. The conventional methods to separate low-quality acid gases release the rest of the CO_2 at near atmospheric pressure and the produced S_8 is often not a marketable product due to its low-quality. Creating an innovative solution to convert the H_2S into S_8 within the dense-phase CO_2 will be beneficial in terms of enabling sulfur recovery from low-quality acid gas while conserving a high-pressure CO_2 stream that would require minimal to no recompression or purification to meet the requirements for sale.

1.4 Sulfur recovery

Producing marketable sulfur could be more desirable as the major source of S_8 is the conversion of H_2S in the acid gas, instead of disposing the acid gas into a reservoir. The removal of H_2S in the separated acid gas can lead to the recovery of S_8 as a by-product. Conventionally available low-pressure sulfur recovery processes are generally divided by the concentrations of H_2S within the acid gas as shown in Table 1-3.[20]

Table 1-3. Low-pressure sulfur recovery processes.[20]

Recovery Process	Claus	Selectox	Liquid Redox
Acid Gas ratio (AG)	> 20% H_2S in AG	2-20 % H_2S in AG	< 2% H_2S in AG

1.4.1 Claus process

The most common method for converting H_2S to S_8 is the modified Claus process. The Claus process is typically used when acid gas streams contain more than 20 % H_2S. The net partial oxidation reaction for Claus process is shown below in Equation 1-4.

$$3\ H_2S\ (g) + 3/2\ O_2\ (g) \rightleftharpoons 3\ H_2O\ (g) + 3/n\ S_n\ (g) \qquad (1\text{-}4)$$

Equation 1-4 is achieved in two steps. Approximately one-third of the H_2S in the acid gas stream is oxidized with oxygen to produce SO_2 at high-temperature in a thermal reactor according to Equation 1-5.

$$H_2S\ (g) + 3/2\ O_2\ (g) \longrightarrow H_2O\ (g) + SO_2\ (g). \qquad (1\text{-}5)$$

The flame stability required to support the thermal reactor is what limits the acid gas quality, where below 20 mol% H_2S cannot sustain a stable flame, even when combusted with O_2 enrichment. The remaining two-thirds of the H_2S is thermally and catalytically reacted with the SO_2 that was produced by Equation 1-5 in the thermal reactor (with waste heat boiler) and catalytic reactors to give elemental sulfur according to Equation 1-6.

$$2\ H_2S\ (g) + SO_2\ (g) \rightleftharpoons 2\ H_2O\ (g) + 3/n\ S_n\ (g). \qquad (1\text{-}6)$$

The reason for having a thermal reactor and several catalytic reactors is because of the thermodynamic equilibrium limitation of the reaction.

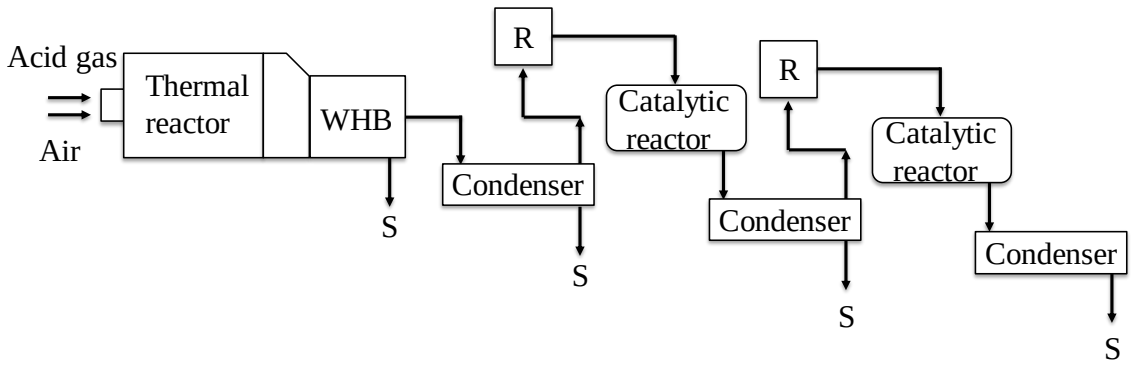

Figure 1-4. Simplified schematic of the Claus process. WHB is a waste heat boiler. R is for reheater, and S is the produced sulfur.

Initially in the thermal reactor, 2/3 of the overall conversion from H_2S to S_n happens. The remaining 1/3 of the overall conversion occurs in two to three catalytic reactors where temperatures are reduced in each subsequent reactor to maximize the recovery of sulfur. The thermal reactor and three catalytic stages can recover up to 98% of the sulfur from H_2S. Between each catalytic stage, there is a sulfur condenser which lowers the sulfur dewpoint temperature, such that the next stage can operate at a progressively lower temperature.

A reducing tail gas treatment unit (TGTU) can be added at the end of the Claus process to reach a recovery of 99.9%.[20,25] In the TGTU, all residual sulfur compounds are reduced back to H_2S using hydrogenation catalysts and excess hydrogen, and the H_2S is then separated by an amine unit and recycled back to the thermal stage.[14]

Other tail gas conversions, such as Superclaus and Euroclaus are also available.[26] These processes are based on a selective oxidation of H_2S to S_8 in the last catalytic reactor as according to Equation 1-7.

$$H_2S + 0.5\ O_2 \rightarrow 1/n\ S_n + H_2O \qquad (1\text{-}7)$$

The selective oxidation is achieved by using an iron oxide-based catalyst with silica support that prevents from establishing the Claus equilibrium.[27] Direct oxidation with the elimination of the Claus activity allows for higher recovery at 99 % to 99.5 %.[20]

When the H_2S concentration is below 40 %, it is difficult to sustain the high-temperatures required in the thermal reactor for the Claus process. This issue can be addressed by preheating the acid gas or air prior to being introduced to the thermal reactor, by adding fuel gas (co-firing), or by oxygen enrichment *via* the introduction of a higher concentration of O_2.[20] Other conversion processes, such as the Selectox process or liquid redox processes (to be introduced in later sections), may be more economical when the H_2S concentrations are below 20 %.[20]

1.4.2 Thermodynamics of the Claus reaction

The thermodynamics of the Claus equilibria were studied by Gamson and Elkins, who developed a chart of theoretical equilibrium conversion of H_2S to sulfur as a function of temperature.[28] A modified Gamson-Elkins plot (Figure 1-5) has been calculated by using a previously developed in-house Gibbs Energy Minimization routine for Claus chemistry equilibria at low-pressure and thermochemical data from the National Institute of Standards and Technology-Joint Army-Navy-Air Force (NIST-JANAF) Thermochemical Tables.[29] Gibbs Free Energy is a thermodynamic potential that measures the available energy (spontaneity) from an isothermal, isobaric thermodynamic system. The reaction quotient for the Claus equilibrium (Equation 1-4) can be expressed as such $Q = [H2S]^3[O2]^{3/2}/[S8]^{3/8}[H2O]^3$. For the reaction quotient to become an equilibrium constant K, a negative Gibbs free energy change (ΔG) of the exothermic reaction would mean a

spontaneous forward reaction. There can be too many different reactions involved with the starting reactants, but at the equilibrium composition the Gibbs Free Energy of the system would achieve the minimum (no more spontaneity because available energy has all been released).

If the initial pressure is 0.1 MPa, the standard Gibbs free energy of formation is ΔG°, and then the Gibbs energy at any pressure p is[30]

$$G = \Delta G^{\circ} + nRT \ln(p/0.1\text{MPa}). \quad (1\text{-}8)$$

If the gas is non-ideal, fugacity is used instead of pressure with the symbol *f*. The fugacity is the pressure departure of non-ideality. The departure ratio from the ideal gas is related by the fugacity coefficient, ϕ. If a gas is behaving ideally ($\phi = 1$), the fugacity is equal to the pressure.

$$f = \phi p \quad (1\text{-}9)$$

In an equilibrium, the total sum of Gibbs energy of each chemical should reach a minimum at constant pressure and temperature. In an ideal gas system comprised of components, *c*, and elements, *m*, the sum of Gibbs energy function is shown in Equation 1-15,

$$\mathrm{G}(T,p) = \sum_{i=1}^{c} y_i\left(\Delta_f G_i^{\circ} + RT\ln(y_i\phi_i p)\right) \quad (1\text{-}10)$$

where y is the mole fraction, $\Delta_f G_i^{\circ}$ is the standard Gibbs free energy of formation, R is the ideal gas constant, T is the absolute temperature, p is the total pressure, and ϕ_i is the fugacity coefficient for species *i*. The only parameters required for the calculation of the equilibrium composition of a mixture *via* GEM are the free energies of formation for the chemical species involved in the equilibrium. The Gibbs free energy of formation data was obtained from JANAF thermochemical tables,[29] which were fitted to a polynomial expression of the form:

$$\Delta_f G_i^\circ = d_i + e_i T + g_i T^2 + h_i T^3 \quad (1\text{-}11)$$

The temperature, pressure, and mole fraction numbers of involved species define the system, the objective is to find the set of mole fraction numbers that result in a minimum Gibbs free energy, subject to mass balance constrains. The following set of equations must be satisfied for the conservation of individual elements:

$$b_j - \sum_{i=1}^{c} a_{ij} n_i = 0 \qquad j = 1, 2, 3, \ldots, m \quad (1\text{-}12)$$

where b_j is the total number of element j in the feed, and a_{ij} is the stoichiometric coefficient of element j in species i. Using Equation 1-10 for a mixture, the concentrations of each species y_i, are iteratively changed to minimize the sum of the Gibbs energy until concentrations fractionally change by $\delta y_i / y_i < 0.00001$ (or any alternative tolerance) by using the Solver tool within Microsoft Excel. The equilibrium concentrations of all species are obtained after minimization of the total system Gibbs energy. Ideal gas conditions are assumed, where $\phi_i = 1$, for the previously developed in-house Gibbs Energy Minimization routine. The modified Gamson-Elkins plot is calculated at 0.1 MPa and at 20 MPa, which is shown in Figure 1-5.

Sulfur has many allotropes in the gas phase, which causes the unusual shape of the conversion curve. At temperatures below 875 K, larger sulfur rings such as S_6 and S_8 are thermodynamically favourable. For Equation 1-4 and $n > 4$, the stoichiometry of gas products is less gas then the reactants; therefore, increasing the total pressure would cause the equilibria to shift towards products (higher S_8 recovery) by Le Chatelier's principal. This phenomenon with increased pressure can be seen in Figure 1-5 with increase in the sulfur recovery from 0.1 MPa to 20 MPa. At temperatures above 875 K, there is a shift in the main sulfur species from S_8 to S_2. In the high-temperature case, increasing the total

pressure would now cause the equilibrium Equation 1-4 to shift away from product due to more gas on product side. This phenomenon with increased pressure can be seen in Figure 1-5 with decrease in the sulfur recovery from 0.1 MPa to 20 MPa. Forming S_2 from larger sulfur molecules is slightly endothermic, thus the trend of recovery increases with temperature above 875 K for each isobar.

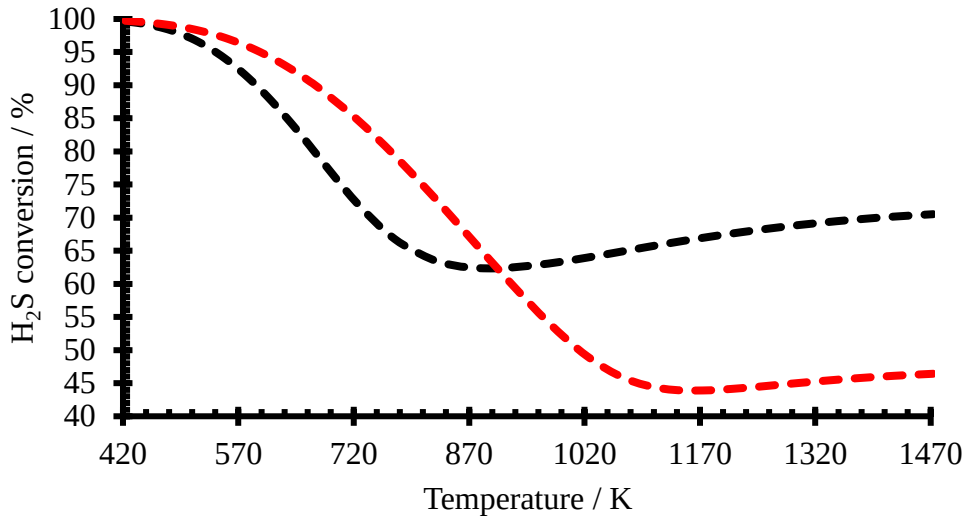

Figure 1-5. Theoretical equilibrium conversion of 25% H_2S, 12.5% O_2, and 62.5% CO_2 mixture to sulfur. The black dotted line (0.1 MPa) and the red dotted line (20 MPa) are calculated from a previously existing GEM model with ideal gas assumption.

Like most applied GEM routines, calculations are aimed at low-pressure H_2S conversions, therefore these calculations do not reflect the effect of non-ideal behavior of high-pressure accurately.[31] The subsequent work involved experimentally measuring S_8 within high-pressure CO_2 and modelling to calibrate non-ideal mixing equation parameters for accurate calculation of the fugacity coefficients. In Chapter 4, research describes substituting ϕ_i with real fluids fugacity coefficients, after which Equation 1-10 was re-minimized for new real-fluid concentrations, y_i.

The interesting conditions for this thesis are in the lower temperature region or $T < 573$ K, where lower temperatures and high-pressures help to drive the equilibrium towards 100 % conversion. For example, the H_2S conversion is 95.4% at 473 K and 0.1 MPa, whereas this conversion is predicted to increase to 98.4% at a higher pressure of 20 MPa. This conversion increase is expected to be even larger if real fluid fugacity coefficients can be incorporated for high-pressure GEM calculations.[32] Again, this subject is revisited in Chapter 4.

1.4.3 Sub dewpoint Claus process

The thermodynamic conversion limitations of the Claus reaction as shown in Figure 1-5, can be improved by taking advantage of the exothermic behaviour of the Claus reaction below 875 K. Here a lower temperature improves recovery, especially below the sulfur dewpoint. Unfortunately, the conditions below the dewpoint of sulfur will eventually lead to catalytic deactivation from sulfur condensation onto solid catalysts, thus blocking the active sites and compromising recovery through kinetic limitations. To mitigate the catalytic deactivation from sulfur condensation, sub-dewpoint Claus processes utilize several catalytic reactors in a cyclic operation to regenerate the catalyst after deactivation. Just before a catalytic reactor is fouled from condensed sulfur, the process flow is diverted to a standby reactor. The saturated reactor is then regenerated using a gas that has been heated to 300–350 °C to vaporize the sulfur, which is directed to a condenser to recover the sulfur.

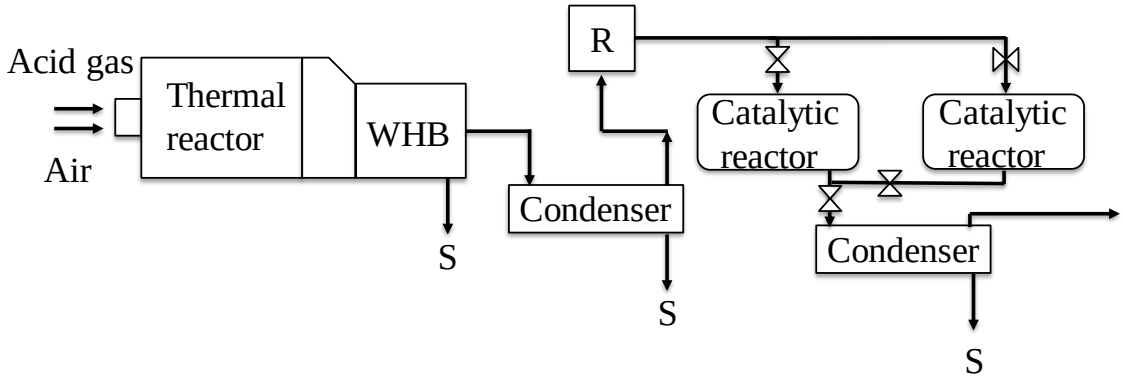

Figure 1-6. Simplified schematic of sub-dewpoint process. WHB is a waste heat boiler. R is for reheater, and S is the produced sulfur.

Commercial sub-dewpoint processes include the Lurgi/SNEA[P] Sulfreen process,[33] the AMOCO CBA process,[34] and the MCRC sulfur recovery process offered by Delta Projects, Inc.[35] Sub-dewpoint conditions are considered in this thesis for the purpose of maximizing the recovery of sulfur by lowering temperatures below sulfur dewpoint conditions.

1.4.4 Selectox process

The Selectox process is entirely catalytic. Although there is no high-temperature thermal stage as in the typical modified Claus process, the chemistry of this heterogeneous catalysis is still considered Claus chemistry, where H_2S is initially oxidized to SO_2.[20] The Selectox is used to process acid gas streams containing 2-20% H_2S, because the thermal reactor within the conventional Claus process is no longer able to sustain the required temperatures with such low-concentrations of H_2S. Typically sulfur is recovered in the range of 90-95%, though further processing such as tail gas treating unit is needed to achieve 99.9% sulfur recovery.[20] This process occurs entirely in the gas-phase, leaving the remaining CO_2 near atmospheric pressure at the end of the process, which will require recompression to transport CO_2 elsewhere. In this thesis, a new method is presented that

will leave CO_2 in a high-pressure supercritical form which reduces the energy requirements for recompression.

1.4.5 Liquid redox processes

Liquid redox processes are used for the removal of less than 2% H_2S in acid gas streams, which is close to the composition of the target acid gas streams of this thesis (~ 1% H_2S in CO_2). Stretford, Unisulf, SulFerox®, and LO-CAT® are some examples of liquid redox sulfur recovery processes.[8] For example, in the LO-CAT®, HS^- ions are formed when H_2S dissolves in an iron chelating solution, and then HS^- is oxidized to elemental sulfur according to Equation 1-13.

$$2\ Fe^{3+}L\ (aq) + HS^-\ (aq) \rightarrow 2\ Fe^{2+}L\ (aq) + S\ (s) + H^+\ (aq), \qquad (1\text{-}13)$$

where "L" is a chelating agent such as ethylenediamine tetraacetic acid (EDTA), hydroxyethyl ethylenediamine triacetic acid (HEDTA) or nitrilotriacetic acid (NTA).[20] Iron would ordinarily precipitate at low-concentrations as either iron hydroxide or iron sulfide,[36] so the chelating agents are required in order to hold the iron ions in the solution. The reduced iron (II) is converted back to the iron (III) form by dissolved oxygen in a separate vessel according to Equation 1-14.

$$2\ Fe^{2+}L\ (aq) + 1/2\ O_2\ (aq) + H_2O \rightarrow 2\ Fe^{3+}L\ (aq) + 2\ OH^-\ (aq). \qquad (1\text{-}14)$$

Liquid redox processes often encounter problems such as absorber plugging, bacterial contamination, and poor-quality sulfur.[8,20] This poor-quality sulfur is often sent to the landfill due to impurity issues. Therefore, a potentially marketable product becomes an environmental liability. This liquid redox process can be incorporated either before or

after the amine sweetening unit. However, this still leads to the energy intensive issue of required recompression of the eventually separated CO_2 due to it being at low-pressure.

For very low-concentrations of H_2S, scavengers can used to selectively remove H_2S. Operation cost increases with increasing quantities of H_2S for non-regenerable scavengers. Regenerable processes such as Vitrisol® is available to reduce the operational cost for large quantities of H_2S.[37]

1.5 Proposed alternative sulfur recovery in high-pressure CO_2

Low-quality acid gas with small concentrations of ~1% H_2S in CO_2 could be a promising source of CO_2 if H_2S can be successfully removed. If low-quality acid gases can be separated using the cryogenic processes, it would be beneficial as the recompression steps of conventional amine separation processes can be minimized or even eliminated. Following a cryogenic separation of acid gas, heterogeneous catalytic conversion of H_2S to S_8 within high-pressure CO_2 can be achieved at low-temperatures, which is advantageous as the equilibrium reaction (Equation 1-2) is exothermic below 875 K. The high-pressure of CO_2 is also beneficial in shifting the equilibrium towards the smaller number of gas molecule in the product side of S_8. The recovered S_8 should be a high-purity marketable product, in contrast to the large amount of waste that liquid redox processes generally produce. While very low-temperatures are beneficial to maximize the conversion of H_2S, decreasing temperatures below the sulfur dewpoint would cause the fouling of the catalyst by sulfur deposition. Therefore, the S_8 dewpoint in high-pressure CO_2 was initially studied in this thesis to determine the optimal conditions for achieving single-phase reaction conditions. The solubility data and the model obtained in this study not only

allowed the determination of the S_8 dewpoint within high-pressure CO_2 but was also used to find the fugacity coefficients of S_8 within high-pressure CO_2 to be used in the subsequent modification of Gibbs Free Energy minimization routine at high-pressure.

The second focus of this thesis work was to study the equilibrium of the H_2S oxidation within high-pressure CO_2. The Gibbs Free Energy minimization routine was established to calculate the high-pressure equilibrium by incorporating fugacity coefficients of the H_2S oxidation equilibrium species within high-pressure CO_2. To verify the calculated results from high-pressure Gibbs Free Energy minimization calculations, oxidation of H_2S within high-pressure CO_2 fluid was experimentally carried out by heterogenous catalysis mainly utilizing γ-alumina and titania at T = 493 to 563 K, p = 10 and 20 MPa, and [H_2S] = 0.5 to 1.7 %. Space velocities of the equilibrium study (3870 to 9310 h^{-1}) was low enough to result in the experimental conversion being close to the Gibbs Free Energy minimization calculated equilibrium conversion.

The final focus of this thesis work was studying the kinetic limitations for H_2S oxidation within the high-pressure CO_2 fluid and relatively high-space velocities. Experiments were carried at T = 423.15 to 513.15 K and p = 10 to 25 MPa using a heterogeneous γ-alumina catalyst. The study was performed with 1% H_2S + 0.5% O_2 within high-pressure CO_2 fluid by following the disappearance of H_2S. Space velocities of the kinentic study (860 to 6330 h^{-1}) was relatively high to result in the experimental conversion being lower to the Gibbs Free Energy minimization calculated equilibrium conversion. From the experimentally obtained kinetic data, a kinetic model was developed to calculate the rate constant over a range of temperatures and pressures.

Chapter 2: Literature Review

2.1 Elemental sulfur

Sulfur is a chemical element with the symbol S, atomic number 16, and atomic mass of 32.06 g mol^{-1}. Its elemental form exists in a cyclic octatomic molecule as S_8 (bright yellow and crystalline) under atmospheric conditions. However, sulfur occurs naturally in a variety of forms. Sulfur can be found in its pure, native form which historically and in literature is often referred as brimstone, meaning "burning stone" because the bright yellow sulfur solids (stone) burns.[38,39] Sulfur can also be often found as sulfide and sulfate minerals. Sulfur also exists in many organosulfur compounds, which can be converted to H_2S through hydrodesulfurization.[40] The sulfide and sulfate forms of sulfur can be converted to S_8 through either oxidative or reductive processes, respectively.

2.1.1 Physical properties of sulfur

Sulfur can exist in two solid forms, an α-solid (orthorhombic) and a β-solid (monoclinic). Because of these two solid phases, sulfur has three triple points shown in Table 2-1.[41] The kinetic melting point is generally the observed melting point, while the thermodynamic melting point is the natural melting point where it can take up to ten hours to form a stable equilibrium sulfur species.[41,42] At high and low temperatures, S_2 and S_8 are the dominant alloptropes respectively. Minor allotropes consisting of S_3, S_4, S_5, S_6, and S_7 are also present throughout the temperature range. This allotropy contributes to the unusual shape of the H_2S to S_n conversion curve as previously discussed in Chapter 1, Figure 1-5.

Table 2-1. Summary of elemental sulfur phase transition points.[41]

Condition	T / K	p / Pa
Triple point (α-β-g)	368.39	0.4868
Triple point (α-β-l)	419.06	124,360,000
Triple point (β-l-g)	388.326	2.4437
Thermodynamic M.P. (β-l)	388.348	101.325
Kinetic M.P. (β-l)	393.5	101.325
Boiling point	717.75	101.325

Homolytic cleavage of S-S electron bond pair occurs above 433 K leading to polymerization of liquid sulfur. Concatenation and reptation between these sulfur polymers cause large changes in viscosity as a function of temperature. The viscosity change of liquid sulfur can range from 7 x 10^{-2} Pa · s at 433 K to a maximum near 93000 x 10^{-2} Pa · s at 460 K.[43] At temperatures > 460 K, depolymerization occurs, causing a decrease in viscosity.[44,45]

2.1.2 Chemical properties of sulfur

Sulfur can be reduced to sulfide (H_2S) or oxidized to sulfates (SO_4^{2-}) with varying oxidation state from -2 to +6. Sulfur is insoluble in water but is highly soluble in carbon disulfide (CS_2) while being slightly less soluble in other nonpolar organic solvents such as benzene and toluene.[46,47] Sulfur solubility in CO_2 increases as the supercritical CO_2 becomes denser with higher pressure. Detailed discussion on the sulfur solubility in high-pressure CO_2 is presented in the following Chapter 3.

2.1.3 Production of sulfur

The world production of sulfur in 2019 was estimated at 79 million tonnes. [48] The Frasch process can be used to recover nearly pure form of S_8. In this process, superheated

water is first pumped into a sulfur deposit to melt the sulfur. This is followed by the addition of compressed air which returns the 99.5 % pure melted product to the surface.[49] However, the Frasch process is expensive and the sources of pure sulfur deposits are limited. This is the reason why it has not been the main supply of S_8 anywhere in the world since early 2000.[40]

The majority of S_8 produced worldwide comes from natural gas and oil sources during the process of removing H_2S.[48] H_2S needs to be removed for safety reasons in addition to producing a valuable commodity in the process. Low-level H_2S (< 530 ppm) exposure can cause eye irritation, a sore throat and cough, nausea, shortness of breath and pulmonary edema. High-level H_2S (> 530 ppm) exposure can result in loss of breathing and eventually fatality.[50,51] In the process of removing H_2S, S_8 is produced as a by-product from the partial oxidation of H_2S during the thermal and catalytic steps. Produced S_8 is a very desirable commodity from the oil and gas industry, with its primary use being the precursor to produce sulfuric acid.

2.1.4 Applications of sulfur

A high percentage (~ 90 %) of the commercial use of produced elemental sulfur is in the production of sulfuric acid (H_2SO_4).[52] For the production of sulfuric acid, S_8 is combusted to produce sulfur dioxide (SO_2) according to Equation 2-1

$$1/8\ S_8 + O_2 \rightarrow SO_2 \qquad (2\text{-}1)$$

SO_2 is then further oxidized to sulfur trioxide (SO_3) with O_2 using a vanadium oxide catalyst according to Equation 2-2.

$$2\ SO_2 + O_2 \rightleftharpoons 2\ SO_3 \qquad (2\text{-}2)$$

Direct absorption of SO_3 into water is avoided to prevent the formation of a sulfuric acid mist due to the exothermic nature of the reaction. Instead, high concentrations of H_2SO_4 (~ 98 %) is used to absorb SO_3 and form oleum ($H_2S_2O_7$) according to Equation 2-3.[53]

$$SO_3 + H_2SO_4 \rightarrow H_2S_2O_7 \quad (2\text{-}3)$$

The $H_2S_2O_7$ is then diluted with water to produce concentrated sulfuric acid (H_2SO_4).

$$H_2S_2O_7 + H_2O \rightarrow 2\ H_2SO_4 \quad (2\text{-}4)$$

The primary use of the produced H_2SO_4 (~ 60 %) is for the production of phosphoric acid (H_3PO_4) used for manufacturing phosphate fertilizers.[52] H_3PO_4 is produced by treating a phosphate-containing mineral such as calcium hydroxyapatite (Equation 2-5) or fluorapatite (Equation 2-6) with H_2SO_4.

$$Ca_5(PO_4)_3OH + 5\ H_2SO_4 \rightarrow 3\ H_3PO_4 + 5\ CaSO_4 + H_2O \quad (2\text{-}5)$$

$$Ca_5F(PO_4)_3 + 5\ H_2SO_4 + 10\ H_2O \rightarrow 5\ CaSO_4 \cdot 2\ H_2O + HF + 3\ H_3PO_4 \quad (2\text{-}6)$$

Sulfur is the most common vulcanization agent. Vulcanization is a chemical process that combines natural rubber and other polydiene elastomers into cross-linked polymers, using sulfur as the bridges between the individual polymers. The vulcanization proceeds *via* ionic vinyl polymerization, where the reaction between sulfur with carbon-carbon double bonds initially forms persulfonium ion intermediates. The intermediates then react further, resulting in a cross-linked rubber.[54]

2.2 Carbon dioxide

CO_2 is a naturally occurring colourless trace gas in the atmosphere. It is also commonly known as a prominent greenhouse gas. While greenhouse gases are generally perceived to be detrimental, CO_2 is a necessary greenhouse gas as it is required to keep the

Earth's atmospheric temperature at a habitable level. Without greenhouse gases, the average surface temperature of Earth would be about 255 K.[55] However, the excess amount of CO_2 emitted since industrialization has resulted in global warming. Ideas of withdrawing CO_2 from the environment are attractive, but they are not yet entirely economically feasible. Most of the CO_2 employed in processes today is collected from the effluents of ammonia plants or separated from natural gas sources.[56] If these anthropogenic sources of CO_2 can be further used in processes such as supercritical fluid extraction or an alternative solvent to conventional organic solvents, it may be the most advantageous and simple form of CO_2 sequestration. A higher demand of industrially available CO_2 can also provide extra incentives for companies to capture the CO_2 for subsequent use rather than releasing it to the atmosphere.

2.2.1 Physical properties of carbon dioxide

The thermodynamic properties of CO_2 have been well documented.[57] The phase diagram of CO_2 is shown in Figure 2-1.

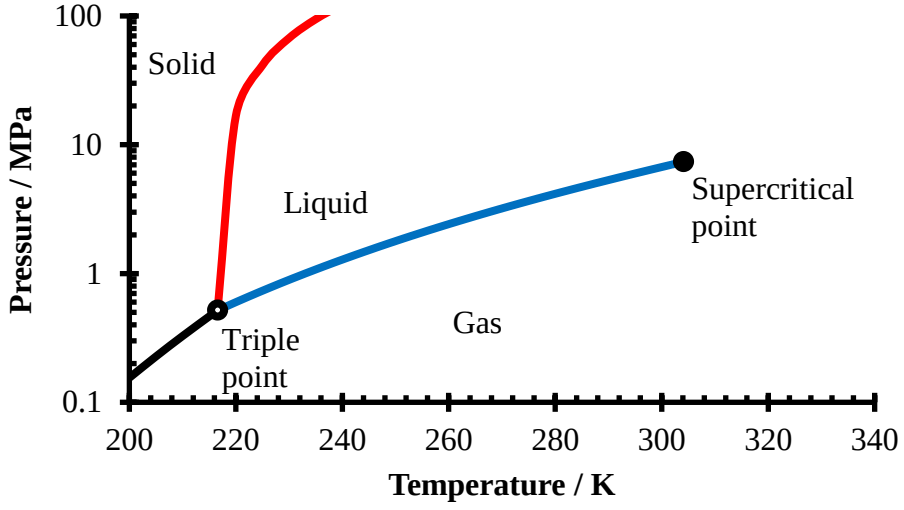

Figure 2-1. The phase diagram of carbon dioxide.[58]

According to the phase diagram, near the atmospheric pressure of 0.1 MPa, CO_2 has no liquid state. The gas deposits directly to a solid at temperatures below 194.65 K and the solid sublimes directly to a gas above 194.65 K. Liquid CO_2 exists only above the triple point at 0.52 MPa and 216.58 K. The critical point is at 7.38 MPa and 304.23 K, and the conditions above the critical point result in CO_2 behaving as a supercritical fluid.[22] When CO_2 is in the supercritical conditions above the critical point, it exhibits behaviours of both a gas and a liquid. For example, supercritical CO_2 can fill its container like a gas while also having a density like a liquid. Near the critical point of CO_2, the thermodynamic properties change rapidly with small changes in the pressure and temperature. This rapid change can be taken advantage of to adapt the properties of CO_2 to a desired point by making small changes in pressure and temperature. For this thesis, higher pressure condition p = 20 MPa is beneficial for the catalytic oxidation of H_2S to maintain a single-phase of the supercritical CO_2 with the produced S_8 dissolved. The solubility of S_8 in CO_2 rapidly decreases with temperature and pressure decrease, so the separation of S_8 and the supercritical CO_2 is achieved by decreasing temperature and/or pressure.

2.2.2 Chemical properties of carbon dioxide

CO_2 cannot be oxidized as it is the product of complete oxidation of organic compounds. CO_2 can be hydrogenated in the presence of noble metal catalysts, such as platinum, to produce carbon monoxide (CO).[59] CO_2 is a potent electrophile, but reactions with nucleophiles are not thermodynamically favoured.[60] The relative inertness of CO_2 is advantageous as an alternative to the conventional organic solvents for preventing undesirable by-products.

2.2.3 Production of carbon dioxide

CO_2 can be found in natural gas sources as an impurity along with H_2S.[2] CO_2 is also a by-product of many industrial processes such as power generation, manufacturing of quicklime and production of hydrogen and ammonia.[56] Producing commercial CO_2 therefore requires recovery and purification from such sources. In almost all cases, CO_2 is vented to the atmosphere at the production point, if it is not recovered for transport and beneficial to be used for other applications.

2.2.4 Applications of carbon dioxide

CO_2 is non-flammable with a high threshold limit value of 5000 ppm at 298 K. The threshold limit value is the maximum daily exposure limit that an individual can be exposed to without experiencing adverse health effects.[7] There are significant advantages in using CO_2 as a solvent compared to conventional organic solvents such as acetone, pentane, and chloroform (threshold limit value of 750 ppm, 600 ppm, and 10 ppm respectively).[7] CO_2 is relatively inert towards reactive compounds, although for this specific thesis, CO_2 does react with H_2S to form a small amount of equilibrium product in the form of carbonyl sulfide (COS) according to Equation 2-7.

$$CO_2 + H_2S \rightleftharpoons COS + H_2O \qquad (2\text{-}7)$$

The high vapour pressure of CO_2 is another safety advantage as the residual CO_2 in final products is not a threat. CO_2 is the only other solvent other than water that does not require process re-evaluation by the United States Food and Drug Administration.[7] The global food industry is taking the advantage of CO_2 as a solvent.[7] Caffeine extraction is one of the most common uses of supercritical CO_2 in the food industry. Caffeine is extracted from coffee

beans at lower temperatures from 313 to 353 K and pressures from 12 to 18 MPa, with residence times up to 30 hours.[61] The extracted caffeine is separated from the supercritical CO_2 into water by reverse osmosis or distillation. These methods are used as they are less energy intensive then depressurization below supercritical point which requires recompression of CO_2 to be used for subsequent extraction. Water can be used as a co-solvent within these extraction processes since CO_2 is a relatively non-polar solvent, and the incorporation of a water co-solvent can increase the extraction yield up to 10 times compared to using CO_2 alone.[62] Here the cross-contamination between water and CO_2 is not a contamination such as with organic contaminations which would require subsequent remediation to eliminate the organic contamination.

The cannabis industry is rapidly expanding due to recent legalization in Canada. Apart from leisurely use of cannabis products, it is gaining a lot of attention from researchers for its medicinal properties. One of the major components contained in cannabis is Δ^9- tetrahydrocannabinol (Δ^9- THC). The Δ^9- THC can be extracted direct from cannabis through use of organic solvents such as hydrocarbons and alcohols with high yield (~ 90 %).[63] In order to avoid potential safety issues associated with the use of organic solvents such as flammability and toxicity, supercritical fluid extraction can be used as an alternative method. Supercritical fluid extraction is non-flammable, does not have toxicity issues, and the separation of the product can be easily achieved by utilizing a pressure decrease. Supercritical fluid extraction is widely used technique including in the pharmaceutical field such as extraction of essential oils.[64-69] Perrotin-Brunel *et al*. utilized supercritical fluid extraction to measure the solubility of Δ^9- THC in CO_2.[70] Their apparatus was operational up to 35 MPa and temperatures from 293 to 423 K. An Isco pump was

used to provide CO_2 into a vessel with Δ^9- THC sample which was placed in an oven for temperature control. Two hours after the system reached the desired temperature and pressure, the CO_2 in the system was circulated using a micropump. The system loop was connected to a high-performance liquid chromatography (HPLC) for the analysis of the sample.

CO_2 is the product when organic compounds are completed oxidized. This is advantageous if CO_2 is to be used as a solvent for oxidation reactions. This is because conventional solvents in oxidation reactions with O_2 will form undesirable by-products from reactions between the O_2 and solvents. For example, conventionally hydrogen peroxide (H_2O_2) is produced via hydrogenation of a 2-alkyl anthraquinone (AQ) over a palladium supported catalyst. The hydrogenated AQ is then oxidized to produce H_2O_2 and regenerate AQ in an organic solvent. The subsequent application of H_2O_2 in an oxidation reaction is considered green as the by-product of the oxidation would be water. However, the manufacturing process of H_2O_2 cannot be considered environmentally friendly because the use of the organic solvent results in a contamination issue. Continuous stirred tank reactors are used to remedy the gas-liquid diffusion limited reaction, which results in a range of AQ residence time, thus over hydrogenation of the AQ can happen to form waste by-products.[71] This contamination issue is circumvented by utilizing distillation, adding another energy-intensive processing step. Due to inertness towards oxidation in addition to being non-flammable, CO_2 was considered as an alternative solvent in the AQ process by adding a fluoroether group to the AQ to make a CO_2-soluble analog to conventional AQ.[72] Despite the promising results, the process was no further pursued as the production of fluoroether-functional AQ was too expensive.

Operating an exothermic reaction in a high-pressure environment must be accompanied by the consideration of additional safety precautions, which could be relieved by the presence of non-flammable CO_2. The high compressibility of supercritical CO_2 can absorb the excess heat evolved from an exothermic reaction and prevent a sudden increase in temperature. Despite the less-than-green manufacturing process of H_2O_2, the AQ process is preferred to avoid direct contact between H_2 and O_2, because mixtures of H_2/O_2 are explosive over a wide range, from a lower flammability limit (LFL) of 4 mol % H_2, to an upper flammability limit (UFL) of 94 mol %.[73] Therefore, CO_2 is considered as an alternative solvent for the direct reaction of H_2 and O_2 to form H_2O_2.[74] In fact, the addition of CO_2 to a mixture of hydrogen and air expands the range of non-explosive level up to 9.5 % in the H_2O_2 production.[75] Here the challenge was the production of CO_2 soluble palladium catalysts.

CO_2 has lower interfacial surface tension compared to conventional organic solvents due to the lower viscosity of supercritical CO_2. This can result in high diffusivity of solutes within the supercritical CO_2, which can wet and penetrate complex reservoirs/catalyst pores faster than conventional organic solvents.[7] Enhanced oil recovery is a good example of where the low-viscosity and high-diffusivity are well utilized. Enhanced oil recovery allows for extra recovery of oils retained in reservoirs due to capillary forces in addition to oils that are immobile or nearly immobile due to high viscosity. Miscible processes, chemical floods, and steam-based methods are generally used in enhanced oil recovery process.[6] Supercritical CO_2 is used in miscible processes because of the miscibility and low-viscosity of supercritical CO_2 at relatively low temperatures and pressures.[76] Supercritical CO_2 is injected into somewhat depleted

reservoirs to pressurize the reservoir as well as provide solvent to dissolve additional oil out of the reservoirs.

Many applications are replacing conventional organic solvents with supercritical CO_2 because of the diffusion limitation across the vapour-liquid interface. The limited solubility of gases in liquid solvents dictates the rate of the reaction. Higher partial pressures of gas reactants are applied to improve the limited solubility of gases in the liquid solvents. The supercritical CO_2 is miscible with gases, therefore eliminating the gas-liquid interface present in conventional organic solvents. Therefore, the rate of the reaction is no longer limited, since the transport resistance of the gas-phase into the liquid-phase has been removed.

The utilization of supercritical CO_2 as a solvent in a gas-phase reaction has not gained attention because the addition of CO_2 will decrease the partial pressures of reactants, leading to a decrease in reaction rate. However, there can still be benefits of using supercritical CO_2 in a gas-phase reaction such as non-flammability and the prevention of catalyst fouling. Addition of CO_2 in a gas-phase reaction will enlarge the non-flammable region, while CO_2 could prevent catalyst fouling by dissolving compounds that would otherwise condense out and block the active sites of the catalyst.[7,77]

This thesis focuses on the conversion of H_2S and O_2 over solid catalysts such as alumina and titania within high-pressure CO_2. The presence of high-pressure CO_2 is beneficial in this typically gas-phase reaction as the equilibrium products have lower partial pressures. Therefore, higher equilibrium conversion of H_2S to S_8 can be achieved by Le Chatelier's principle. Additional advantages from the utilization of supercritical CO_2 are the added safety in relation to the exothermal reaction and the prevention of catalyst

fouling, with increased S_8 solubility in high-pressure CO_2. Furthermore, the higher sulfur dewpoint in high-pressure CO_2 allows for the reaction temperature to be lower than that of the same reaction near atmospheric pressure. This allows for improved conversion of H_2S to S_8 by taking advantage of the exothermic nature of the reaction.

Processes utilizing high-pressure CO_2 require high-pressure equipment, which can be a potential safety hazard in comparison to comparable low-pressure processes. It should be noted that the low-density polyethylene polymerization process has been in operation since the 1940s, with conditions at p = 200 to 300 MPa and 520 K with a highly flammable component.[78] High-pressure CO_2 processes utilizing relatively lower pressures, from 10 to 20 MPa, should be readily achievable with current technologies.

2.3 S_8 solubility in high-pressure CO_2 measurements

In this thesis, solubility of S_8 within high-pressure CO_2 is explored and discussed. There are limited literature data available surrounding this topic, with the available literature data being limited to temperature conditions below 394 K. Previous studies focused on sulfur solubility in low-temperatures due to the flow assurance within pipeline conditions. In addition, the recent paper by Serin *et al*. did not agree with previous works by Kennedy *et al*. and *Gu et al*. in terms of the determined solubility values.[79-81] There are inconsistencies even within the limited literature at lower temperatures, and no available data at higher temperatures.

Kennedy and Wieland published the first experimental measurements in 1960 of S_8 in CO_2 at T = 339.15 K, 367.15 K, and 394.15 K and p = 6.9 MPa to 41.4 MPa.[81] In their study, CO_2 was introduced into the sulfur equilibrium reactor, which contained 18 cm^3 of

solid sulfur. While the equilibrium time was not described in their paper, the sulfur saturated CO_2 was sampled at a rate of 1 L h^{-1}. The sulfur was then filtered through a glass tube filled with Pyrex glass wool. The quantification of deposited sulfur was determined using the American Society for Testing and Materials (ASTM) Lamp Sulphur Method. The sulfur is flushed out using a sulfur-free natural gas and combusted with oxygen. The combustion products of the gas and sulfur were neutralized by a solution of sodium carbonate contained in the absorber, and back-titrated to calculate the amount of S_8 as in the ASTM Lamp Sulfur method. The volume of CO_2 passing through the sulfur vessel was measured by absorption in Ascarite (asbestos impregnated with sodium hydroxide). The main idea of measuring sulfur solubility in CO_2 is similar between literature studies and this thesis, but the quantification methods for sulfur and CO_2 are different.

Gu *et al*. did a similar study to determine the solubility of S_8 in CO_2 at T = 363.2 K and 383.2 K and p = 12.07 MPa to 40.52 MPa.[80] A stainless-steel reactor was used to contain solid sulfur and CO_2 was introduced into the reactor to establish equilibrium. The reactor volume was 300 cm^3, which was installed in a rocking device immersed in an oil bath. This system was able to operate up to 50 MPa and 423 K. After 20 hours of mixing, the sulfur saturated CO_2 was sampled from the reactor while the pressure in the reactor was kept constant with a piston. The sample loop was rinsed with 100 cm^3 of carbon disulfide to dissolve the sulfur collected, which was weighed after CS_2 was evaporated. This may be the reason for their inaccurate sulfur solubility numbers if a small amount of residual sulfur from the evaporated CS_2 was not accounted for their solubility numbers. The remaining CO_2 was measured through a gasometer to quantify the amount of gas sampled. The amount of sulfur weighed was related to the amount of CO_2 to determine the solubility of

sulfur in CO_2. The similar CS_2 wash is utilized in the work of this thesis, but the residual sulfur from the evaporated CS_2 was accounted in this thesis (Appendix, A2).

Similarly, Serin *et al*. used a stainless-steel equilibrium reactor with a piston where solid sulfur and CO_2 were able to establish equilibrium.[79] The reactor had a maximum working volume of 500 cm^3 and was able to operate under conditions up to 50 MPa and 473.15 K. CO_2 was introduced into the equilibrium reactor filled with sulfur. A gas booster was used to pressurize nitrogen for the pressure regulation by the piston. A heating band was used to control the temperature, and the reactor was equipped with a stirrer. The sulfur saturated CO_2 was sampled while the piston maintained the pressure of the reactor. Two 5 micrometer filters were used to ensure that no undissolved solid sulfur would exit the equilibrium reactor. The sulfur saturated CO_2 was passed through two stainless-steel bottles filled with a trapping mixture containing triphenyl phosphine (TPP). TPP reacts with the sulfur to form sulfur triphenyl phosphine (TPPS),[82] which is analyzed by Gas Chromatography (GC) equipped with a flame photometric detector (FPD) in a phosphorous mode.[83] The remaining CO_2 went through a mass flow meter to ensure the measurement of the gas volume sampled. Their experimental results were obtained at T = 333.15 and 363.15 K and p = 10 to 30 MPa. The same quantification method for S_8 is used for this thesis, but the sample loops were washed with CS_2 to make sure all the deposited sulfur was collected. The results obtained by Serin *et al*. agreed with this thesis work, and the data from their study was also included in the sulfur solubility in CO_2 modeling work (Chapter 3).

2.4 Heterogeneous catalysis experiments

In this thesis, the catalytic oxidation of H_2S within high-pressure CO_2 is discussed. Many studies are available in the literature for the heterogeneous oxidation of H_2S to form S_8 over various catalysts, none are conducted using high-pressure CO_2 as the solvent.[84-93] Most of these studies were conducted at near atmospheric pressures compared to that used in this thesis (p = 10 to 25 MPa). However, they provide some insights surrounding the equilibrium mechanisms and kinetics of the reaction. There are many metal oxides options for the catalyst for the reaction with the following activity relationship.[94]

$$V_2O_5 >> TiO_2 > Mn_2O_3 > La_2O_3 > CaO > MgO > Al_2O_3 > ZrO_2 > Cr_2O_3 >> SiO_2$$

where V_2O_5 is the most active per unit area, being 16 times more active than TiO_2 and 73 times more active than Al_2O_3.[94] This sequence is based on the number of reacted molecules per unit area, while reordering the sequence based on the activity per mass gives the following relationship.[94]

$$TiO_2 > V_2O_5 \approx Al_2O_3.$$

In addition to the more than acceptable activity per mass of Al_2O_3 towards the desired reaction, the low-cost associated with the production of the catalyst has been the reason why alumina-based catalysts are the most widespread in industrial practice.[94] For this reason, the main catalyst used in this thesis was Al_2O_3 although TiO_2 was also explored. Unlike the conventional Claus process utilizing a thermal reactor, the lower temperature conditions of this work do not result in the production of CS_2.[13] With this issue negated, the catalyst choice does not need such rigorous consideration.

Catalysts provide active sites for the adsorption of reactants, and lower activation energy for the transition state of the reaction allowing for increase in reaction rate constants. The potential energy change over the heterogeneous catalysis is shown in the Figure 2-2.

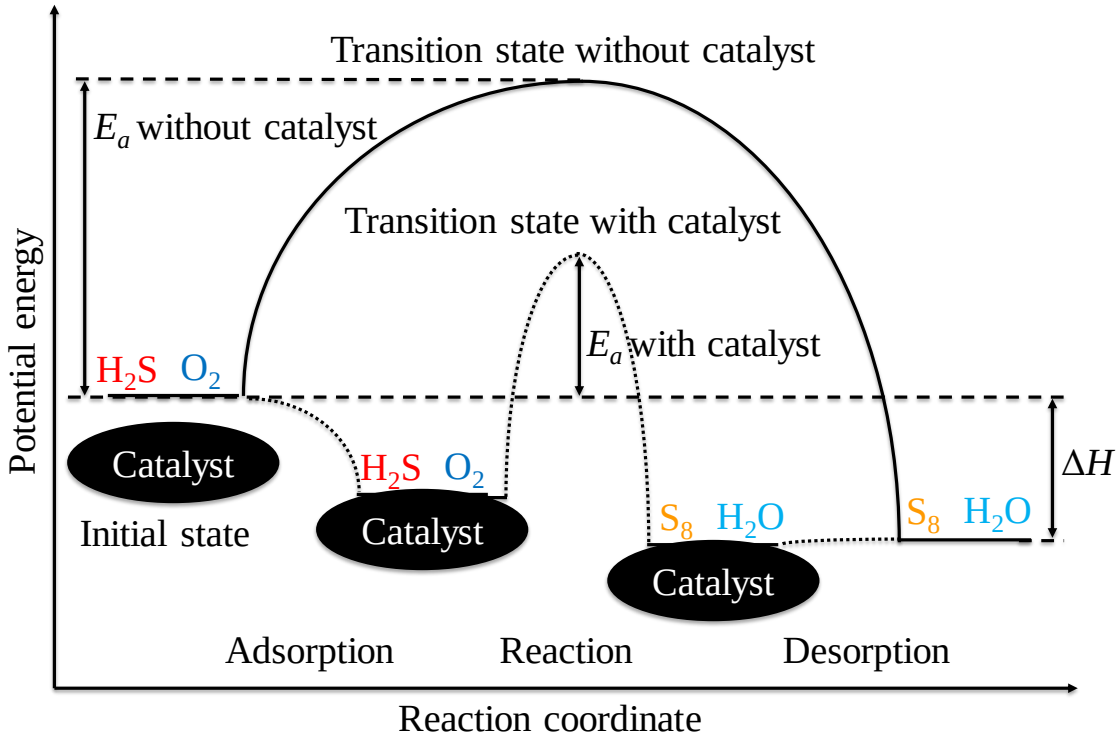

Figure 2-2. Schematic of potential-energy diagram over the heterogeneous catalysis. The black catalyst circles represent the surface-active site.

The activity of a Claus catalyst is directly proportional to the number of accessible surface-active sites, where a higher surface area (m^2/g) leads to a higher mass activity.[95] Condensation of liquid sulfur within the pores of the catalyst is known to decrease the performance of the Claus catalyst by blocking the active sites.[96] This is called catalyst fouling, where the physical deposition of sulfur onto the catalyst resulting in activity loss due to the blocked active sites. Catalyst fouling is detrimental as it causes a reduction in

the reaction rate. Introducing additional meso- and macropores within the catalyst pellets can improve the catalytic performance by increasing the available surface area, enabling sulfur pore condensation in micropores to be less of a detrimental factor in overall catalytic performance.[97] In addition to catalyst deactivation, fouling can cause disintegration of catalyst particles and in extreme cases can plug the catalytic reactor. To decrease catalyst deactivation by sulfur condensation in this work, the catalysts were regenerated by flowing CO_2 through the reactor at 563 K to evaporate the condensed sulfur between experiments.

Heterogeneous catalysis generally proceeds according to the following seven steps.[98] The steps are explained in terms of an H_2S reactant to an S_8 product.

1. External film diffusion. Bulk diffusion of H_2S through the boundary layer (CO_2) surrounding the catalyst particle to the external catalyst surface.
2. Internal pore diffusion. Diffusion of H_2S through the porous network of the catalyst to the catalytic active sites.
3. Adsorption. Adsorption of H_2S onto the catalyst active sites.
4. Reactions. Reactions of H_2S to S_8 on catalytic sites.
5. Desorption. S_8 desorption from the catalytic active site
6. Internal pore diffusion. Diffusion of S_8 through the porous network towards the external catalyst surface.
7. External film diffusion. Bulk diffusion of S_8 from the external catalyst surface through the boundary layer (CO_2) to the bulk gas stream.

Diffusion processes within steps of 1, 2, 6, and 7 have small dependences on temperature ($T^{1/2}$ or $T^{3/2}$) compared to the chemical processes of steps 3, 4, and 5 (also Figure 2-2) which have large temperature dependences with activation energies of 20 – 200 kJ mol^{-1}.[98] The

rates of chemical processes are exponentially dependent on temperature and have relatively large activation energies compared to the diffusional processes at low reaction temperatures. In this case, the chemical steps are the rate-limiting processes as shown in the Figure 2-3.

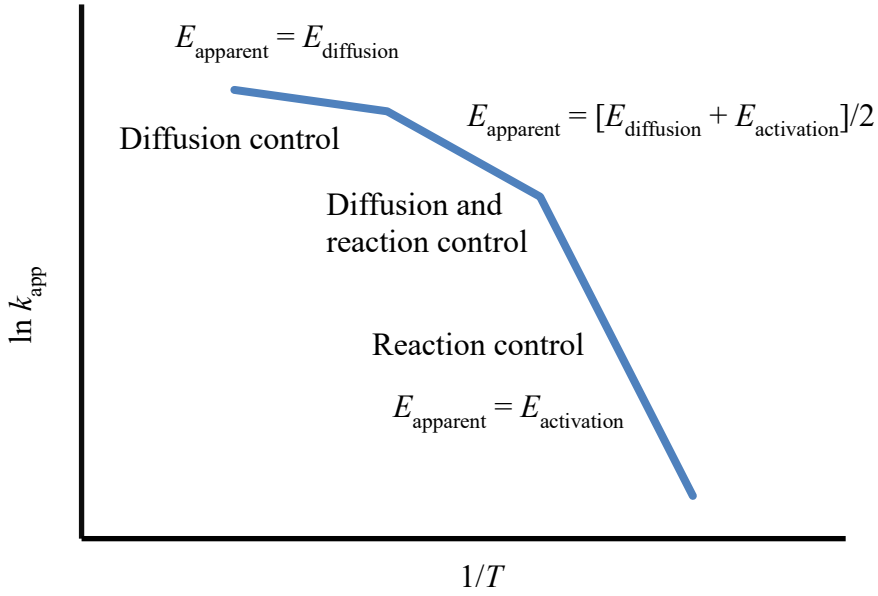

Figure 2-3. Temperature dependence of a typical catalytic reaction in Arrhenius plot form. The slope is $-E_{apparent}/R$. The figure is adapted from Bartholomew and Farrauto.[98]

As the reaction temperature increases, the rates of the chemical steps increase exponentially and the rate limiting process shifts from being chemical to being diffusional. At high reaction temperatures, the chemical reaction is so rapid that reactions occur on the exterior surfaces of the catalyst even before reactants can diffuse into the pores of the catalyst. In this case, diffusion steps with a temperature dependence of only $T^{3/2}$ (E_{act} = 4-8 kJ mol^{-1}) become rate limiting.[98] At intermediate reaction temperatures, both pore diffusion and the surface chemical reactions can influence the rate-limiting process. Therefore, the temperature dependence is an average of the activation energies for both chemical and diffusional steps.[98] These relationships between the rate constants and temperatures are

explained in gas phase reactions.[98] The reaction studied in this work is in high-pressure dense phase CO_2 which may affect the diffusion of reactants towards the catalyst and/or the chemical steps of the reactions.

Two main types of mechanisms for bimolecular surface reactions are the Langmuir-Hinshelwood (LH) and Eley-Rideal (ER) mechanisms.[98] In the LH mechanism, both reactants are adsorbed onto the surface of catalysts before they react with one another. Whereas in the ER mechanism, only one of reactants is adsorbed onto the surface of the catalyst while the other molecule reacts with the adsorbed reactant directly. For the selective oxidation reactions over metal oxide catalysts, the Mars-van Krevelen (MvK) or redox mechanism should also be considered. This mechanism involves steps where the oxidized catalyst surface oxidizes the reactant and then the catalyst surface is re-oxidized by the gas phase oxygen.[99] The involvement of MvK type mechanism can be detected by separating oxidation and reduction steps (swing). The evidence for the MvK type mechanism is when the rates and selectivities of the swing and the continuous catalytic reactions are similar.[100,101] In contrast to MvK, a concerted mechanism occurs when the interaction of oxygen with a catalyst and the formation of the products take place simultaneously in the presence of both reagents only.[94] The evidence of concerted mechanism is when the rates and selectivities of the swing and the continuous catalytic reactions would be different. Davydov *et al*. found that with alumina and titania catalysts, the conversion of reagents in a mixture was approximately three times higher than the conversion of the separated interaction of H_2S or SO_2 with steady-state catalysts.[94] They concluded that on alumina and titania catalysts, the Claus reaction proceeds mainly by the concerted mechanism.[94]

Detailed suggested equilibrium mechanism of H_2S conversion to S_8 is shown in Figure 2-4.[102] The mechanism was based on sulfation on catalysts, which is the formation of sulfur oxyanion intermediate species confirmed by ion chromatography. The direct oxidation of H_2S to S_8 is suggested to be a kinetic mechanism without the formation of sulfur oxyanions.[26] Therefore, the evidence of sulfur oxyanions on catalysts can suggest the equilibrium mechanism reaction instead of the kinetic direct oxidation mechanism.

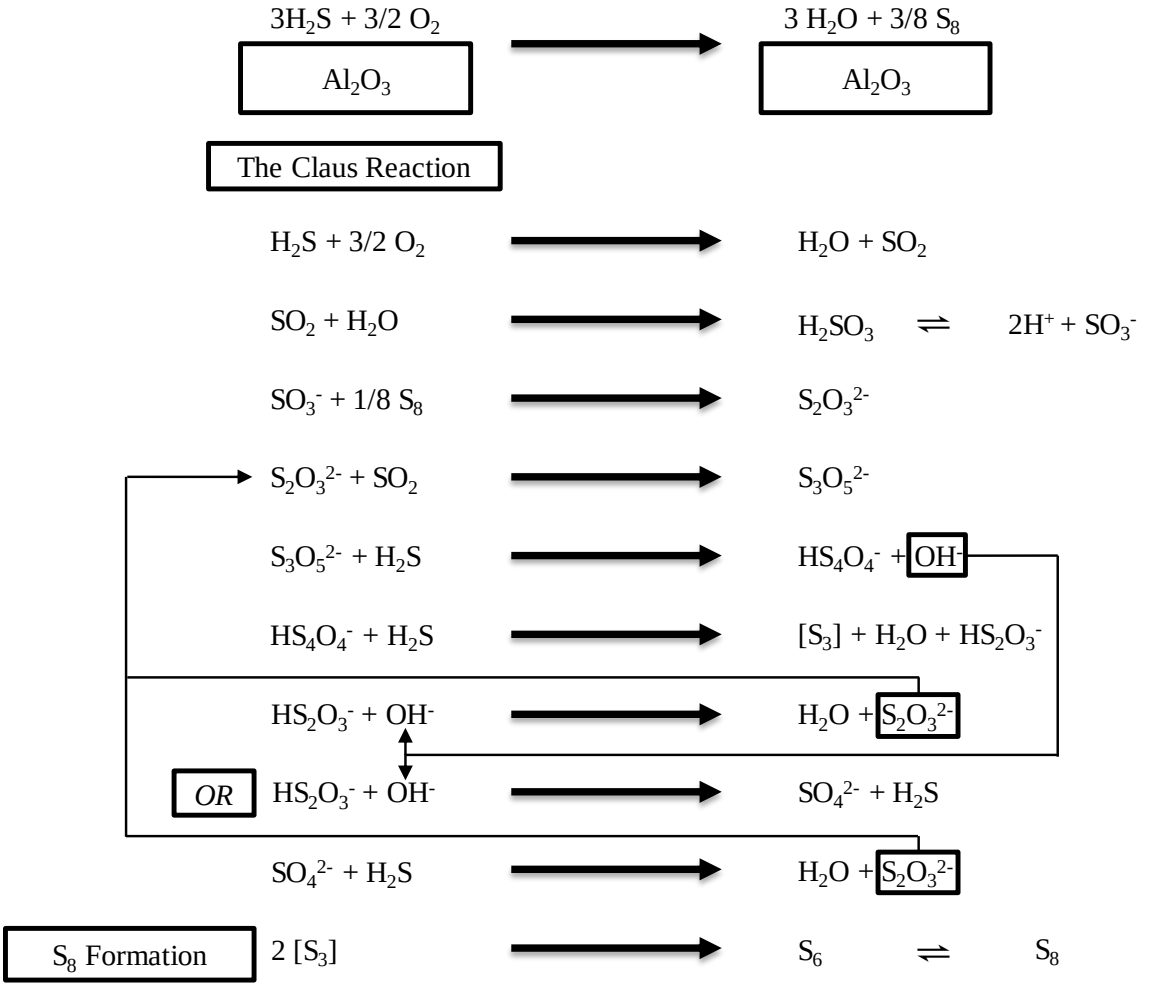

Figure 2-4. Suggested mechanisms of sulfur formation on an alumina catalyst adopted by Clark *et al*.[102]

2.4.1 Laboratory flow reactors for heterogeneous catalysis

For heterogeneous catalysis, a flow through reactor is generally used instead of a batch reactor.[98] In a batch reactor, materials are loaded into a reaction vessel and are well mixed then left to react for a certain period of time. The product mixture is then discharged out of the vessel. Since the composition changes with time, this process is considered an unsteady-state operation.

The flow reactor can also be called a continuous tubular reactor since reagents are pumped through a pipe or tube. The chemical reaction proceeds as the reagents travel through the pipe or tube which contains catalysts.[98] Continuous flow reactors are generally used for industrial catalytic processes, being either fixed-bed or fluidized-bed reactors. As the name may suggest, fixed-bed reactors have catalyst particles fixed with respect to the reactor while fluidized-bed reactors have catalyst particles that move relative to each other and the reactor.[98]

Fluidized-bed reactors generally have very good temperature control which is advantageous for reactions requiring efficient heat transfer, for example, exothermic or endothermic reactions.[98] In addition, fluidized-bed reactors are beneficial for processes with rapid catalyst deactivation due to the ability to continuously regenerate and/or replace spent catalyst without the system being shut-down.[98] On the downside, fluidized-bed reactors may be complex, expensive and high-maintenance.[98] Complications such as formation of large gas bubbles occur in fluid-catalyst contact, which leads to less efficient mass transfer and reaction processes. As a result, only small variations in residence time are possible, which limits possible conversion. Although the ability to continuously

regenerate and/or replace spent catalyst is an advantage, the continuous attrition and loss of catalyst can be extensive and expensive.[98]

Fixed-bed reactors are the most widely used for heterogeneous catalysis due to their flexibility and efficiency while remaining inexpensive and low-maintenance.[98] Fixed-bed reactors allow for a large variation in operating conditions and contact time. They allow for a long residence time which enables near complete reactions to occur. Most importantly, they are the only practical and economical reactor at high-pressures.[98] A fixed-bed catalyst reactor was chosen in this work since the most important criteria was the consideration of high-pressures. A general disadvantage of using fixed-bed reactors is that heat transfer is poor in a large fixed-bed, making temperature control and measurement difficult.[98] This poor heat transfer is less of an issue in this work because the high-pressure CO_2 fluid is about ~ 450 times more dense which requires a much smaller reactor size compared to typical gas reactors. Another disadvantage of fixed-bed reactors is that regeneration or replacement of the catalyst is difficult, requiring complete shut down of the system.[98]

Space velocity is an important variable for continuous flow reactors. Space velocity is the relationship between volumetric flow and reactor volume in a chemical reactor.

Space velocity ($time^{-1}$) = volumetric flow (volume/time) / volume of the reactor (2-8)

For example, with a typical space velocity for a Claus process of 1200 h^{-1}, the volumetric flow per hour equates to 1200 reactor volumes per hour. In other words, the amount of time that reactants spend in a reactor (residence time) is inverse of the space velocity. This is not directly translated at high-pressure due to the reduced volume (increased density), so for this thesis, standard (273.15 K and 0.1 MPa) space velocity is used by conversion

through densities. For the high-pressure vessel, the standard space velocity of 1200 h^{-1} equates to an actual space velocity of 2.67 h^{-1} because the fluid is 450 times denser (563 K and 20 MPa).

2.4.2 Other heterogeneous catalysis processes at higher pressures

Some common heterogeneous catalytic processes that utilize higher pressures include ammonia synthesis and Fischer-Tropsch synthesis.[98] Ammonia is synthesized by a relatively simple reaction at 723-773 K and 30 MPa:[98]

$$3\ H_2 + N_2 \rightleftharpoons 2\ NH_3 \qquad (2\text{-}9)$$

Ammonia synthesis has some similarities to the high-pressure Claus reaction that is being studied in this thesis. Due to the decrease in volume of the products and its high exothermicity, the reaction is thermodynamically favourable at high-pressures and low-temperatures. Modified Fe and Ru are the typical active metals of choice where Fe is 10-20 times more active than Ru.[103]

Fischer-Tropsch synthesis produces liquid hydrocarbons from the synthesis gas, composed of CO and H_2.

$$CO + 3\ H_2 \rightleftharpoons CH_4 + H_2O \qquad (2\text{-}10)$$

$$CO + 2H_2 \rightleftharpoons 1/n\ C_nH_{2n} + H_2O \qquad (2\text{-}11)$$

Equilibrium calculations by Anderson highly favour methane formation (Equation 2-10) over the formation of heavier hydrocarbons (Equation 2-11).[104] Thus, catalysts for Fischer-Tropsch synthesis require careful consideration with high selectivity towards heavier hydrocarbons over methane. Ni catalysts produce methane, while Co, Fe, and Ru catalysts selectively promote the synthesis of heavier hydrocarbons under typical synthesis

conditions (453-543 K and H_2/CO = 1-2).[98] In addition to the catalyst choice, reaction conditions can affect the selectivity shift from C_{2+} hydrocarbons to methane with increasing H_2/CO ratio, increasing reaction temperature, and decreasing pressure.[98] Selective catalysts are also available for the direct oxidation of H_2S to S_8 (SuperClaus as described in Chapter 1). However, this thesis studies the experimental equilibrium conversion and modeling to calculate the theoretical equilibrium conversion, which does not require such a rigorous selection of catalyst as mentioned earlier.

2.4.3 Heterogeneous catalysis of the Claus reaction

Various kinetic expressions have been used by numerous authors and different conclusions were reached regarding to the reaction orders with respect to the reactants.[84-93] The general methods to investigate catalyses between these studies were similar in that initial gaseous components were flowed separately through corresponding thermal conductivity mass flow controllers. The resulting gas mixture then passed through a catalytic reactor that could be temperature controlled. The analysis of the feed and product streams were completed using a GC. Sulfur filter was used to collect the produced sulfur prior to the GC. The methodology of carrying out the high-pressure catalysis in this thesis is similar, however the delivery of the mixture differs by preparing two separate high-pressure mixtures (H_2S/CO_2 and O_2/CO_2) prior to transferring into two separate syringe pumps. These syringe pumps enable flow control of the high-pressure mixtures.

The sulfur collected in the sulfur filter prior to the GC would normally be quantified for mass balance and be compared to the GC results. However, sulfur mass balance was not feasible for this thesis because of the high-pressure conditions and the toxicity of H_2S.

Ensuring a leak-free system was of significant importance and disassembling/reassembling the system between experiments would be time consuming due to the required leak-testing. According to the literature, the H_2S conversion % obtained from GC generally matches well with the collected sulfur mass balance.[92] Therefore, the GC results alone were determined to be sufficient in this work.

The kinetics of the Claus reaction were studied by many over a range of conditions and catalysts. For example, McGregor *et al*. studied above 515 K over commercial bauxite and obtained an activation energy of 31.1 kJ mol^{-1},[84] while Dalla Lana *et al*. studied from T = 483 to 563 K over γ-alumina with the obtained activation energy = 30.7 kJ mol^{-1}.[85] In addition, George studied from T = 523 to 623 K using a cobalt molybdate catalyst with calculated activation energy = 23.0 kJ mol^{-1}.[86] Liu used γ-alumina from T = 473 to 596 K and the activation energy was 30.8 kJ mol^{-1}.[87] Quft *et al*. studied the sulfation of alumina upon Claus activity above 540 K.[88] El Masry explored the effect of forced feed composition cycling on the time-average of the Claus reaction from 463 to 573 K over bauxite and obtained activation energy = 35.1 kJ mol^{-1}.[90] Alternatively, Birkholz *et al*. used T = 400 to 548 K in their modelling of a fluidized bed Claus plant as an alternative to the conventional fixed bed Claus process with the obtained activation energy of 30.8 kJ mol^{-1}.[91] While all of these studies showed the kinetics of the catalytic reaction between H_2S and SO_2, which are the reaction effluents of the thermal reactor in the modified Claus process, they did not study the kinetics between H_2S and O_2. The general kinetic expression derived from aforementioned studies is as follows:

$$-d[H_2S]/dt = \frac{k[H_2S]^a[SO_2]^b}{(1+K_{H_2O}[H_2O])^c} \quad (2\text{-}12)$$

where the coefficient, *a*, is always 1, *b* is mostly ~ 0.5, and *c* is generally 1 or 2. Most expressions were obtained at temperatures above the dewpoint where a couple literature studies specified that involvement of water applies when there is no sulfur deposition onto catalysts from the reaction.[86,88] Water can therefore compete with the reactants for the active sites if reaction conditions are above sulfur dewpoint. However, if reaction conditions involve sulfur deposition onto catalysts, there was no change in reaction rates with and without water (c = 0).[93] Mendioroz *et al*., attributed that the deposited sulfur prevented from water being adsorbed.[93] In these literature cases, the O_2 would have been converted to SO_2 in the thermal reactor and therefore the feed gas entering the catalytic reactors would be H_2S and SO_2. However, for the purpose of entirely catalytic process in this thesis, the feed gas entering the catalytic reactor would be H_2S and O_2. While the reaction between H_2S and SO_2 remains, it is an intermediate step that is not shown in the apparent kinetic expression.

$$-d[H_2S]/dt = k[H_2S]^a[O_2]^b \quad (2\text{-}13)$$

The only relevant literature study to our knowledge that discusses similar reaction between H_2S and O_2 at elevated pressures is the kinetic study by Dowling *et al*., who used pressures up to 6.9 MPa which is comparable to that used in this work at p = 10 to 25 MPa.[92] Their kinetic expression resulted in an overall second order reaction, being first order with respect to both H_2S and O_2. The calculated activation energy was 62.2 ± 8.3 kJ mol^{-1}. They also found a change in the order of H_2S from 1 at lower H_2S partial pressures, to 0 at higher H_2S partial pressures, which was the indication for the reaction proceeding as the ER mechanism. [92,98] The kinetic expression of Dowling *et al*. was adapted for use in this thesis (Chapter 5).

Chapter 3: Solubility of Elemental Sulfur in Dense Phase Carbon Dioxide from T = 324 to 424 K and p = 10 and 20 MPa

This manuscript has been published in the *journal of natural gas and engineering*.

3.1 Introduction

Apart from methane, lean natural gas can contain various concentrations of H_2O, H_2S and CO_2. Many production fluids, such as lean shale gas fluids, contain a low-level of H_2S (< 0.1%) which is accompanied with larger amounts of CO_2 (*ca.* 10%).[2] Both acid gas components (H_2S and CO_2) must be removed from the sales gas because CO_2 has no heating value and H_2S is toxic.[3,4] Removed CO_2 rich fluids can be injected into storage/disposal reservoirs or cleaned up for sale as a secondary value added product for enhanced oil recovery or as a solvent for other green processes.[7] Conversion of the H_2S to elemental sulfur by partial oxidation (sulfur recovery) has the potential to add a third valuable material, which can be sold for sulfuric acid production used in mining and fertiliser production.

Depending on the concentration of H_2S in the acid gas, different separation and recovery techniques can be used.[14] At high-levels of H_2S, one can recover and sell the elemental sulfur (S_8) by oxidation within a Claus process. For these lower-levels of H_2S, the Claus front-end reactor will not sustain a stable acid gas flame and other low-level techniques must be selected, *e.g.*, aqueous redox chemistry or scavenging with non-regenerable solids/liquids.[14,20,105] There are some low-level oxidation processes in various solvents; however, all these processes are aimed at oxidation in non-volatile solvents. Due

to solvent/sulfur reactions, these processes rarely produce marketable sulfur and they are difficult to operate; therefore, sulfur is often landfilled.[106] As CO_2 is relatively inert, recovery in a high-pressure CO_2 stream could lead to higher purity product.

Our current research is aimed at exploring the option to partially oxidize the H_2S to elemental sulfur within the high-pressure CO_2, by addition of stoichiometric O_2. This can be accomplished using a solid catalyst, where the direct oxidation reaction is given by

$$3\ H_2S\ (g) + 3/2\ O_2\ (g) \rightleftharpoons 3\ H_2O\ (g) + 3/8\ S_8\ (g). \qquad (3\text{-}1)$$

Equation 3-1 can also be accomplished in two steps as the modified Claus process, where approximately one-third of the H_2S in the acid gas stream is reacted with oxygen to produce SO_2,

$$H_2S\ (g) + 3/2\ O_2\ (g) \rightleftharpoons H_2O\ (g) + SO_2\ (g), \qquad (3\text{-}2)$$

and the remaining two-thirds of H_2S are then reacted with the SO_2 to give S_8,

$$2\ H_2S\ (g) + SO_2\ (g) \rightleftharpoons 2\ H_2O\ (g) + 3/8\ S_8\ (g). \qquad (3\text{-}3)$$

Regardless of the possible surface mechanism on a given catalyst or final process design, the overall objective of any partial oxidation shown in equation 3-1.

A simplified diagram for a proposed production treatment and recovery was introduced in the Chapter 1, Table 1-3. The catalytic process is aimed at temperatures $T < 523$ K to maximize the sulfur recovery by shifting the equilibrium towards the products, where lower temperatures are more favorable; *i.e.*, the reaction equilibrium is exothermic. If possible, it would be ideal to carry out any catalytic reaction at conditions that are above the sulfur dewpoint (produced sulfur below the solubility limit) in order to prevent deactivation of the catalyst by sulfur deposition. Before exploring this region, we required

the sulfur solubility in dense phase CO_2. Note that this exploration of the phase behavior is necessary before designing any oxidation process in CO_2.[7]

There are limited data available in the literature for elemental sulfur solubility in pure CO_2 and there were no solubility data for $T > 393$ K.[79-81] This paucity in data is due to the fact that previous experiments were carried out for flow assurance studies, where the coldest temperature in the production stream is more important.[92] In this work, the solubilities of elemental sulfur in dense phase CO_2 were measured from T = 323.75 to 424.05 K and at p = 10 and 20 MPa. Two thermodynamic models were calibrated with the experimental solubility data, (i) a previous Virial Equation Model and (ii) a new Fluctuation Solution Theory correlation. While both can be used to calculate sulfur solubility, the Fluctuation Solution Theory correlation provides a more physically reasonable extrapolation for the lower temperatures and higher pressures.

3.2 Experimental

3.2.1 Materials

The sources, purities and pre-experiment analyses of chemicals used in this study are reported in Table 3-1. Air prilled sulfur was obtained from Keyera Energy, Strachan, Alberta (2012). The purity was reported previously by Sofekun *et al*., (99.992%).[43] High-purity CO_2 (Laser Grade 99.9995%) and helium (Ultra High Purity Grade 99.999%) were obtained from Praxair. Analytic reagent grade carbon disulfide (CS_2) was obtained from EMD. All chemicals including xylene (99.3% Anachemia), triphenyl phosphine (TPP, 99% Alfa Aesar) and triphenyl phosphate ($TPPO_4$, 98% Eastman) were used without further purification.

Table 3-1. Purity of chemicals used in this study, chemical supplier, and the analysis procedure used for verification.

Chemical Name	Source	Analysis Method	Purity / mol %
carbon dioxide	Praxair Inc.	GC-TCD/FID/SCD	≥99.9995
carbon disulfide	Sigma Aldrich	GC-TCD/FID/SCD	≥99.9
sulfur	Keyera	see reference 15	99.992
triphenyl phosphine	Alfa Aesar	GC-TCD/FID/SCD	99
triphenyl phosphate	Eastman	as received	98
xylene	Anachemia	as received	99.3

3.2.2 Solubility apparatus

For solubility studies, a custom flow-through bed saturator was built as shown in Figure 3-1. A Teledyne Isco 260D syringe pump was used to maintain constant pressure between in a 50 cm^3, SS-316, vessel packed with *ca.* 45 g sulfur prill, *i.e.*, the pump supplied more CO_2 as samples were removed from the outlet. The sulfur packed vessel was placed in a Hewlett Packard 5890 Series GC oven, which maintained temperatures to within 0.01 °C. A high-precision pressure transducer, Keller series PA-33X with a reported full-scale accuracy of 0.004% at 100 MPa, was used to measure the pressure of the vessel. The pressure transducer was calibrated from 5 to 25 MPa using a Pressurements Limited T3800/4 deadweight tester, where the average drift and precision was found to be within 0.00076 MPa. The temperature of the system was measured by a 100-ohm, four-wire platinum resistance thermometer connected to a Pico Technology PT-104 USB data logger, previously calibrated according to the International Temperature Scale of 1990.[107] Data collection was completed using LabVIEW software, which also allowed for apparatus control *via* a single control module (Appendix, A3).[108]

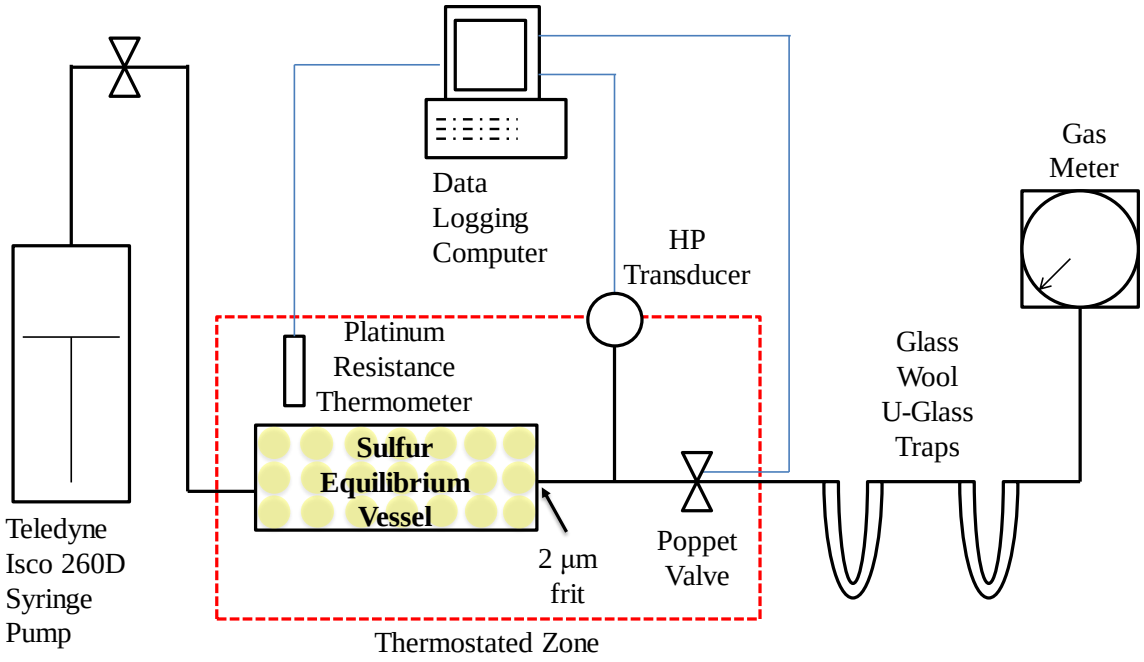

Figure 3-1. Schematic of in-house built sulfur solubility measurement apparatus.

3.2.3 Procedure

The sulfur equilibrium vessel was loaded with *ca.* 45 g of sulfur and the oven was set to the desired temperature. CO_2 was then introduced into the vessel at the desired pressure using the syringe pump and the vessel was left for 48 hours to equilibrate. After this time, the sulfur saturated CO_2 fluid was slowly released to ambient pressure and temperature using a VICI on/off poppet valve (Valco Instruments Co. Inc.), which was set to open for very short intervals (0.03 seconds) every 6 minutes. Upstream of the valve there was a 0.2 µm filter to prevent any particulate non-dissolved sulfur from exiting the vessel. The released fluid, now at ambient pressure, flowed through two glass-wool *u*-traps before reaching a diaphragm dry-gas flow meter (Singer 802), for measuring the net discharged CO_2. Sulfur has very low-vapor pressure; therefore, it was assumed that all the dissolved sulfur was deposited in the outlet of the valve and in the glass-wool traps upon expansion

of the released CO_2 fluid and cooling at room temperature. Analytical results verified that the final trap had negligible captured sulfur. After 48 to 60 hours of releasing sulfur saturated CO_2, the outlet of the poppet valve, the transfer lines and the traps were washed with CS_2 to dissolve any deposited S_8. The CS_2 wash was evaporated and the residue was re-dissolved in a xylene-triphenyl phosphine solution where S_8 reacted with TPP to form TPPS.[82] The diluted solution was then analyzed using a GC equipped with a pulsed flame photometric detector (PFPD) in phosphorus mode to quantify the total deposited sulfur.[83] The amount of sulfur was related to the net volume of CO_2 that had exited the saturation vessel to give the solubility of S_8 in CO_2.

The analysis of deposited sulfur was completed on a Varian CP-3800 GC/PFPD and a Rxi-5ms Restek column (fused silica capillary, 15 m x 0.32 mm i.d., 1.0µm film thickness). All analyses used helium as the carrier gas at a column flow rate of 6 mL min^{-1}, with a 20 mL min^{-1} detector makeup. The injector and detector temperatures were set at 553 and 573 K respectively, and the column was operated isothermally at 523 K. The solvent for the GC analysis was prepared by dissolving 5.0 g of TPP and 1.0 g of $TPPO_4$ as an internal standard in 1 L xylene.

3.3 Results and discussion

3.3.1 Elemental sulfur solubility in carbon dioxide

Sulfur solubilities in CO_2 were measured at pressures of p = 10.12 and 20.12 MPa and temperatures between T = 323.75 to 424.05 K. The solubility data for this work are reported as grams of sulfur per standard ($T_{standard}$ = 273.15 K and $p_{standard}$ = 0.1 MPa) cubic meter of CO_2 (g Sm^{-3}) in Table 3-2 and mole fraction, x. Each condition was measured two

or more times to verify that there was no volumetric or kinetic uptake effect, *i.e.*, different accumulation times were used. The uncertainties are reported as the standard deviation, where the pressure and temperature drift during the course of the experiments were larger than the measurement reported precision in the experimental section.

Table 3-2. Average experimental solubilities of elemental sulfur in carbon dioxide.

^{a}T / K	^{a}p / MPa	n	g / Sm^{-3}	u / g Sm^{-3}	x	u(x)
323.75	10.12	3	0.014	0.002	0.0000013	0.0000001
323.75	20.12	5	0.124	0.030	0.0000108	0.0000026
348.95	10.12	2	0.014	0.002	0.0000012	0.0000002
348.95	20.12	2	0.211	0.007	0.0000184	0.0000006
374.15	20.12	3	0.281	0.028	0.0000246	0.0000025
424.05	10.12	4	0.254	0.027	0.0000222	0.0000023
424.05	20.12	4	0.795	0.030	0.0000695	0.0000026

[a] Standard deviation in u are $u(T)$ = 0.01 K, $u(p)$ = 0.04 MPa; n is the number of experiments performed; (g Sm^{-3}) denotes grams of sulfur per standard cubic meter of CO_2 (g Sm^{-3}) ($T_{standard}$ = 273.15 K).

In this region of the phase diagram (much larger pressures than the sulfur vapour pressure), the experimental results indicate that the solubility of sulfur increases with pressure and temperature. The effect of pressure on sulfur solubility can be explained by the increase of the CO_2 fluid density, whereby dense CO_2 fluid is a more effective sulfur solvent due to the increased intermolecular interactions. The opposite effect of pressure is expected at lower pressures near the sulfur vapour pressure, where the pressure dependence is dominated by Raoultian ideality. The effect of temperature on sulfur solubility at any pressure is due to the sulfur vapor pressure increase.

The experimental solubility data along with literature values are shown in Figure 3-2 in addition to the Virial Equation based solubility model of Dowling *et al.*[92] The new experimental data appear to be consistent with literature data from Serin *et al.*[79] While the

experimental temperatures do not match Serin *et al*., those literature data at T = 333.2 and 363.2 K are aligned between the experimental data at T = 323.2 and 373.2 K. The solubility of sulfur in pure CO_2 from other reports are less consistent,[80,81] which has been previously recognized by Dowling *et al*.,[92] and Serin *et al*.[79] The solubilities calculated using the existing model by Dowling *et al*.,[92] are consistently lower than the experimental data for p > 15 MPa. These deviations are likely a result of the model being calibrated for sour gases; therefore, a fit-for-purpose model was calibrated for pure CO_2 for more accurate solubility calculations.

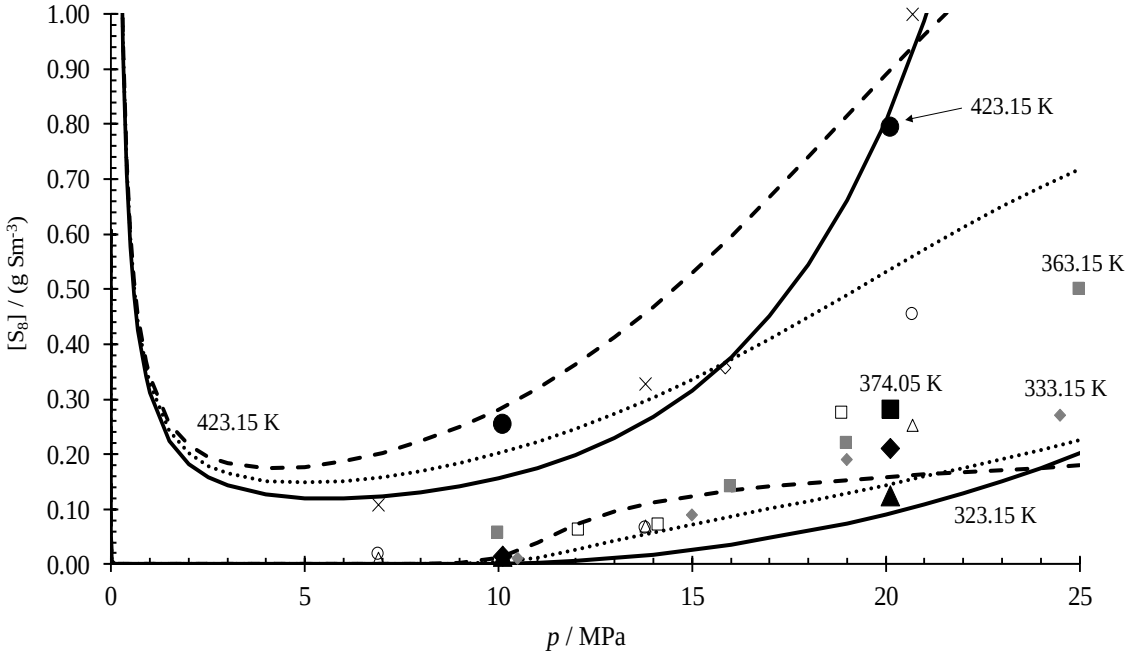

Figure 3-2. Sulfur solubility in CO_2 up to p = 25 MPa and 323.15 K < T < 424.15 K. This study: (●), 424.05 K; (■), 374.05 K; (◆), 348.95 K; (▲), 323.75 K. Serin *et al*. 2010: (◆), 333.15 K; (■), 363.15 K. *Gu et al*. 1993: (□), 363.2 K; (◇), 383.2 K. *Kennedy et al*. 1960: (△), 338.71 K; (○), 366.48 K; (×), 394.26 K. Models: *Dowling et al*. 2012: ••••••••, recalibrated virial model, Equation 3-6;--------, Fluctuation Solution Theory correlation, Equation 3-9; ———. Two example sulfur solubilities were calculated using models at 325.15 K and 423.15 K.

For both models investigated in this work we have used the equality of fugacity for pure S_8 and S_8 in CO_2, which can be calculated using the fugacity coefficient at the infinite dilution limit, ϕ_1^∞

$$\phi_1^\infty = \frac{f_1^{\alpha,\beta \text{ or } \lambda}}{y_1 p}, \tag{3-4}$$

where y_1 is the mole fraction of S_8 in CO_2, $f_1^{\alpha,\beta \text{ or } \lambda}$ is the fugacity of the dense phase elemental sulfur and p is the total pressure. The fugacity of pure elemental sulfur has been calculated from the equations of Marriott and Wan. For the fugacity coefficient for elemental sulfur, two models were examined: (i) a recalibration of the Virial model of Dowling *et al*.[92] and (ii) a Fluctuation Solution Theory correlation reported by O'Connell *et al*.[109]

3.3.2 Virial model

The volume explicit virial equation expresses the deviation of the properties of a real gas from the ideal gas law equation as an infinite power series in reciprocal volume (or density). The virial equation yields relatively simple expressions for computing fugacity coefficients as a function of temperature, pressure and composition; however, it normally requires many coefficients for extension into the high-pressure dense-phase region. The virial model used previously by Dowling *et al*.[92] was based on the volume explicit virial equation for infinite dilution fugacity, where the solvent volume was calculated using the dimensionless Helmholtz energy equations compiled by the National Institute of Standards and Technology (NIST).[58] Using the virial equation, the fugacity coefficients for sulfur in a high-pressure fluid is calculated by

$$\ln Z\phi_1 = 2\rho\sum_i y_i B_{1i} + \frac{3}{2}\rho^2\sum_i\sum_j y_i y_j C_{1ij} + \mathrm{K}\ , \qquad (3\text{-}5)$$

where ρ is the molar density of the fluid mixture and Z is the compressibility factor. B_{1i} and C_{1ij} are the second and third virial coefficients, respectively. It is likely that the final fitted virial coefficients for S_8 compensates for a portion of the allotropic chemical equilibria.

Dowling *et al.*,[92] expanded equation 3-5 for two components (S_8(1) and CO_2(2)) and truncated at the third virial coefficient. At the infinite dilution limit, all components with terms y_1 are assumed to be insignificant (*i.e.*, fugacity coefficient is calculated at the infinite dilution limit, therefore $y_1 = 0$), which provides the following simplification for calculation of the fugacity coefficient:

$$\ln \phi_1^{\infty} = 2y_2 B_{12}\rho + \frac{3}{2}y_2^2 C_{122}\rho^2 - \ln Z\,. \qquad (3\text{-}6)$$

This simplification for the solubility of solids in compressed gas phases has been described by Quiram *et al.*,[110] who recognized that the truncated virial equation alone is not rigorous at high-pressure or in high-density regions. To improve the calculation, the model was implemented using the Span and Wagner equations-of-state to calculate the densities and compressibility factors for the high-pressure CO_2. Here a virial correlation is improved considerably by using high-accuracy densities.[92] The equilibrium condition at sulfur saturation is

$$y_1 = f_1^{\alpha,\beta \text{ or } \lambda} \Big/ p\exp\left[2y_2 B_{12}\rho + \frac{3}{2}y_2^2 C_{122}\rho^2 - \ln Z\right]. \qquad (3\text{-}7)$$

Both data from Table 3-2 and those of Serin *et al.*[79] were used for fitting Equation 3-7, using least square regression with the logarithmic form of Equation 3-7. The best-sub-set found contained the second virial coefficient as a temperature dependent function:

$$B_{12} = a_{12} + \frac{b_{12}}{T}, \tag{3-8}$$

[$a_{12} = (3.88 \pm 0.79)\times10^{-4}$ m^3 mol^{-1}, $b_{12} = -0.324 \pm 0.031$ m^3 K mol^{-1}, $C_{122} = (2.32 \pm 0.19)\times10^{-8}$ m^6 mol^{-2}; all uncertainties shown at 95% confidence]. The sum squared error (SSE) improved from 0.183 to 0.092 when compared to the virial coefficients of Dowling *et al.*,[92] and the coefficient of determination (R^2) increased by a small amount (0.88 versus 0.89); see Table 3-3.

Table 3-3. Sum of squared errors and coefficients of determination between experimental [S_8] and calculated values using different models.

	Dowling *et al.* [92]	**Virial**	**FST**
SSE	0.183	0.092	0.078
R^2	0.88	0.89	0.95

The important disadvantage that the truncated virial equation has is its inapplicability at high-densities. The virial equation is frequently not useful at densities greater than 50% of the critical density.[111] Although the virial equation follows the Raoultian ideality at higher temperature and lower pressure, there is still limitation when it comes to dense, low-temperature fluids where intermolecular forces are strong. If the gas density exceeds the truncated virial equation limit, empirical equations of state are mostly used to relate the fugacity.[111] A substantial improvement over the truncated virial equation was found using the Fluctuation Solution Theory correlation, which does not require truncation like the Virial equation.

3.3.3 Fluctuation Solution Theory

The generalized Krichevskii parameter, defined through Fluctuation Solution Theory, has proven to provide a good correlation for the partial molar volumes of several neutral aqueous solutes and solvent properties, including aqueous CO_2.[112] Similar to sulfur in CO_2, the equation of O'Connell *et al.*,[112] was recently found to be a good function for the molar volumes of water in CO_2 by Deering *et al.*[113] Using this approach, infinite dilution fugacity coefficient for a sulfur solute is provided by Equation 3-9:

$$\ln(\phi_1^{\infty} / \phi_2^{o}) = (a-b)/\bar{V}_2^{o} + b[\exp(c/\bar{V}_2^{o}) - 1]/c \qquad (3\text{-}9)$$

where ϕ_1^{∞} is the fugacity coefficient for S_8 at infinite dilution, ϕ_2^{0} is the fugacity coefficient for pure CO_2, and *a*, *b*, *c* are fitting coefficients. The molar volume of pure CO_2, $\bar{V}_2^{o}$, was calculated using the Span and Wagner equation-of-state.[57] As pointed out by O'Connell *et al.*,[112] as well as Deering *et al.*,[113] Equation 3-9 has a minimum number of empirical parameters, where three fitting coefficients is equivalent to the truncated virial equation used previously. The equation is theoretically justified, representing the ideal gas properly at high *T* and low *p* and the departure from ideality with the second cross virial coefficient. Also, the equation behaves well near the supercritical point. The resulting curves indicate that Equation 3-9 would represent the proper behaviour of real fluid with proper limits at the both ends of densities. If using a virial equation, such curves can only be theoretically obtained by containing infinite number of parameters. In this case, the fugacity coefficients were calculated from the experimental solubilities and then used to optimise *a*, *b* and *c* by minimization of a sum-squared-error objective function. Again, the parameters (*a* = -384.581 $cm^3\ mol^{-1}$, *b* = 10684.072 $cm^3\ mol^{-1}$ and *c* = -1.498 $cm^3\ mol^{-1}$) were fitted using only the solubilities measured within this study and Serin *et al.*[79] Based on the fitted

parameters of Equation 3-9, the sulfur saturation diagram for several concentration limits has been shown in Figure 3-3. Note that the steep increase in the saturation solubility lines at the lower temperature and higher pressure is where the truncated virial equation is limited. In fact, several cubic equations of state also fail to correctly describe this high-pressure region.

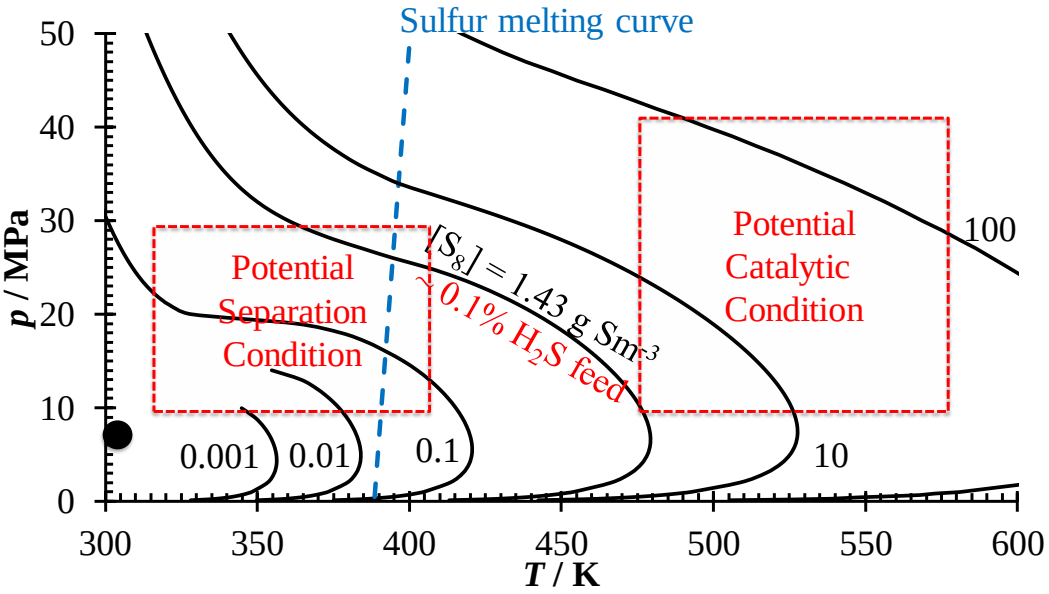

Figure 3-3. Sulfur saturation diagram for CO_2 using FST from 0 to 50 MPa and 300 to 600 K. Each solid black line represents the vapor – liquid (if to the right of sulfur melting curve) or vapor – solid (if to the left of sulfur melting curve) equilibria at labeled sulfur solubility. The blue dotted line is sulfur melting points at temperatures and pressures.

Because the Fluctuation Solution Theory correlation results in the more accurate calculation than the virial model in the high-pressure region, it was used to assess the viability of a non-sub-dewpoint oxidation process. The catalytic conditions were initially considered for T < 523 K for practical process temperatures and to achieve the highest conversion at the equilibrium limit. The solubility limit of 1.432 g Sm^{-3} is shown to fall within the considered process conditions, which, at full conversion, only represents a fluid limited to [H_2S] < 0.1 mol%. Thus, any fluid with [H_2S] > 0.1 mol%, will generate

depositable sulfur and catalytic conversion would result in a sub dewpoint process with intermittent catalysis conversion. Note that our target fluid was for the conversion of 1% H_2S in CO_2.

The model shows that a non-sub-dewpoint processes may be possible at a higher temperature than initially considered. However, increasing T will decrease the total possible conversion of H_2S to S_8. Increasing temperature to a point where the catalytic condition is above the expected sulfur dewpoint, but still low enough for a sufficient conversion of H_2S, will be the focus of this project in association with experimental catalysis. It should be noted that the fugacity coefficients for elemental sulfur, as calculated using Equation 3-9, are to be used in future Gibbs Energy Minimization studies to explore any significant improvement in reaction equilibria. Future studies will need to find temperature ranges that work for different inlet H_2S concentrations as well as the catalytic efficiency under the effect of feed fluid impurities.

Another highlighted area on the Figure 3-3 are the potential separation conditions to deposit elemental sulfur out of CO_2 stream after conversion. When the temperature and/or pressure is reduced below a certain sulfur solubility, most of elemental sulfur should saturate out of CO_2 stream, while maintaining CO_2 in a liquid/supercritical form.

3.4 Conclusion

The elemental sulfur solubilities in supercritical CO_2 were measured from T = 323.75 to 424.05 K at p = 10 and 20 MPa. The solubility increased with increasing temperature and pressure following the sulfur vapour pressure and the CO_2 solvent density changes. Both a truncated Virial equation and a Fluctuation Solution Theory equation were

optimized with experimental solubilities of elemental sulfur using three fitting coefficients. The results showed that the Fluctuation Solution Theory correlation provides a better description of the solubilities and a more physically realistic extrapolation to higher density CO_2 (higher pressure and lower temperature).

In the context of a low-H_2S sulfur recovery process, the Fluctuation Solution Theory correlation showed that it may be possible to oxidize a stream with less that 0.1% H_2S in CO_2 while remaining as a single phase. However, the target stream for our process was 1% H_2S, where 85% of the produced sulfur product was calculated to deposit on the catalyst surface. Finally, we note that fugacity coefficients which can be calculated from this work and used within Gibbs Free Energy minimization routines when simulating equilibrium limits at high-pressures.[114]

Chapter 4: Experimental High-pressure Hydrogen Sulfide Partial Oxidation and Equilibrium Calculation by Gibbs Energy Minimization

This manuscript has been published in the *Industrial & Engineering Chemistry Research*.

4.1 Introduction

A significant amount of geological natural gas sources contains small quantities of acid gas species (H_2S and CO_2). One example of this would be from the Horn River shale gas play in northeast British Columbia, Canada, where produced gas can contain up to 10% CO_2 and 0.1% H_2S.[1,2] Because of the low-heating value of CO_2, the toxicity of H_2S,[3,4] and the corrosion potential of both species, these acid gas components must be removed before the sales gas is transported to consumers. For many conventional natural gas sources, this removal (treatment) is most often completed using aqueous alkanolamines to preferentially absorb the acid gases from the high-pressure production stream and discharge the separated acid gas at a low-pressure during solvent regeneration. The H_2S in the low-pressure acid gas discharge is often then converted to S_8 through partial oxidation:

$$3\ H_2S\ (g) + 3/2\ O_2\ (g) \rightleftharpoons 3\ H_2O\ (g) + 3/8\ S_8\ (g). \quad (4\text{-}1)$$

Industrially, this is typically achieved through the modified Claus process, which utilizes a thermal stage (Equation 4-2) and several lower temperature catalytic stages (Equation 4-3) which help overcome thermodynamic equilibrium limitations. Claus produced S_8 is then marketed for many industrial purposes, including, predominantly for sulfuric acid production within the phosphate fertilizer and mining industry.

$$H_2S\,(g) + 3/2\,O_2\,(g) \longrightarrow H_2O\,(g) + SO_2\,(g) \quad (4\text{-}2)$$

$$2\,H_2S\,(g) + SO_2\,(g) \rightleftharpoons 2\,H_2O\,(g) + 3/n\,S_n\,(g) \quad (4\text{-}3)$$

For low-quality acid gas mixtures, such as that from a shale gas, the low-concentration of H_2S in the acid gas mixture causes the acid gas to be less flammable and not sufficiently combustible to sustain a stable flame in the thermal stage of a Claus plant; therefore, low-sulfur recovery processes with only catalytic stage(s) are used. The majority of low-level sulfur recovery processes do not directly produce a sulfur of sufficient purity for many consumers; therefore, the S_8 is less marketable.

As an alternative to S_8 recovery, acid gases can be compressed for disposal by sub-surface injection or for transportation of a purified and salable CO_2 stream. Due to the high cost of recompression for CO_2, low-pressure alkanolamine discharge of a low-quality acid gas may not be the most efficient choice. Unlike the conventional aqueous alkanolamine separation processes, cryogenic separation of acid gases from raw natural gas sources results in a high-pressure dense phase fluid, which requires little or no compression before transportation.[9-11] While cryogenic separation of acid gas provides the energetic advantage of preserving high-pressure dense fluid, there is no current technology to convert H_2S to S_8 in high-pressure CO_2.

Converting H_2S to S_8 within high-pressure CO_2 would be beneficial to eliminate the post-recovery compression of CO_2 and to form high-quality, marketable S_8 and CO_2 simultaneously. Due to an expectation of lower sulfur dewpoints at elevated pressures, heterogeneous catalytic conversion of H_2S to S_8 (or an initial mixture of S_x species) can be achieved at lower temperatures compared to atmospheric processes, which is advantageous from an equilibrium perspective, as the reactions are exothermic. Alternatively, a sub-

dewpoint catalytic process is still expected to favour S_8 recovery at higher pressure through the reduction in volatile species, see Equation 4-1. In this context, elemental sulfur dewpoints in high-pressure CO_2 were studied previously to provide an initial guideline for testing conditions.[12] Downstream separation of S_8 and CO_2 may be achievable through further temperature reduction to below the sulfur dewpoint. The separated supercritical CO_2 fluid can become a marketable product for enhanced oil recovery or as a solvent for several green processes.[6,7]

Previous thermodynamic modelling efforts for S_8 dissolved in CO_2 resulted in correlations for the high-pressure fugacity of S_8, which can be used within Gibbs Free Energy minimization routines to calculate overall reaction equilibria at elevated pressure.[12,114] This study reports calculations using a modified high-pressure Gibbs Free Energy minimization routine, which are compared to experimentally measured sulfur recoveries from low-level H_2S in CO_2 fluids. Experimental equilibrium recoveries were obtained by flowing high-pressure H_2S + CO_2 and O_2 + CO_2 fluids across γ-alumina or titania beds at velocities from 3800 to 9300 h^{-1}, T = 493.15 to 563.15 K and p = 10 & 20 MPa (0.5 to 1.7 % H_2S and 0.25 to 0.85 % O_2).

4.2 Methods

Safety note. The experiments described here involved toxic H_2S. The experimental bay is equipped with two Honeywell E3Point H_2S detectors and a KOH caustic scrubbing system is used for treating reaction effluent before entering the building exhaust system. The detectors are set to alarm at 5 ppm H_2S (local) and 15 ppm H_2S (facility wide), where the low-level alarm is one half of the eight-hour time weighted average exposure limit in

Alberta (in accordance with the University of Calgary's H_2S Code of Practice standard).[115,116]

4.2.1 Materials

The sources, purities and pre-experiment analyses of chemicals used in this study are reported in Table 4-1. All chemicals were used without further purification but were verified by gas chromatography.

Table 4-1. Purity of chemicals used in this study, chemical supplier, and the analysis procedure used for verification.

Chemical Name	Source	Purification Method	Analysis Method	Purity / mol %
Carbon dioxide	Praxair Inc.	Used at specification	GC-TCD/FID/SCD	≥ 99.9995
Hydrogen sulfide	Linde	Used at specification	GC-TCD/FID/SCD	≥ 99.9
Oxygen	Praxair Inc.	Used at specification	GC-TCD/FID	≥ 99.993
Helium	Praxair Inc.	Used at specification	GC-TCD/FID	≥ 99.999
Compressed Air	Praxair Inc.	Used at specification		Breathing grade

4.2.2 Mixture preparation

Feed mixtures were made gravimetrically in 500 mL SS316 vessels using a high-precision (Mettler Toledo XP26003L) mass comparator with a calibrated accuracy at ±0.001 g. Either H_2S or O_2 was first introduced into an evacuated vessel and CO_2 was then added using an SFT-10 Supercritical Fluid Pump. While gravimetric concentrations were used throughout the experiments, the mole fraction of both mixtures also was confirmed by gas chromatography. The results of one example are summarized in Table 4-2. Both H_2S/CO_2 and O_2/CO_2 mixtures were equilibrated for a minimum of two weeks before GC

measurement. Note that the temperatures and pressures of the sample vessel, the transfer lines, as well as the syringe pumps were always maintained above the two-phase region of the mixtures to prevent a composition change. Table 4-2 also shows the concentration after transfer to the reactor inlet pumps (bypassing the catalytic bed) to ensure that the mixtures have not partitioned during transfer from the synthetic vessels.

Table 4-2. Example mixture of 0.49 % H_2S in CO_2 and 0.24 % O_2 in CO_2.

Solutes	*x* / % by mass	*x* / % by GC/TCD	*x* / % (bypass) by GC/TCD
H_2S	0.4919 ± 0.0012	0.4952 ± 0.0261	0.4921 ± 0.0253
O_2	0.2445 ± 0.0006	0.2446 ± 0.0093	0.2267 ± 0.0108

x (bypass) refers to the GC determined concentration of the fluid bypassing the catalytic bed and verifies that the fluids within the experimental set-up have not changed during transfer from the synthetic mixture vessels. For this example, the fluids are bypassing the catalytic bed at 553.15 K and 20.12 MPa. Verification was performed for every condition measured.

4.2.3 High-pressure oxidation apparatus

For high-pressure heterogeneous catalysis, a custom fixed-bed reactor was built, and the schematic is shown in Figure 4-1. Two Teledyne Isco 260D syringe pumps were used to maintain constant flow of H_2S/CO_2 and O_2/CO_2 mixtures. The ~ 0.5 mL reactor (3 mm i.d.) was packed with ~ 0.5 g of catalyst (crushed and sieved with 50 and 80 mesh) to have a minimum of 10 catalyst particles across the reator diameter. The catalyst filled reactor was placed in a Hewlett Packard 5890 Series Gas Chromatography oven, which maintained temperatures to within ±0.01 K. A high-precision pressure transducer, Keller series PA-33X with a reported full-scale accuracy of 0.004% at 100 MPa, was used to measure the system pressure. The pressure transducer was calibrated from 5 to 25 MPa using a Pressurements Limited T3800/4 deadweight tester, where the average drift and precision was found to be within 0.00076 MPa. The temperature of the system was

measured by 100-ohm, four-wire platinum resistance thermometers connected to a Pico Technology PT-104 USB data logger, previously calibrated according to the International Temperature Scale of 1990.[107] Data collection was completed using LabVIEW software,[108] which also allowed for apparatus control *via* a single control module. The calibration and response factor of GC can be found in the Appendix (A4).

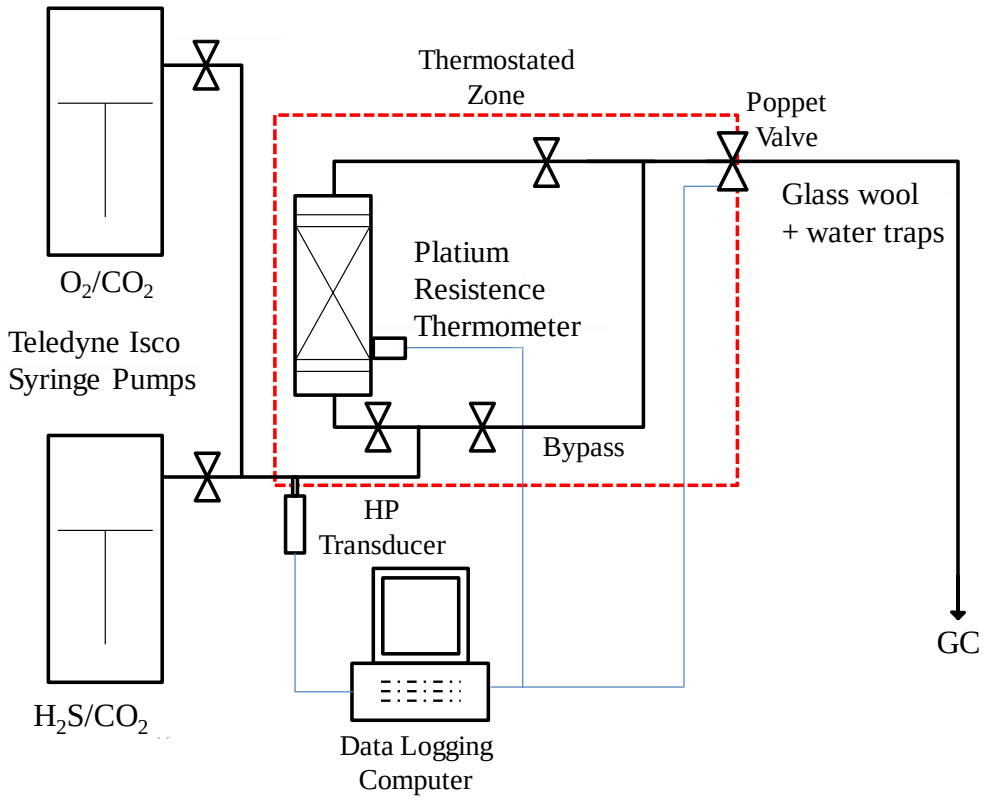

Figure 4-1. Schematic of high-pressure heterogeneous catalytic H_2S partial oxidation apparatus.

4.2.4 Procedure

The initial mixtures of H_2S/CO_2 and O_2/CO_2 were flown through a bypass to a GC equipped with a TCD for the verification of H_2S and O_2 concentrations. Here standard space velocity was calculated using the flow rates from the syringe pumps and equations of state described in the GEM minimization section. After the verification and adjustment

of H_2S and O_2 concentrations to a 2:1 ratio, the fluids were directed through the catalytic bed, *i.e.*, there was no reaction when bypassing the catalyst. At this point, the syringe pumps were pushing the mixtures through the bed with standard (273.15 K and 0.01 MPa) space velocity (SV) higher than 3800 h^{-1}. When the pressure of the system reached a set point, a VICI on/off poppet valve (Valco Instruments Co. Inc.) would open and close automatically to release a small volume element of the system, as well as to send a gas sample towards the GC. At the exit of the poppet valve, the gas passed through glass wool traps and a phosphorus pentoxide (P_2O_5) trap prior to the GC to knock out the produced elemental sulfur and water, respectively. The analysis of reaction effluents was completed on a Bruker 450-GC Gas Chromatograph with an Agilent GS-GasPro column (bonded porous layer open tubular, 30 m x 0.32 mm i.d.). All analyses used helium as the carrier gas at a column flow rate of 2 mL min^{-1}, with a 14 mL min^{-1} detector makeup. The detector temperature was set at 423.15 K, and the column was operated initially at 313.15 K for 5 minutes, after which the temperature was increased to 463.15 K at 20 K min^{-1} rate, then held at that temperature for 4.5 minutes. While sulfur product for multiple tests was recovered at the outlet of the valve for analysis of purity, a quantitative recovery for mass balance during each test was not feasible.

4.2.5 Carbon content in sulfur analysis

To measure the total carbon content in the produced elemental sulfur, 100 mg of the produced sulfur sample was fully combusted in a quartz ampoule charged with 0.1 MPa O_2. The combustion of the sulfur was completed in a tube furnace (Thermolyne Model 21100) at 1073 K. The Chromatographic analysis for CO_2 was carried out using an SRI

8610 gas chromatograph with a GOW-MAC model 952 thermal conductivity detector to determine the CO_2 content, which was converted to carbon content using the ideal gas equation.[117]

4.2.6 Catalyst characterization

Commercially available γ-alumina and anatase titania Claus catalysts were used in this study in addition to a titania nanofiber doped alumina (2.5 wt% TiO_2 on Al_2O_3).[118] This latter material was incorporated for future sub-dewpoint work, where it was thought that the nanofibers might allow for easier regeneration due to less pore condensation. Regardless, mostly low-space velocity and high-temperature results (equilibrium and single-phase) are reported in this study. These materials were crushed and sieved to 50 mesh due to the size of the bed (0.3 mm i.d.).

A series of characterizations were carried out in order to understand any physical or chemical property changes to catalyst materials after use. Thermal gravimetric analysis (TGA) was conducted to find out how much elemental sulfur was present on used catalysts on a TA TGA 55 system, where the catalysts were heated at 10 K per minute until 383 K (sulfur melting point), then held for 2 hours. The samples were then heated at 10 K per minute until 873 K (sulfur boiling point) and held for 2 hours before cooling back to room temperature. Gas flow was dried helium at 20 mL min^{-1} (5 mL min^{-1} through the balance and 15 mL/min through the furnace). The N_2 isotherms, Brunauer, Emmett & Teller (BET)[119] surface areas and Barrett, Joyner & Halenda (BJH)[120] pore size distributions for the catalysts were determined by N_2 adsorption at 77 K on a 3Flex Surface Characterization Analyzer (Micromeretics). Ion chromatography (IC) samples were prepared using 0.10 M

NaOH to extract sulfate and sulfite from the spent catalysts. These extractions were conducted under an inert environment in a N_2 glove bag to prevent oxidation of sulfur compounds by air.

4.2.7 GEM calculations

For this process to be viable, a model which can calculate chemical equilibria over a wide range of concentrations, temperatures, and pressures is required for design and operation. Gibbs Free Energy minimization routines for calculation of multicomponent equilibria are not new; however, commercially available Gibbs Free Energy minimization software is not available for real fluid high-pressure calculations within CO_2. Our calculations were based on an in-house routine previously developed for Claus chemistry equilibria at near atmospheric pressures using an MS Excel Solver routine and thermochemical data from the JANAF tables.[29] Like most applied Gibbs Free Energy minimization routines in this area, our previous spreadsheet was aimed at calculating H_2S conversion and sulfur recovery at low-pressures. As such, Gibbs Energy is calculated using ideal gas partial pressure, *i.e.*, where the fugacity coefficients are at unity, $\phi_i = 1$. By implementing the fugacity coefficient of the real high-pressure fluid, the high-pressure total Gibbs Energy function is

$$G(T,p)=\sum_{i=1}^{c} y_i\left(\Delta_f G_i^{\circ}+RT\ln(y_i\phi_i p\right) \qquad (4\text{-}4)$$

In Equation 4-4, where y is the mole fraction, $\Delta_f G_i^{\circ}$ is the standard Gibbs free energy of formation, R is the ideal gas constant, T is the absolute temperature, p is the total pressure, and ϕ_i is the fugacity coefficient for species i. For the first iteration in our calculation, ideal gas is assumed and standard Gibbs free energies of each species are calculated using only

the reference thermochemical data from the JANAF Tables, see Table 4-3.[29] The sum of the Gibbs free energies of all species is then iteratively minimized by changing the concentrations of all species until concentrations fractionally change by $\delta y_i/y_i < 0.00001$. The Gibbs energy is then minimized further after updating fugacity coefficients using equations of state with appropriate mixing coefficients or fugacity correlations. This procedure is repeated until the concentrations no longer change (again for $\delta y_i/y_i < 0.00001$).

Table 4-3. Reference enthalpies and entropies were used in the oxidation equilibrium calculation.

Species	$\Delta_f H^{298\,K,0.1MPa}$ / (kJ mol^{-1})	$\Delta_f S^{298\,K,0.1MPa}$ / (J K mol^{-1})
H_2O	-285.830	69.95
CO_2	-393.522	213.795
H_2S	-20.502	205.757
COS	-141.744[a]	231.581
CS_2	116.943	237.977
SO_2	-296.842	248.212
O_2	0	205.147
S_2	128.600	228.165
S_3	141.461	269.517
S_4	145.771	310.646
S_5	109.370	308.638
S_6	101.922	354.076
S_7	113.679	407.673
S_8	100.416	430.311

[a]COS enthalpies of formation are from Deering *et al.*[114]

Fugacities are calculated using reference quality reduced Helmholtz equations where possible. The reduced Helmholtz energy reference equations-of-state for fugacity coefficient calculations are the Span and Wagner for CO_2,[57] Lemmon and Span for H_2S[121] and Wagner and Pruß for H_2O.[122] The Helmholtz mixing coefficients were optimized for H_2S-CO_2 by Kunz and Wagner.[123] Mixing parameters for H_2O and COS in CO_2 were reported by Deering *et al.*,[113,114] while carbon disulfide and sulfur dioxide within CO_2 were reported by Commodore *et al.*[124] For dense phase sulfur, the model of Marriott and Wan for S_8 is used.[41] Elemental sulfur fugacity coefficients within CO_2 can be calculated using a Fluctuation Solution Theory model fitted to the experimental solubility of S_8 within CO_2.[12] This fugacity coefficient is applied to all sulphur allotropes, i.e., S_2, S_3, and other species up to S_8. Previously, these types of high-pressure equilibrium calculations have been described for COS hydrolysis in high-pressure CO_2; however, that system only contains 4 species in one phase versus 14 species in up to two phases here. Only two iterations after implementation of fugacity coefficients were necessary for high-pressure equilibrium convergence (using the same tolerance as stated previously).

4.3 Results and Discussion

4.3.1 GEM calculations

With the ability to calculate (i) the elemental sulfur dewpoint within CO_2 and (ii) the equilibria of H_2S oxidation to S_8,[12] the optimal equilibria conditions for production of S_8, from low-quality acid gas (1% H_2S) while keeping produced S_8 dissolved within the CO_2 fluid was calculated and shown in Figure 4-2. The black line in Figure 4-2 represents the sulfur phase pocket for the condition where 1% H_2S is converted to S_8.[12] Conditions

within the phase-pocket would result in condensation of S_8 or sub-dewpoint conversion. The conditions to the right of or above the black line are favourable regions for maintaining S_8 dissolution in CO_2. The blue lines represent H_2S conversion from 95 to 98 % recovery. To the left of these blue lines (lower temperature and higher pressure) shows conditions for above 98% recovery. The GEM calculation for conversion of H_2S to S_8 was greater than 99.9% for T < 370 K, regardless of the total pressure. Compared to the atmospheric pressure near 0.1 MPa, conversions were improved at high-pressures up to as much as 15 % depending on the temperature. Seven of the nine reported tests were conducted in the single-phase region at 20 MPa and two were conducted at 10 MPa.

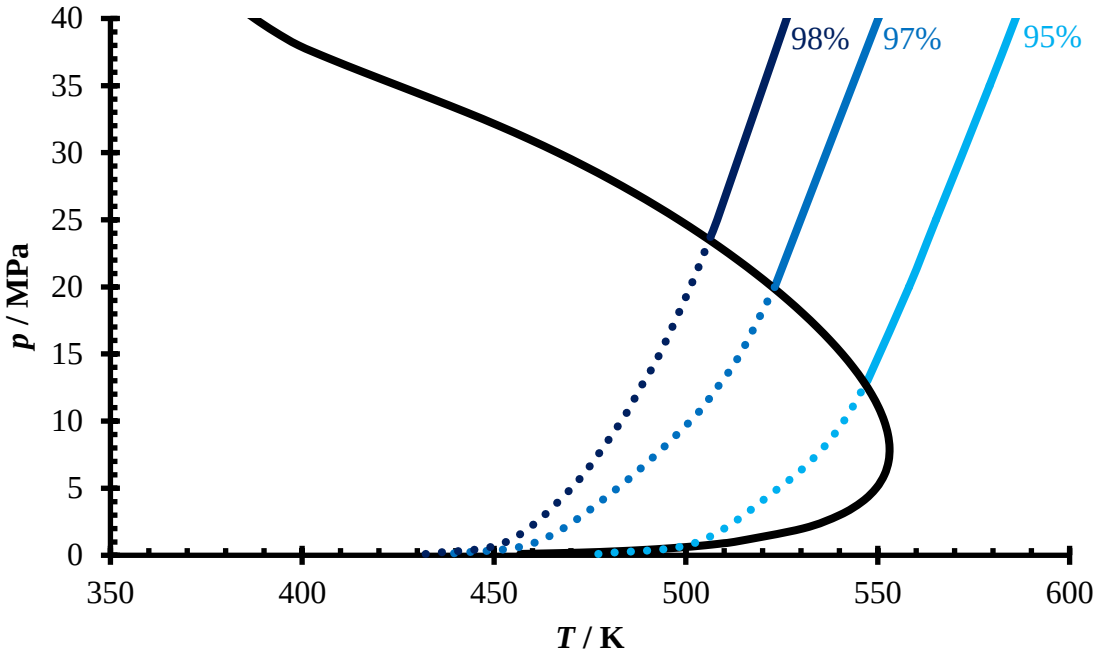

Figure 4-2. Sulfur recovery diagram using GEM routine. Blue lines represent sulfur recovery. The black line is the sulfur saturation line in CO_2 when all of 1 % H_2S converted to S_8.

4.3.2 Experimental H_2S Oxidation Data

The experimental H_2S conversion (or sulfur recovery) was determined by the following Equation 4-5:

$$H_2S\ \text{Conversion}(\%) = 100\left(\mathbf{1} - \frac{y_{H_2S}^{init.} - y_{H_2S}^{fin.} - y_{COS}^{fin.} - y_{SO_2}^{fin.} - 2y_{CS_2}^{fin.}}{y_{H_2S}^{init.}}\right) \quad (4\text{-}5)$$

In Equation 4-5, $y_{H_2S}^{init.}$ is the initial H_2S concentration, and $y_x^{fin.}$ indicates the final concentrations for sulfur compounds detected at the GC. An example of a typical experiment is shown in Figure 4-3 for 1.68% H_2S + 0.84% O_2 just after a fresh Al_2O_3 catalyst had been loaded into the catalyst bed (20 MPa, 562.97 K and 5370 h^{-1}). The recovery was noticeably lower for a short induction period after loading with fresh catalyst in several tests. This low initial recovery supports a Claus type mechanism, where Equation 4-3 requires some amount of sulfation on the surface before full catalytic activity is achieved.[102] For this reason, we believe that direct oxidation is not a significantly fast mechanism; however, future studies may attempt to utilise a direct oxidation catalyst, where Claus equilibria may not be involved in the overall kinetics. The TiO_2 catalyst did not require an initial sulfation time; however, the TiO_2 was already sulfated before being loaded into the reactor bed (see subsequent analysis). The final conversion for each test is calculated using the steady state (equilibrium) region of the data. For example, with the test shown in Figure 4-3, the final 31 data points were averaged.

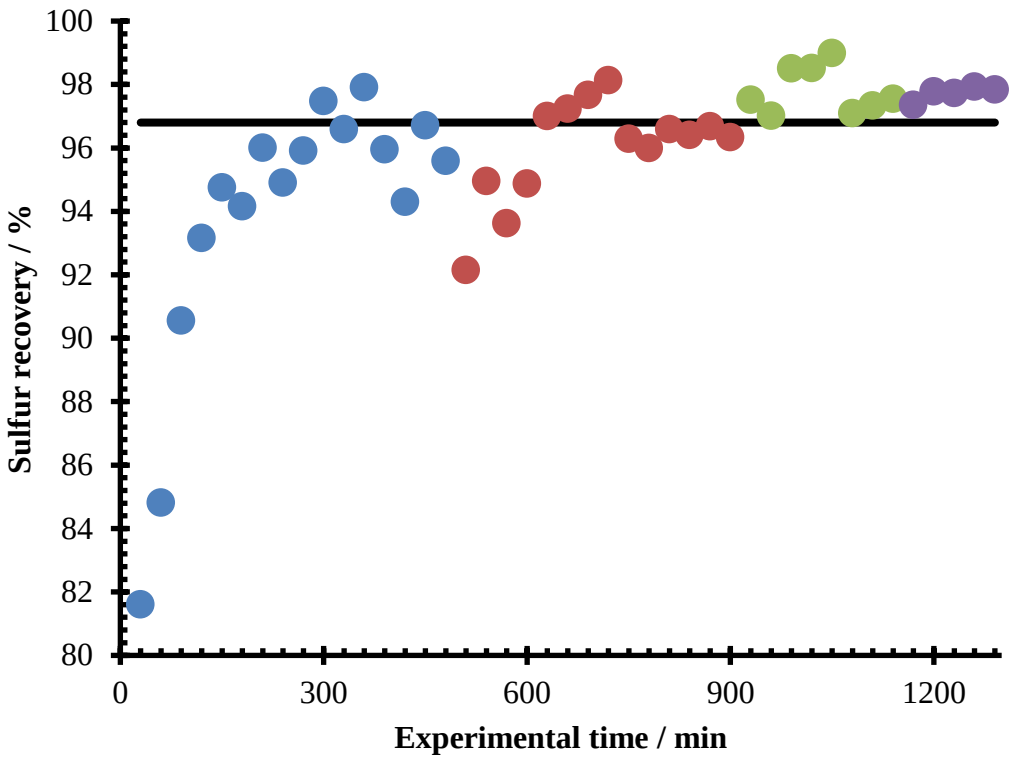

Figure 4-3. Sulfur recovery with 1.68% H_2S + 0.84% O_2 after a fresh Al_2O_3 catalyst loading (20.00 MPa, 562.97 K, 5370 h^{-1}). The line indicates calculated equilibrium with our GEM routine and the different colour data points represent different experimental days.

The measured H_2S conversions for 1 % H_2S are compared to the GEM calculations at 10 and 20 MPa total pressure in Figure 4-4 (TiO_2, Al_2O_3 and 2.5 wt% TiO_2 doped Al_2O_3). There was a more significant sensitivity to pressure increase in conversion at higher temperature, where the equilibrium conversion limit is less favourable for sulfur due to the exothermic nature of the reaction. The high-pressure is expected to favour the production of elemental sulfur provided the equilibrium sulfur speciation is still predominantly greater than S_3. The experimental conversions showed reasonable agreement compared to calculated conversions from the GEM minimization shown in Figure 4-4.

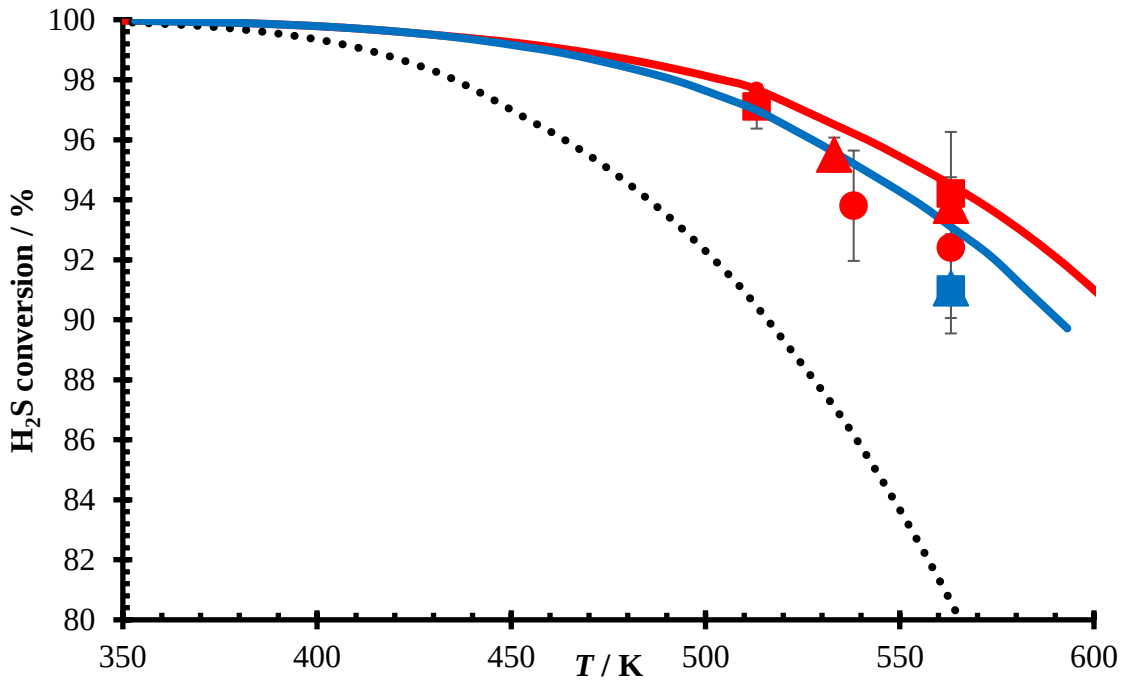

Figure 4-4. H_2S conversion of 1 % H_2S + 0.5 % O_2 in high-pressure CO_2. The solid lines were calculated equilibrium at high-pressures (red = 20 MPa and blue = 10 MPa) with real fluid fugacity coefficients, and the dotted line was calculated near atmospheric pressure (0.1 MPa). Al_2O_3, squares; TiO_2, circles; 2.5 wt% TiO_2 doped Al_2O_3, triangles.

Conversion data for our experiment conditions are reported in Table 4-4. The data in Table 4-4 shows only a very small difference between the real fluid GEM calculation versus an ideal gas GEM calculation at pressure. We note that three of the experiments with the Al_2O_3 catalyst were calculated to be in a sub-dewpoint region; 0.77% H_2S at 502.79 K; 0.95% at 512.79 K and 1.68% H_2S at 493.15 K. For 0.77% H_2S at 502.79 K we did not measure a drop in sulfur conversion. This conditions is within 8 K of the calculated dewpoint at 100% conversion; therefore, we believe this may not be deep enough into the phase pocket to cover the catalyst with sulfur and/or an 8 K difference may be within the uncertainty margin of the phase pocket calculation. The 1.68% H_2S at 493.15 K experiment was more than 50 K below the calculated dewpoint and conversion began to suffer after

about 7 hours. Several other sub-dewpoint experiments were attempted, but at these space velocities, the catalyst bed capacity for elemental sulfur is quite low. Sub-dewpoint operation requires a catalyst regeneration cycle and a larger bed, and these aspects were not incorporated into this study. For the test at 0.95% at 512.79 K we did not observe a deactivation but were able to demonstrate that the catalyst had deposited sulfur on it (see TGA results). Again, this last test is very close to the saturation temperature.

Table 4-4. Calculated and experimental H_2S conversion for the oxidation of H_2S above Al_2O_3 or TiO_2 catalysts.

T / K	SV / h^{-1}	Ideal GEM calc. conversion / %	Real GEM calc. conversion / %	Exp. Conversion / %
Feed composition: 0.495% H_2S + 0.248% O_2 (Al_2O_3)				
553.15	5260	93.0	94.0	94.4 ± 2.5
Feed composition: 0.77% H_2S + 0.385% O_2 (Al_2O_3)				
502.79[b]	4620	98.0	98.0	97.1 ± 0.4
533.15	3870	96.2	96.3	96.7 ± 0.3
562.93	5370	93.5	94.1	95.0 ± 0.5
Feed composition: 0.95% H_2S + 0.475% O_2 (Al_2O_3)				
512.79[b]	4720	97.8	97.8	97.1 ± 0.7
562.94	5370	94.1	94.5	94.2 ± 2.1
564.03[a]	9310	92.6	93.9	91.1 ± 2.0
Feed composition: 1.00% H_2S + 0.50% O_2 (TiO_2)				
538.15	3870	96.3	96.3	93.8 ± 1.1
563.15	5370	94.2	94.5	92.4 ± 1.0
Feed composition: 1.00% H_2S + 0.50% O_2 (2.5 wt% TiO_2 doped Al_2O_3)				
533.15	3870	96.6	96.6	95.5 ± 0.6
563.15	5370	94.2	94.5	93.8 ± 0.9
563.15[a]	9310	92.8	94.0	91.0 ± 2.0
Feed composition: 1.68% H_2S + 0.84% O_2 (Al_2O_3)				
493.15[b]	4400	98.8	98.8	98.5 ± 0.5
562.97	5370	95.4	95.4	95.5 ± 0.7

$\sigma(T)$ = 0.02 K; [a] indicates two experiments at p = 10.09 MPa, whereas all other experiments are for p = 20.00 ± 0.02 MPa; [b] indicates a sub-dewpoint condition before any observable catalyst deactivation; the reproducibility for experimental conversion is reported as the standard deviation for 6 to 30 points (3 to 15 hours).

Measured and calculated H_2S concentrations were in statistical agreement shown in Table 4-4 (within 2 standard deviation). Compounds such as CS_2 and thiols were not detected, where the absence of CS_2 was expected from the equilibrium calculations. Thermodynamically unstable CS_2 is often present in Claus plant catalyst beds due to hydrocarbon reacting within the thermal stage or from hydrocarbon destruction across a catalyst. In application, a hydrocarbon impurity within the CO_2 stream would likely lead to other reaction intermediates in this process and possibly catalyst fouling. COS is an equilibrium species which we observed with calculated and with the experimental results. In over 70% of our experiments, the calculated concentration of COS agreed with the GC results. We note that COS and SO_2 proved difficult to measure when flashing the CO_2 fluid to the GC injector.

The final purity of produced S8 was determined to be ~ 99.984% based on the carbon content of 127-159 ppmw, which was below the 250 ppmw nominal premium Canadian export specifications.[117] Fresh and used catalysts were characterized to find out what physical and chemical changes happened after the reactions. Thermogravimetric analysis was carried out to determine if produced sulfur was deposited onto the catalyst (Figure 4-5). Surface area change and pore size distribution were also determined by nitrogen adsorption. Decrease in surface area was found beyond the 50 m^2g^{-1} expected from the hydrothermal aging (Figure 4-6), around pore diameters shown in pore size distribution (Figure 4-7). We were also able to find evidence of sulfate by ion chromatography (Table 4-5). The formation of sulfate on the catalyst supports that the main mechanism of the equilibrium reaction (Figure 2-4).

4.3.3 Thermogravimetric analysis (TGA)

Thermogravimetric analysis was conducted on a spent Al_2O_3 catalyst to confirm condensed liquid sulfur, where the 0.95% H_2S at 512.79 K was the final experiment before removing the catalyst. Although this last temperature is slightly below the calculated dewpoint, it was unknown if sulfur was depositing on the surface (the sulfur partial pressure was on the same magnitude as the calculated partial pressure). Figure 4-5 shows the mass loss profile of the spent Al_2O_3 catalyst in the temperature range of 600-850 K. The loss of up to 8 weight % in the range of 670-800 K was attributed to the evaporation of elemental sulfur deposited on the catalyst.

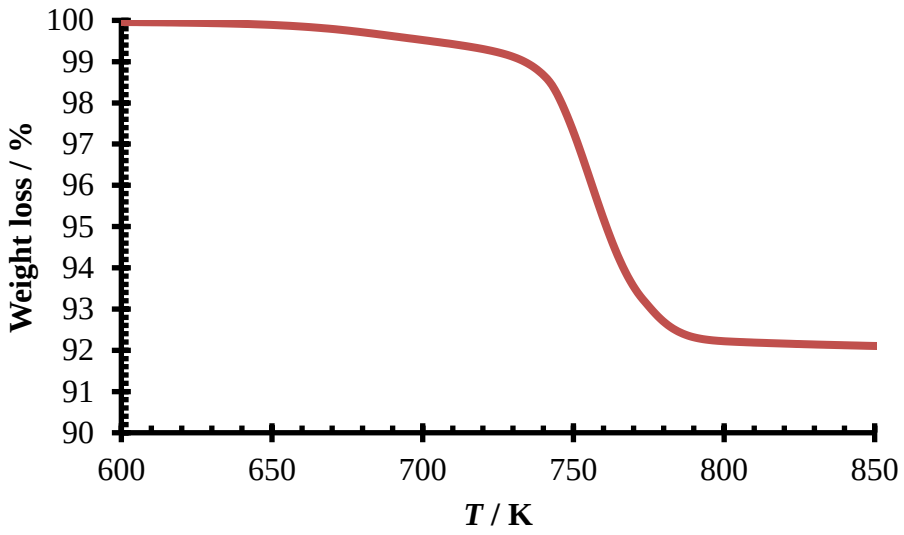

Figure 4-5. TGA results of used Al_2O_3. Weight loss with increasing temperature was attributed to the evaporation of elemental sulfur that was deposited onto the catalyst.

4.3.4 N_2 physisorption

BET surface area and pore size distribution for virgin and spent catalysts were determined by N_2 adsorption. The isotherms for TiO_2 and Al_2O_3 are shown in Figure 4-6. Both TiO_2 and Al_2O_3 showed type IV isotherms, which was expected for these mesoporous

catalysts. The Al_2O_3 catalyst showed a higher initial surface area; however, after the Claus reaction tests, the BET specific surface area of Al_2O_3 decreased from 341 to 166 $m^2\ g^{-1}$. Although relatively less, the TiO_2 catalyst also experienced a specific surface area decrease from 122 to 89 $m^2\ g^{-1}$.

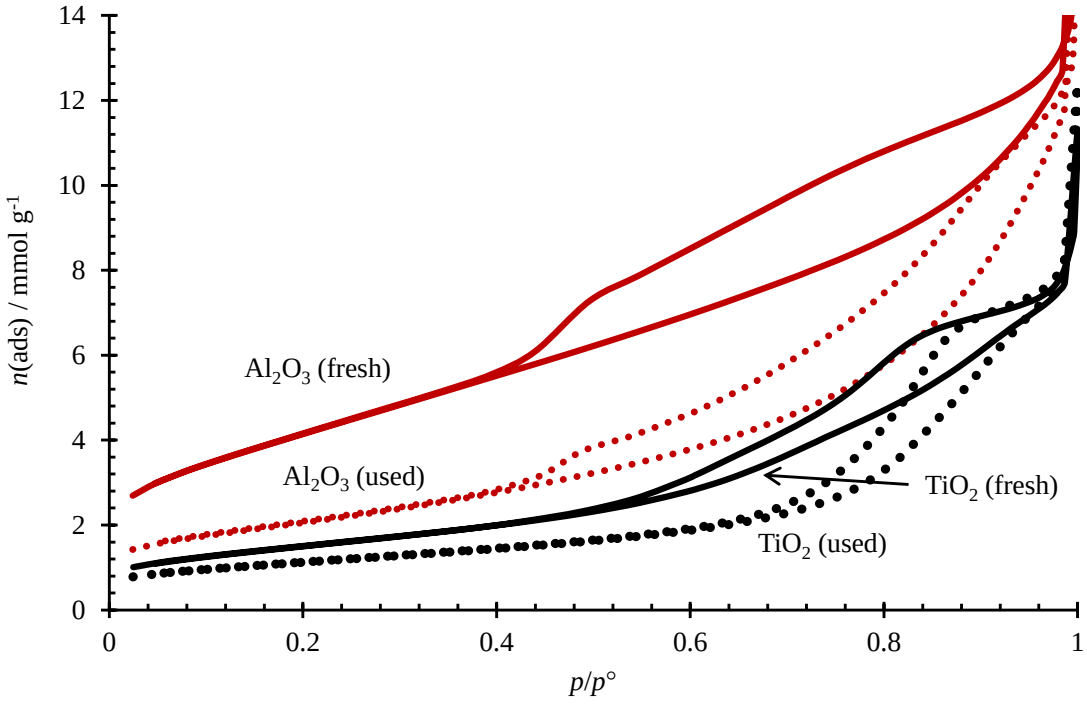

Figure 4-6. Fresh and used N_2 BET Isotherms for Al_2O_3 and TiO_2 catalyst materials. Note the decrease in gas adsorption in used catalysts.

Decreases in specific surface area is quite common for Al_2O_3 catalyst materials, where hydrothermal aging is thought to be the primary cause; however, this reduction is well beyond the ca. 50 $m^2\ g^{-1}$ expected. Again, using our solubility calculations and TGA results, we believe that sulfur deposition contributed more significantly to the loss of specific surface area. The change in pore volume distributions are shown in Figure 4-7, where Al_2O_3 lost a significant pore volume for ca. 3.6 nm pores and TiO_2 lost significant pores at ca. 4.7 nm.

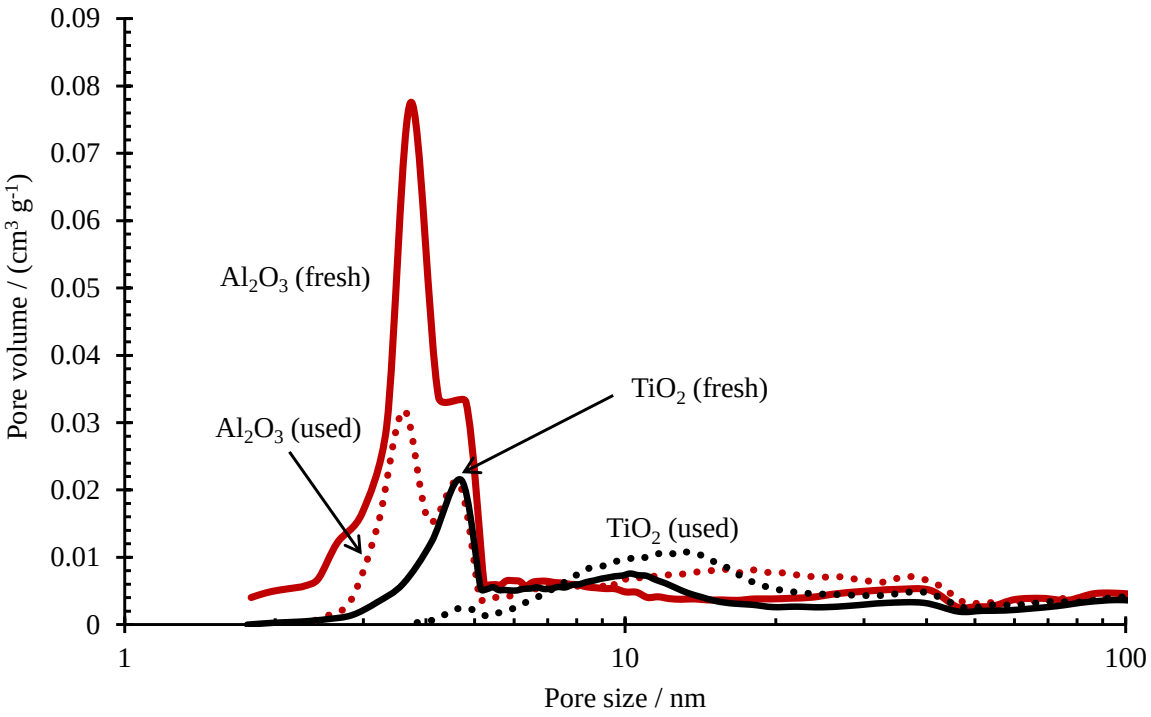

Figure 4-7. BJH pore size distribution for fresh and used catalyst. Note the decrease in pore volumes due to the sulfur pore deposition.

Ideally, one could measure pore condensation and compare to calculated pore condensation by using the Kelvin equation, if the temperature is above the dewpoint. This would provide an independent test of our sulfur solubility model. However, purging and depressurizing a high-pressure catalyst bed does introduce significant error (sulfur loss) and these high-pressure catalyses experiments were quite challenging.

4.3.5 Sulfate species on the surface

The IC results for the surface washes are shown in Table 4-5. Sulfur oxy-anion species are suggested intermediates in the Claus reaction.**Error! Bookmark not defined.** We note that thiosulfate and sulfite were not detected at any significant amount. As suggested in Figure 4-3, the Al_2O_3 showed a build-up of sulfate, whereas the TiO_2 did not undergo

sulfation during the tests. Again, the involvement of sulfate intermediate with the surface Claus reaction in the overall conversions observed here, is required to achieve the equilibrium predicted by the GEM calculations.

Table 4-5. Sulfate, sulfite and thiosulfate concentrations of catalysts.

Sample	Al_2O_3 (fresh)	Al_2O_3 (used)	TiO_2 (fresh)	TiO_2 (used)
SO_4^{-2} (wt. %)	0.003	2.46	6.36	5.92
SO_3^{-2} (wt. %)	0.041	0.007	0.016	0.021
$S_2O_3^{-2}$ (wt. %)	0.001	0.009	0.001	not detected

4.4 Conclusions

The oxidation of H_2S in supercritical CO_2 is being explored as a low-level sulfur recovery process together with the production of commercially utile liquid CO_2. In order to determine the limits of such a process, the possible equilibrium conversion has been independently investigated using a high-pressure GEM calculation and experimental conversions over Al_2O_3, TiO_2 and TiO_2 doped Al_2O_3 catalyst materials. Overall, both experimental and calculated conversions were in agreement and suggest that conversion increased with decreasing temperatures and increasing pressures.

Initial sulfation of the Al_2O_3 material, plus the agreement between equilibrium GEM calculations and experimental results, suggest that the modified Claus reaction is a significant contributor to the overall conversion mechanism. A possible future study could be conversion over a direct oxidation catalyst on a support which may not support Claus catalysis, thus higher conversions might be possible.

We note that formation of COS was also found to be at equilibrium, while CS_2 and/or thiol was not detected. Where these studies only included highly pure CO_2, another

future study could include hydrocarbon impurities, which would be present in any cryogenically separated acid gas.

Finally, the equilibrium oxidation of 1% H_2S in high-pressure CO_2 showed that the conversion to elemental sulfur increases by 12 % at 550 K by increasing the total pressure from 0.1 to 20 MPa. While increasing pressure even higher than 20 MPa could be explored to further increase the H_2S conversion, 20 MPa may be a practical limit for high-pressure processing and the kinetics of the reaction could be slowed due to the kinetic limitations at such high-pressures. Therefore, the future direction of this project will include a kinetic study at relatively faster space velocities.

Chapter 5: The Kinetics of Hydrogen Sulfide Oxidation within High-pressure Carbon Dioxide

This manuscript is intended to be published and will be submitted to *Industrial & Engineering Chemistry Research*.

5.1 Introduction

Previously, the effect of temperature and pressure on H_2S conversion whilst avoiding the sulfur dewpoint in high-pressure CO_2 was studied.[12,13] Upon later separation, the formed S_8 can be a marketable product to be used in fertilizer production while the high-pressure CO_2 fluid can be sold for enhanced oil recovery or as a solvent for other green processes.[6,7] For 1 % H_2S in CO_2, a pressure of 20 MPa can increase the H_2S conversion by as much as 12% at 550 K in comparison to the conventional near-atmospheric pressure reactions. Standard (273 K and 0.1 MPa) space velocities > 1000 h^{-1} provided satisfactory residence times (inverse of space velocity) for reactions to reach equilibria above 513K and up to 20 MPa.[13] Decreasing temperature below sulfur dewpoint and increasing pressure higher were attempted in pursuit of further improvement in H_2S conversion. It was found that temperatures below 513 K and pressures above 20 MPa, the oxidation reaction would require much longer residence times to establish the calculated equilibrium by high-pressure Gibbs Free Energy minimization routine.[13]

When considering a dense phase supercritical CO_2 medium for heterogeneous catalysis, strong cluster effects can influence the kinetics of H_2S adsorption onto a surface due to the constraints imposed on trace H_2S by the surrounding cluster of high-pressure CO_2.[125] The rate limiting process could be enhanced by the presence of high-pressure CO_2

in either the diffusional steps or the surface chemical steps. This phenomenon could require a lower space velocity of the H_2S oxidation reaction at lower temperatures and/or higher pressures than the typical space velocity of near atmospheric pressure processes at 1200 h^{-1}. A kinetic study was carried out to understand the change in kinetic limitations of H_2S within high-pressure CO_2 fluids and to provide an understanding for possible industry implementation.

The investigation of H_2S oxidation kinetics within a high-pressure CO_2 fluid was carried at T = 423.15 to 513.15 K, p = 10 to 25 MPa, and space velocity = 860 to 6330 h^{-1} over γ-alumina. The study was performed with 1.00 % H_2S + 0.50 % O_2 within high-pressure CO_2 fluid following the disappearance of H_2S by GC. The general form of the rate expression for the oxidation of H_2S in the presence of O_2 based on the stoichiometry can be written as:

$$-d[H_2S]/dt = -2d[O_2]/dt = k[H_2S]^a[O_2]^b \quad (5\text{-}1)$$

where t is the residence time, and k is the rate constant. A similar study done by Dowling *et al.*, at lower pressures was utilized here as a starting point for the kinetics of the reaction.[92] The reaction order with respect to each reactant was found to be a = 1 and b = 1, being determined by oxidation of H_2S at p = 0.69 to 6.9 MPa, using pseudo-order with respect to H_2S and first order with respect to O_2, then vice versa.[92] Ideally, the reaction order and surface adsorption mechanisms should be experimentally determined by repeating the similar process done by Dowling *et al.*, at elevated pressures. However, making high-concentrations of H_2S mixtures at high-pressures was an undesirable safety hazard and not necessary as the H_2S concentration of interest in this work is only ~ 1%. The upper pressure of 6.9 MPa studied by Dowling *et al*. was in a proximity of the lower

pressure of 10 MPa studied in this work, and the kinetic results from Dowling *et al*. was adapted for the kinetics of H_2S oxidation in high-pressure CO_2.

For bimolecular surface reactions, the rate expression can be considered as a Langmuir-Hinshelwood (LH) mechanism where both species are adsorbed to the γ-alumina surface or an an Eley-Rideal (ER) mechanism whereby one of the species adsorbs before reacting with the other gas specie.[98] Dowling *et al*. found a shifting-order rate behaviour of ER mechanism with respect to H_2S with excess O_2, where the shifting in reaction order from 1 to 0 as increasing partial pressure of H_2S.[92,98] Since H_2S and O_2 react with 2 to 1 stoichiometry, $[H_2S]_{final} = [H_2S]_{initial} - 2x$ and $[O_2]_{final} = [O_2]_{initial} - x$, where x is the amount of reactant consumed. With an assumption that at any time, $1/2[H_2S] = [O_2]$ and substituting it into Equation 5-1 with gaseous reactants can simplify to Equation 5-2:

$$-d[H_2S]/dt \approx \{k\phi_{H_2S}\phi_{O_2}[H_2S]^2\}/2 \quad (5\text{-}2)$$

where ϕ_{H_2S} and ϕ_{O_2} are the fugacity coefficients of H_2S and O_2, and for $\phi_{H_2S}\phi_{O_2}$ values were calculated using REFPROP.[58] The integration of this second-order rate law and replacing concentration terms with fugacity, *f*, yield Equation 5-3.

$$\frac{1}{f_{H_2S,\,final}} = \frac{1}{f_{H_2S,\,initial}} + \frac{k}{2}t \quad (5\text{-}3)$$

The experimentally obtained kinetic data were used to fit the Equation 5-3, and a kinetic model was developed to calculate the minimum *t* required, or the maximum space velocity allowed for H_2S oxidation to establish equilibrium calculated by Gibbs Free Energy minimization routine at high-pressure.[13] Further correlation was necessary in order to calculate the rate constant from temperature, pressure, and the concentration of H_2S. The pre-exponential factor in the Arrhenius equation, *A*, for bimolecular gas reactions is dependent on temperature and pressure according to the following relationship:[30]

$$A = (e^2 k_B T/hp) \exp(\Delta S^{\ddagger}/R), \quad (5\text{-}4)$$

where k_B is the Boltzmann constant ($1.38 \times 10\text{-}^{23}$ m^2 kg s^{-2} K^{-1}), h is the Planck constant (3.976×10^{-32} m^2 kg min^{-1}), T is the absolute temperature, p is pressure in MPa, and R is the ideal gas constant in units of m^3 Pa mol^{-1} K^{-1}. The pressure term is added because of the pressure dependence of the pre-exponential factor as well as to keep consistency in units. $\Delta S^{\ddagger}$ is the entropy of activation in m^3 Pa mol^{-1} K^{-1} where

$$\Delta S^{\ddagger} = S^{\ddagger} - S_{initial} \quad (5\text{-}5)$$

$S^{\ddagger}$ is the entropy of the activation complex and $S_{initial}$ is the entropy of the initial mixture. Experimental measurements were used in order to develop a correlation to calculate $\Delta S^{\ddagger}$ values for any desired temperature or pressure.

5.2 Experimental

5.2.1 Materials

The sources, purities and pre-experimental analyses of all chemicals used in this study are reported in Table 5-1.

Table 5-1. Purity of chemicals used in this study, chemical supplier, and the analysis procedures used for verification.

Chemical Name	Source	Analysis Method	Purity / mol %
Carbon dioxide	Praxair Inc.	GC-TCD/FID/SCD	≥99.9995
Hydrogen sulfide	Linde	GC-TCD/FID/SCD	≥ 99.9
Oxygen	Praxair Inc.	GC-TCD/FID	≥ 99.993
Helium	Praxair Inc.	GC-TCD/FID	≥ 99.999
Air	Praxair Inc.		Breathing grade

All chemicals were used without further purification but were verified by GC.

5.2.2 High-pressure oxidation apparatus

Kinetic experiments were carried out in the same experimental apparatus as previous Chapter as in Figure 4-1. The details of the experimental apparatus and preparation of reaction mixtures were described in the previous chapter. The same SS-316 reactor was used, with an internal volume of ~ 0.5 mL (0.3 mm inner diameter) filled with ~ 0.5 g of commercially available γ-alumina catalyst crushed below 300 micrometer particle size. Two 2 μm filters were used for both inlet and outlet of the reactor to ensure that no solid particles would travel through the 1/16" lines to prevent blockage of the system.

5.2.3 Procedure

Using the constant flow feature of the Teledyne Isco Pumps, the initial mixtures of H_2S/CO_2 and O_2/CO_2 were flown through the catalytic reactor with 2:1 ratio of H_2S to O_2. The syringe pumps were set at constant flows for the mixtures with standard space velocity high enough (860 to 6330 h^{-1}) to result in steady concentrations of H_2S distant from the high-pressure GEM calculated equilibrium H_2S concentrations.[13] When the pressure of the system reached a set point, for example 20 MPa, a VICI on/off poppet valve (Valco Instruments Co. Inc.) poppet valve would work as a back-pressure regulator by opening and closing automatically to release and maintain the pressure of the system near the set point. The release of pressure doubled to sample the reaction effluent which passed through a glass wool trap and a P_2O_5 trap prior to the GC to remove the produced S_8 and water,

respectively. The analysis of reaction effluents was completed on a Bruker 450-GC with an Agilent GS-GasPro column equipped with a thermal conductivity detector.

5.3 Experimental Results and Calculation Methods

5.3.1 Determination of the high-pressure H_2S oxidation Kinetics

For the heterogeneous catalysis of H_2S, oxidation at 483.15 K and 20 MPa was first studied to correlate an increase in an initial rate to an increase in an alumina surface area. A feed mixture of 1.00 % H_2S and 0.50 % O_2 was used. This correlation was achieved by comparing fresh zeolite 13X and fresh γ-alumina. The fresh zeolite 13X had an initial surface area of 583 $m^2\ g^{-1}$, which was synthesized and characterized by Wynnyk *et al.*[126] Their energy dispersive X-ray spectroscopy (EDX) analysis showed that the Si/Al mole ratio of the product to be 1.8, which was used to estimate the available alumina surface as ~ 208 $m^2\ g^{-1}$. The surface area of fresh γ-alumina was determined as 341 $m^2\ g^{-1}$ in the previous study.[13] The initial rate constants at the conditions mentioned above were 4757 $MPa^{-1}\ min^{-1}$ for γ-alumina and 2828 $MPa^{-1}\ min^{-1}$ for 13X. The rate constant ratio of γ-alumina/13X was 1.68, which was closely related to the available alumina surface area ratio of γ-alumina/13X at 1.64. These results demonstrate that diffusion steps were not the rate limiting processes.

The results of the kinetic experiments performed over γ-alumina with the feed mixture of 1.00 % H_2S and 0.50 % O_2 are shown in Table 5-1. Table 5-1 provide the relevant temperature and pressure conditions, residence times converted from space velocity, average % H_2S conversion by GC (at minimum 3 steady points), and the fugacity of H_2S within high-pressure CO_2 calculated by REFPROP with the optimized mixing

coefficients by Commodore *et al*.[58,124] Note that the steady H_2S conversions were achieved away from equilibria at most conditions (minimum GEM theoretical H_2S equilibrium conversion of 98 %),[13] except the conditions at higher pressures and higher temperatures were limited by the slowest flow settings of the Isco pumps.

Table 5-1. Experimental results for the 1% H_2S/0.5% O_2 feed in the γ-alumina catalytic reactor.

Temperature (K)	Pressure (MPa)	% Conversion of H_2S[a]	Space Velocity / h^{-1}	Residence Time (minutes)	Fugacity H_2S (MPa)
423.15	10	0.0	0	0.000	0.816
423.15	10	8.7	6330	0.010	0.743
423.15	10	20.0	3170	0.019	0.651
423.15	10	48.2	930	0.065	0.420
453.15	10	0.0	0	0.000	0.858
453.15	10	33.7	4660	0.013	0.566
453.15	10	39.7	3260	0.018	0.515
453.15	10	54.9	2050	0.029	0.385
483.15	10	0.0	0	0.000	0.890
483.15	10	64.3	3260	0.018	0.315
483.15	10	77.7	2050	0.029	0.197
483.15	15	0.0	0	0.000	1.268
483.15	15	62.3	4090	0.015	0.340
483.15	15	77.2	3580	0.017	0.288
483.15	20	0.0	0	0.000	1.615
483.15	20	95.8	5370	0.037	0.065
483.15	20	96.8	4300	0.056	0.049
513.15	25	0.0	0	0.000	2.075
513.15	25	92.0	3760	0.015	0.164
513.15	25	94.6	860	0.022	0.109

[a] H_2S GC analysis: $(\{[H_2S]_{initial} - [H_2S]_{final} - [COS]_{final} - [SO_2]_{final}\}/[H_2S]_{initial}) * 100$.
[b] Only condition that is not sub-dewpoint.

The experimental kinetic data of high-pressure H_2S catalysis within CO_2 were used to fit the second overall reaction rate law (Equation 5-3), where the slope = $k/2$ in Figure 5-1.

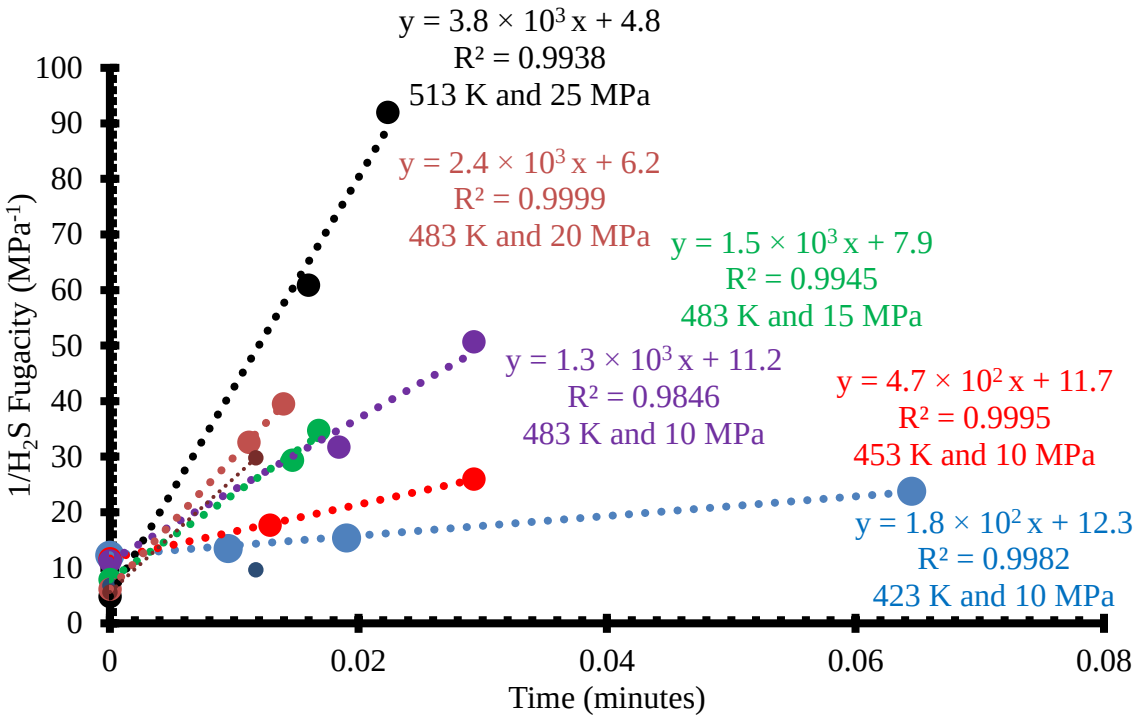

Figure 5-1. Second order kinetic plot for H_2S. The slope of each plot is the second order rate constant, and the y-intercept of each plot is the $\frac{1}{f_{H_2S,\ initial}}$.

The activation energy for H_2S oxidation can be determined from the rate constants at 423.15, 453.15, and 483.15 K at a constant pressure of 10 MPa for the 1.00 % H_2S + 0.50 % O_2 mixture in CO_2 shown in Table 5-2.

Table 5-2. Overall second order rate constants (MPa^{-1} min^{-1}) for H_2S oxidation in the catalytic reactor.

Temperature (K)	Pressure (MPa)	k (MPa^{-1} min^{-1})
423.15	10	353 ± 11
453.15	10	940 ± 68
483.15	10	2563 ± 331

The Arrhenius plot for the H_2S oxidation in the catalytic reactor is presented in Figure 5-2. The apparent activation energy for H_2S oxidation was determined from the Arrhenius plot *via* slope = -*E*a/R, providing a value of 56.1 ± 2.5 kJ mol^{-1} which is in agreement with the literature values of 62.2 ± 8.3 kJ mol^{-1} and 56.5 kJ mol^{-1} obtained at lower pressures.[92,93] This was within the typical range of > 30 – 50 kJ mol^{-1} for surface-reaction controlled catalytic processes involving adsorption or the reaction of adsorbed species in the rate limiting process.[92] The agreement in between activation energy of this work and literature supports that the similar reaction pathways is occurring and justifies the adaption of the literature rate expression. The pre-exponential factor, *A*, determined from the y-intercept of the Arrhenius plot, was found to be 2.86 ± 0.08 × 10^9 MPa^{-1} min^{-1} at 10 MPa.

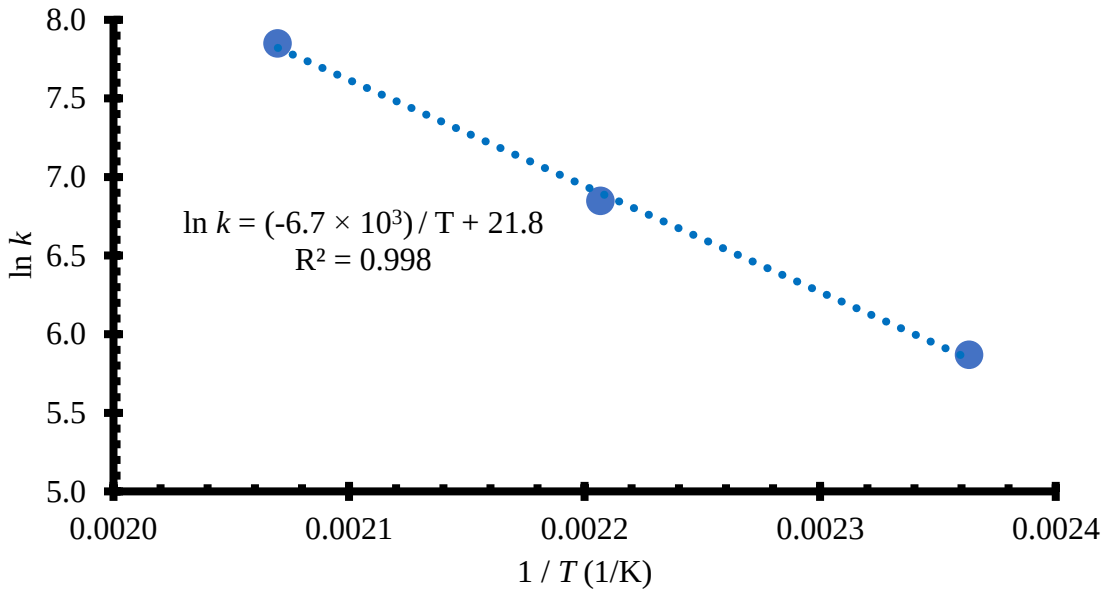

Figure 5-2. Arrhenius plot for H_2S oxidation in the catalytic reactor.

5.3.2 Modelling of the high-pressure H_2S oxidation Kinetics

For the kinetic model at high-pressure, it was first necessary to correlate the change of pre-exponential factor, *A*, with varying temperatures pressures. First, $\Delta S^{\ddagger}$ was calculated from Equation 5-4 using the experimental results over three temperatures 423.15, 453.15, and 483.15 K at a constant pressure of 10 MPa as shown in Table 5-3.

Table 5-3. Entropy of activation for H_2S oxidation in the catalytic reactor at three temperatures and 10 MPa.

Temperature (K)	Pressure (MPa)	$\Delta S^{\ddagger}$ (m^3 Pa mol^{-1} K^{-1})
423.15	10	-30.2
453.15	10	-30.8
483.15	10	-31.3

The negative values for $\Delta S^{\ddagger}$ indicated that the entropy decreased on forming the transition state. This negative $\Delta S^{\ddagger}$ was expected for the heterogeneous catalysis as two reactants formed a single activated complex.[127] This also agreed with previous kinetic studies, where the mechanism of the reaction was described as a bimolecular surface reaction occurring *via* the Eley-Rideal mechanism.[92,98] Increasing the temperature at constant pressure decreased the entropy of activation, meaning that S_i is relatively higher than $S^{\ddagger}$. Higher S_i indicates more disorder with increasing temperature compared to $S^{\ddagger}$. However, the pre-exponential factor did not change as the decrease in $\Delta S^{\ddagger}$ was offset by the increase in temperature in Equation 5-4.

The entropy of activation over pressures 10, 15, 20, and 22.5 MPa at 483.15 K were calculated as shown in Table 5-4 from the experimental data. Fugacity coefficients of H_2S were suspected to decrease with increasing pressure of CO_2 due to the more constrains imposed on H_2S by CO_2, which would lead to lower reaction rates.[128] In fact, fugacity

coefficients of H_2S did decrease with increasing pressure as shown in Table 5-4, but there was an initial increase in reaction rate constant.

Table 5-4. Entropy of activation and H_2S fugacity coefficient for H_2S oxidation in the catalytic reactor at different pressures.

Temperature (K)	Pressure (MPa)	$\Delta S^{\ddagger}$ (m^3 Pa mol^{-1} K^{-1})	A (MPa^{-1} min^{-1})	H_2S fugacity coefficient[58]
483.15	10	-31.3	2.94×10^9	0.89
483.15	15	-26.2	3.54×10^9	0.85
483.15	20	-20.2	5.46×10^9	0.81
483.15	22.5	-20.4	4.72×10^9	0.79

Increasing pressure up to 20 MPa increased $\Delta S^{\ddagger}$ initially, indicating relative decreases in S_i compared to $S^{\ddagger}$. Therefore, the initial reaction mixture became more ordered with increasing pressure. The pre-exponential factor was seen to increase as the increase in pressure was outweighed by the increase in $\Delta S^{\ddagger}$ in Equation 5-4. Above 20 MPa, $\Delta S^{\ddagger}$ decreased, meaning the initial reaction mixture became more disordered compared to the adsorbed activation complex. While this is unexpected at high-pressures, the trend was confirmed by other experiments and shown in Figure 5-3. This phenomenon could be caused by the initial reaction mixture being unable to reach the surface of the catalyst due to the resistance of the dense CO_2. As a result, the apparent S_i is seen to increase, likely from the reactants failing to adsorb to the catalytic surface and form the activation complex. Both increasing pressure and decreasing $\Delta S^{\ddagger}$ contributed to a decreasing pre-exponential factor above 20 MPa in Equation 5-4.

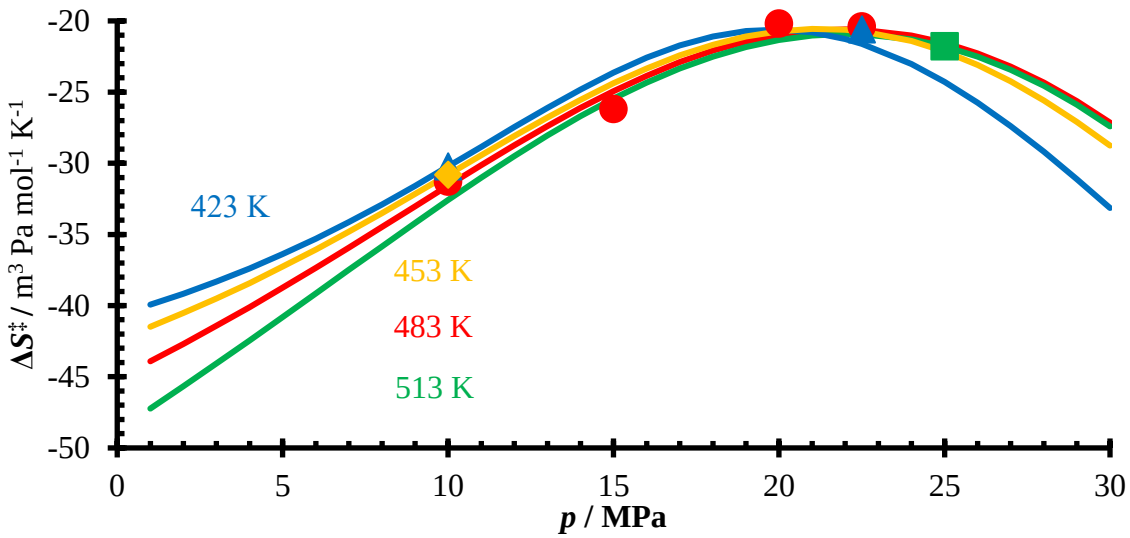

Figure 5-3. Entropy of activation as a function of pressure. Blue triangle and line are 423 K, orange diamond and line are 453 K, red circles and line are 483 K, and green square and line are 513 K.

In order to account for the shifting trend in the entropy of activation, varying pressures and temperatures were related to $\Delta S^{\ddagger}$ in Figure 5-3. The experimentally obtained $\Delta S^{\ddagger}$ was fitted adapting the change in entropy of the free molecule by the Clausius-Clapeyron relation ($\Delta S = \frac{dp}{dT}\Delta V$) resulting Equation 5-6.

$$\Delta S^{\ddagger} = a\Delta S\text{-}b \tag{5-6}$$

It was found that the entropy of activation was a function of partial molar volume of H_2S in the mixture ΔV, dp/dT, and molality, M. Partial molar volume was calculated by the density differences of H_2S within the mixture and the pure CO_2. Densities and dp/dT (at constant volume) were calculated from REFPROP.[58] Parameters a and b in Equation 5-6 were empirically correlated to temperatures and resulted in the following Equation 5-7:

$$\Delta S^{\ddagger} = \exp(0.01656T)\frac{290.9}{M}\frac{dp}{dT}\left(\frac{\rho_{H_2S,\,mix} - \rho_{CO_2}}{\rho_{H_2S,\,mix}\,\rho_{CO_2}}\right) - (0.0005349T^2 - 0.4104T + 118.5) \tag{5-7}$$

Equation 5-7 was used over at T = 423 to 513 K and p = 1 to 30 MPa to establish Figure 5-3. The shifting trend of $\Delta S^{\ddagger}$ was confirmed while the peaks of $\Delta S^{\ddagger}$ slightly change depending on temperatures.

At a given temperature, the maximum $\Delta S^{\ddagger}$ would result in the fastest kinetics in the supercritical CO_2. The maximum $\Delta S^{\ddagger}$ with respect to the pressure would be where the derivative of $\Delta S^{\ddagger}$ with respect to p equals 0. The only pressure dependent terms in Equation 5-7 are the dp/dT and the partial molar volume of H_2S. This information is very useful, because even without carrying out an actual kinetic experiment in supercritical CO_2, it is possible to find at what pressure the kinetics of a reaction would be the fastest by calculating where the maximum of the dp/dT multiplied by the partial molar volume given temperature and H_2S concentration.

Correlating these maximums with respect to temperature and pressure, a Widom line with respect to H_2S within CO_2 can be obtained. Widom lines are used to decribe ridges for lines of maximums of thermodynamic characteristics in the supercritical fluids (in this case, $\Delta S^{\ddagger}$).[129] This specific Widom line should be where the chemical reaction rate should be the fastest. This Widom line resembles the subcritical boiling process and occurs as the extension of the coexistence line into the supercritical region without discontinuity in the "phases" present in the subcritical boiling process. Instead of a discontinuity, there is a line that represents the maxima of $\Delta S^{\ddagger}$ which divides gas-like supercritical CO_2 solvent and liquid-like supercritical CO_2 solvent. However, the Widom line only suggests at what temperature and pressure the reaction would be the fastest, not how fast the reaction would be. Kinetic experiments are therefore still necessary to find out the rate constants.

The increasing constrains from high-pressure CO_2 resulted in decreasing partial molar volume of H_2S. This is initially beneficial in terms of the volume of activation, $\Delta V^{\ddagger}$, which is the volume change in going from the initial reactants to the activated state. $\Delta V^{\ddagger}$ has a relationship with the rate constant according to Equation 5-8.[30]

$$\left(\frac{\partial \ln k}{\partial p}\right)_T = -\frac{\Delta V^{\ddagger}}{RT} \tag{5-8}$$

Therefore the rate constant will increase with increasing pressure if $\Delta V^{\ddagger}$ is negative.[30] The negative $\Delta V^{\ddagger}$ means that the activation complex has a smaller volume than the initial reactants. Increasing pressure can speed up the formation of activation complex by reducing the volume of the reactants closer to (but not smaller than) the volume of the activation complex. In non-catalyses conceptual form, increasing rate constants can also be related to the increased number of collisions between the reactants due to the cage effect of CO_2. This effect of CO_2 caging in the solute molecule is also known as the Franck-Rabinowitch effect.[130] Therefore, these effects combined reduce the time required for the reactants to form the activation complex. This results in an overall increase in the rate constants with the initial pressure increase up to ~ 20 MPa. This phenomenon is similar to gaseous reactions in a gaseous medium with increasing pressure.[92] This pressure region can be considered to be where the supercritical CO_2 is a more gas-like solvent for H_2S. Increasing the pressure even further will eventually get to the point where the reactants are in disadvantage as the caging effect from high-pressure CO_2 are too great, potentially isolating reactants within cages and limiting the adsorption of the reactants. The further increase in pressure also will influence resulting in the positive $\Delta V^{\ddagger}$ by decreasing the volume of reactants even smaller than the activation complex. These effects can slow down the formation of the activation complex from the reactants, and therefore shifting the rate

constant in decreasing manner. This resembles gaseous reactions in a liquid medium, and this pressure region can be considered to be where liquid-like supercritical CO_2 exists with respect to H_2S.

Using Equation 5-7 to calculate $\Delta S^{\ddagger}$, followed by Equation 5-4, the pre-exponential factor was iteratively calculated using Solver in Microsoft Excel to match the entropy of activation at each temperature and pressure. This was necessary because the entropy of activation is negative, which would give $\exp(\Delta S^{\ddagger}/R) = 0$. Inserting Equation 5-4 into the Arrhenius equation yields:

$$k = [(e^2 k_B T/hp) \exp(\Delta S^{\ddagger}/R)] \exp(-E_a/RT) \quad (5\text{-}9)$$

Using the equation above, the rate constants were calculated, and these calculated constants were compared to the rate constants obtained from the experimental study in Table 5-5. The calculated rate constants were in agreement with experimental rate constants.

Table 5-5. The comparison of experimentally obtained and calculated rate constants.

Temperature (K)	Pressure (MPa)	experimental k ($MPa^{-1}\ min^{-1}$)	99.6 % standard error[a] ($MPa^{-1}\ min^{-1}$)	calculated k ($MPa^{-1}\ min^{-1}$)
423.15	10	353	± 33	345
453.15	10	940	± 204	991
483.15	10	2563	± 993	2422
483.15	15	3081	± 691	3589
483.15	20	4757	± 120	4332
423.15	22.5	485	n/a	432
483.15	22.5	4112	n/a	4015
513.15	25	7541	± 1807	7542

[a] 99.6% standard error is from 3 times standard deviation of experimental rate constant.

Combining Equation 5-3 and Equation 5-9, the minimum residence time required to reach equilibrium can be calculated by obtaining k and the fugacity of H_2S at equilibrium.

$$t = \left(\frac{1}{f_{H_2S}} - \frac{1}{f_{H_2S,\,initial}} \right) \left\{ \frac{2}{[(e^2 k_B T/hp)\exp(\Delta S^{\ddagger}/R)]\exp(-E_a/RT)} \right\} \quad (5\text{-}10)$$

Using the S_8 solubility model in high-pressure CO_2, the high-pressure GEM routine of H_2S conversion to S_8, and now using the high-pressure kinetic model of H_2S conversion to S_8, the optimum conditions for removing H_2S of low-quality acid gas can be calculated as shown in Figure 5-4.[12,13] For the low-quality acid gas of 1% H_2S in CO_2, at most 14.3 g Sm^{-3} of solubility is required to dissolve all S_8 converted from 1% H_2S in the stream. This condition corresponds to the black line seen in Figure 5-4. The target conditions should be to the right and/or above this black line if maintaining single-phase reaction is desired. Next, using the updated high-pressure GEM, certain conversion percentages (blue lines) can be plotted depending on the *T* and *p*. Again, the only areas of interest are above the sulfur solubility line (black) as shown by the solid blue lines whereas the dotted the blue lines should be avoided in order to prevent sulfur deposition on the catalyst. Finally, using the kinetic model, the space velocity lines (red lines) were calculated. These red lines, at the *T* and *p*, represent the maximum space velocities allowed to reach the calculated equilibrium by high-pressure GEM. At 563.15 K and 20 MPa, all the produced S_8 should stay dissolved in CO_2, and an H_2S conversion of 94.6 % should be achievable, while the maximum space velocity of 5050 h^{-1} should be allowed. If higher than 97% conversion is desired with a space velocity of 1000h^{-1}, a *T*, *p* condition can be chosen on the red 1000h^{-1} space velocity line, that is still to the right/above the sulfur solubility line (black), but to the left of the 97 % conversion line.

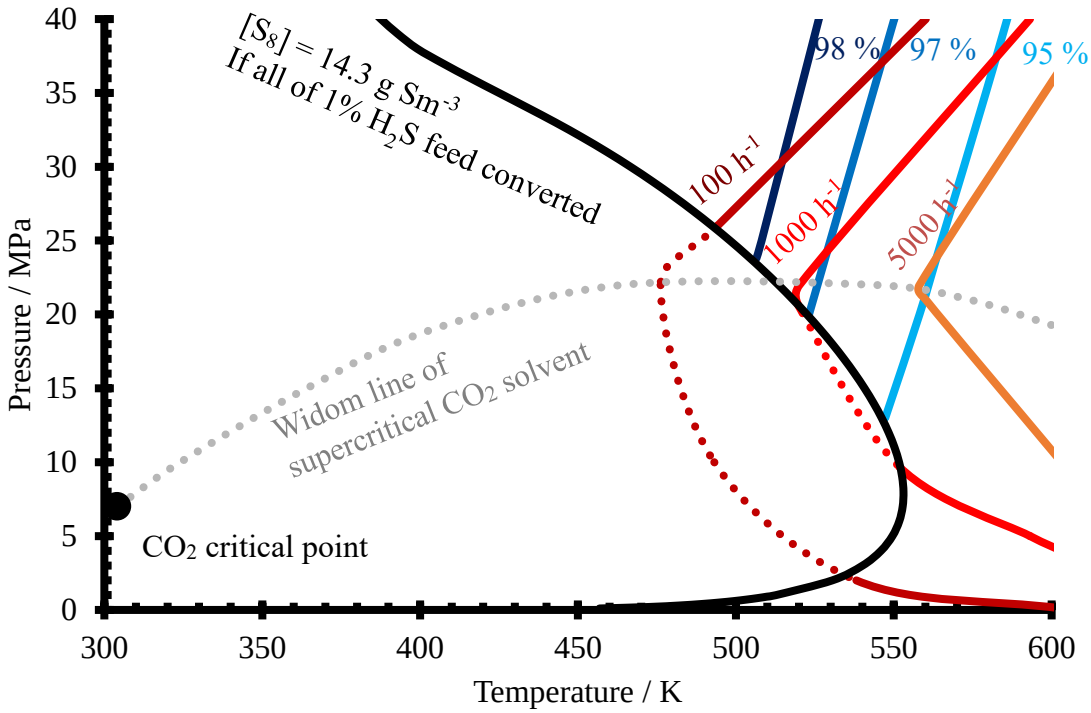

Figure 5-4. Calculated space velocity from the kinetic model. The red lines represent space velocities that can provide enough residence time for the reaction to reach the calculated equilibrium by high-pressure Gibbs Energy Minimization routine. To the right side of the 1000 h^{-1} red line can reach equilibrium while flowing the reaction mixtures above 1000h^{-1}, and to the left side of the red line would require space velocity below 1000h^{-1} to reach equilibrium. The general error between the calculated and experimentally obtained space velocity was around 20 h^{-1}.

Note that Widom line in grey dotted line is also present in Figure 5-4. This line represents the fastest kinetic conditions on the *T* and *p* diagram and where a "phase-transition" between gas-like and liquid-like supercritical CO_2 solvent is occurring for the H_2S oxidation reaction. Above the Widom line is where the high-pressure CO_2 acts as liquid-like supercritical medium for the reaction whereas below the Widom line, the high-pressure CO_2 is more of gas-like supercritical medium for the reaction. As the conditions move away from the Widom line, the kinetics of the H_2S oxidation within high-pressure CO_2 would be slower. This Widom line has an initial increase with increasing temperature

up to ~ 500 K and decreases back down slightly at higher temperatures above 550 K. This is because of the slight viscosity increase of the solution above 550 K shown in Figure 5-5.[58] This viscosity increase results in a lowering pressure conditions of the Widom line at higher temperatures.

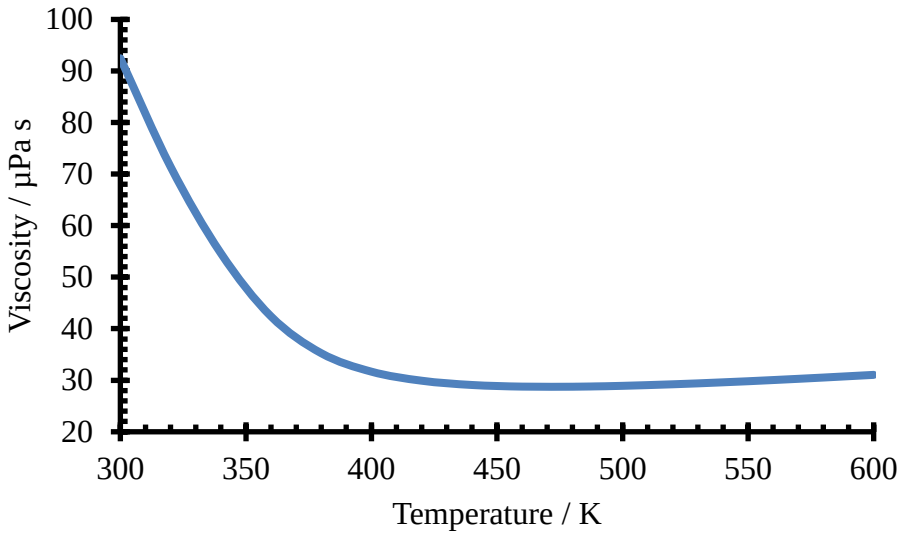

Figure 5-5. Viscosity of 1 % H_2S in CO_2 as a function of temperature at 20 Mpa.

Increasing pressure and lowering the temperature could increase the H_2S conversion further, but the improvement in conversion would come at the cost of either depositing S_8 onto the catalyst surface due to the conditions being below the sulfur dewpoint or slowing down the reaction because of the longer residence time required to establish the calculated equilibrium. For example, at 453.15 K and 25 MPa the H_2S conversion can improve to 99.5 % according to high-pressure GEM calculation.[13] However, the maximum standard space velocity possible calculated from the kinetic model is 20 h^{-1} and the produced S_8 would condense out of high-pressure CO_2 onto the catalysts.[12]

5.4 Conclusions

The oxidation of H_2S in high-pressure CO_2 is suggested as an alternative method to remove H_2S following the cryogenic separation of low-quality acid gas from natural gas sources. The heterogeneous catalytic H_2S oxidation in high-pressure CO_2 was studied to understand the kinetic limitations of dense phase CO_2 and to provide guideline for possible industry implementation. From the measured average rates at T = 423 to 563 K and p = 10 to 25 MPa, several parameters were determined such as the activation energy, pre-exponential factor, and entropy of activation. Increasing temperature was found to increase the rate constants, while increasing pressure increased the rate constants up to ~ 20 MPa whereas above this pressure, the rate constants were found to decreased due to the surface chemical limitation. The kinetic model was constructed by correlating entropy of activation to temperature, pressure, and concentration of H_2S. This kinetic model allowed for calculation of entropy of activation over a range of temperature, pressure, and H_2S concentration which was used to calculate the pre-exponential factor within Arrhenius equation. The rate constants can be calculated from the Arrhenius equation to find the minimum residence time required to reach the H_2S oxidation equilibrium calculated by the Gibbs Energy Minimization calculations at high-pressure. Overall, both experimental and calculated rate constants were in good agreement and supported that either at low-temperatures or high-pressures, the H_2S oxidation within high-pressure CO_2 requires much longer residence time to reach the thermodynamic equilibrium.

Chapter 6: Conclusions and future work

6.1 Conclusions

An alternative process for handling a low-quality acid gas has been discussed in this thesis. The H_2S oxidation in a high-pressure CO_2 fluid improves the equilibrium conversion towards S_8 compared to the low-pressure conversion. It has been demonstrated that high-pressure CO_2 can dissolve more S_8 compared to the low-pressure conditions because of the density increase of supercritical CO_2. This S_8 solubility increase in high-pressure CO_2 allows for the oxidation processes to run at lower temperatures versus an atmospheric pressure process, which improves the conversion by taking the advantage of the exothermic nature of the equilibrium without crossing the dewpoint. In addition, the higher acid gas pressure can improve the reaction rate until the pressure condition of the CO_2 solvent reaches the Widom line. For pressure conditions above the Widom line, the dense liquid-like CO_2 starts to limit the adsorption of the reactants to the active sites and/or decrease the rate of the reaction at the surface with further increase in pressure. As the activation energy is not different with larger pressure, this limitation in the surface rate due to a lower pre-exponential factor (less collisions) caused by (a) lower surface adsorption or surface concentration and/or (b) lower surface mobility.

The best conditions for the produced S_8, while still maintaining a single-phase within high-pressure CO_2, were studied with the custom-built saturation system to define conditions that would prevent catalyst fouling by sulfur deposition. The conditions for the solubility tests were at T = 323.75 to 424.05 K and at p = 10 and 20 MPa. High-temperatures and high-pressures were related to higher S_8 solubility in CO_2 due to the

higher vapour pressure of S_8 and the dense CO_2 solvent. The experimental S_8 solubilities in CO_2 were in good agreement with the most recent solubility data from literature.[79] Both a truncated Virial equation and Fluctuation Solution Theory correlation were fit to the experimental data to model the sulfur fugacity coefficient in high-pressure CO_2. Fluctuation Solution Theory provided a comparable correlation for the solubilities, and a more physically realistic extrapolation to higher density CO_2. Vapour-liquid equilibrium lines can now be calculated from the solubility model over a range of temperature and pressure. These vapour-liquid-equilibrium lines were used as guidelines for carrying out the H_2S oxidation reaction conditions without condensing S_8 out of CO_2 streams. The solubility model was also used to provide the fugacity coefficients of S_8 within dense CO_2 for the modification of Gibbs Energy minimization routine at high-pressure.

A custom heterogeneous catalytic system was built to study the best conditions required to oxidize low-levels of H_2S within high-pressure CO_2. The equilibria of H_2S + O_2 to S_8 and H_2O were studied above the S_8/CO_2 phase pocket to improve the sulfur recovery while maintain a single-phase reaction. The experimental oxidation results were obtained by flowing high-pressure mixtures of $[H_2S]$ = 0.5 to 1.7 % at T = 493.15 o 563.15 K, p = 10 & 20 MPa, and standard space velocity = 3800 to 9300 h^{-1} over Al_2O_3, TiO_2 and TiO_2 doped Al_2O_3 catalyst materials. The experimental equilibrium conversions of H_2S were compared to the high-pressure Gibbs Energy Minimization routine which was modified to accurately calculate theoretical equilibrium composition at high-pressures. The modification of a previously existing in-house ideal gas Gibbs Energy Minimization routine was accomplished by incorporating fugacity coefficients of various chemical species (including S_8 fugacity coefficients from Fluctuation Solution Theory) involved in

the equilibrium under high-pressure CO_2. Increasing pressure and decreasing temperature increased the conversion of H_2S to S_8 by 12 % at 550 K by increasing the total pressure from 0.1 MPa to 20 MPa according to both experimental and calculated results.

In an attempt to increase the sulfur recovery even further, temperatures inside the S_8/CO_2 phase pocket and higher pressures were also explored, which resulted in finding out the kinetic limitations of surface chemical steps at low-temperatures and high-pressures. Finally, the kinetics of H_2S oxidation in high-pressure CO_2 were studied at T = 423 to 563 K and p = 10 to 25 MPa with standard space velocity = 860 to 6330 h^{-1} over γ-alumina. The experimentally obtained kinetically limited conversion results were used to develop a model which can calculate the minimum residence time required to establish the calculated equilibrium conversion within high-pressure CO_2. In the process of developing the kinetic model, a Widom line was found, which connects entropy of activation maxima versus temperature and pressure. This Widom line corresponds to the fastest possible kinetic conditions for H_2S conversion within CO_2.

Overall, three applicable models were obtained from this thesis, S_8 solubility in high-pressure CO_2, high-pressure H_2S equilibrium oxidation conversion to S_8, and the kinetic model to calculate the minimum residence time for the equilibrium to establish over a range of temperature, pressure, and [H_2S]. These three models can be used to calculate potential operation conditions for the high-pressure H_2S oxidation within CO_2, which can provide guideline for a possible industry implementation of the process proposed in this thesis.

6.2 Future work

The kinetically limited results for H_2S oxidation in HP CO_2 were only carried out with γ-alumina catalyst, which is one of the most common catalyst used for such processes. Thus, the kinetic model described in this thesis only applies for γ-alumina and may be different for different catalysts. Any change will most likely be due to variable surface area, but the kinetics of the reaction may be affected by other factors. Future kinetic studies can include other commonly used catalysts such as titania.

The only mixture studied in the kinetic part of the thesis was 1% H_2S in CO_2, because it was the first target concentration for low-level acid gas and large enough to obtain reasonable analytic results. While the kinetic model did include the concentration of H_2S in CO_2 in molality, it was never experimentally confirmed for other initial H_2S concentrations. Experimental confirmation with various concentrations of H_2S can increase the versatility of the kinetic model over a wide range of [H_2S].

In the kinetic study, the kinetic limitation region was not completely determined to see which processes were contributing to the kinetic limitation. While a preliminary experiment showed that the diffusion process was not the limiting factor, and the experimentally obtained activation energy suggested that the surface chemical process was a limiting factor. However, the presence of high-pressure CO_2 can influence the kinetic limitation region to be in the intermediate of chemical and diffusional limited processes (**Figure 2-3**). A further study is recommended to determine if the kinetic limitation is either only the surface chemical process or the combination of the surface chemical and diffusional processes.

This thesis focused on the best conditions for the heterogeneous catalysis of H_2S oxidation within high-pressure CO_2, which was to provide a guideline for processing conditions within the catalytic stage. However, the downstream of the catalytic stage will also need to include the separation of produced S_8 from CO_2. The conditions are defined from the solubility studies that can condense most of S_8 out of CO_2, but the methods to separate these potentially marketable products have not been explored yet. Separation by condensation of sulfur liquid may be possible just below 400 K, according to Figure 3-4 in Chapter 3. For the 1% H_2S, more than 99% of converted S_8 should be condensed out of the supercritical CO_2.

If propane and butane are present in the raw sour natural gas, a cryogenic distillation may not be sufficient to separate these hydrocarbons and the acid gas due to the similarity in volatilities. Cryogenic separation of frozen acid gas and liquid butane and propane may be possible, or a Ryan-Holmes process can be utilized. The Ryan-Holmes process modifies the relative volatility of CO_2 with respect to H_2S by using a hydrocarbon-based additive like *n*-butane.[131] This can be an advantage if butane is already present within the feed gas, because the additive used in the Ryan-Holmes process may be no longer additive. Although these processes may allow for the bulk separation of acid gas, producing the purest acid gas is a challenge when impurities are present in the feed fluid.

Another future study could be carrying out the oxidation of H_2S with the impurities present. Promoting a complete oxidation of trace propane and butane in addition to the oxidation of H_2S may be possible by adding additional stoichiometric amount O_2, but this will reduce the overall H_2S conversion from extra water produced. Extra CO_2 produced from the combustion may also dilute the reactants and reduce the rate of the reaction. The

presence of the hydrocarbons over the heterogeneous catalysis of H_2S run into problems such as catalyst fouling, unwanted by-product from incomplete oxidation of hydrocarbons. These problems can further decrease the catalytic efficiency and the H_2S conversion efficiency.

Appendix

A.1 Statement of contribution

Co-author contribution (Dr. Marriott)

Dr. Marriott has contributed in the development, supervision and publication of all the work presented in this thesis. His support has been critical in this thesis with feedback, technical knowledge, proofreading and submission of all manuscripts.

Co-author contribution (Mr. Connor Deering)

Mr. Deering has co-author publications presented in this thesis. His understanding of physical chemistry has been crucial in helping me to understand the relationship between thermodynamic properties and mathematical models. Connor also completed the thermogravimetric analysis in the Chapter 4. Mr. Deering has always provided great feedback for all my work and proofread all manuscripts and this thesis.

Co-author contribution (Mr. Mitchell Stashick)

Mr. Stashick has co-authored the manuscript presented in Chapter 4. Mr. Stashick helped me carry out the carbon content analysis in the produced elemental sulfur. He also provided a lot of feedback for ideas and understandings of many aspects in this thesis.

Co-author contribution (Mrs. Nancy Chou)

Mrs. Chou has co-authored the manuscript presented in Chapter 4. Mrs. Chou completed the ion chromatography in the Chapter 4. She has been a great help throughout the analytical aspects in this thesis.

A.2 Residual sulfur from CS_2

The amount of residual sulfur from evaporated CS_2 was quantified by evaporating different amounts of CS_2 in beakers. The residue from CS_2 evaporation was quantified by the sulfur quantification analysis discussed in the Chapter 3. The amount of sulfur quantified was related to the amount of CS_2 evaporated to result in the Figure A-3.

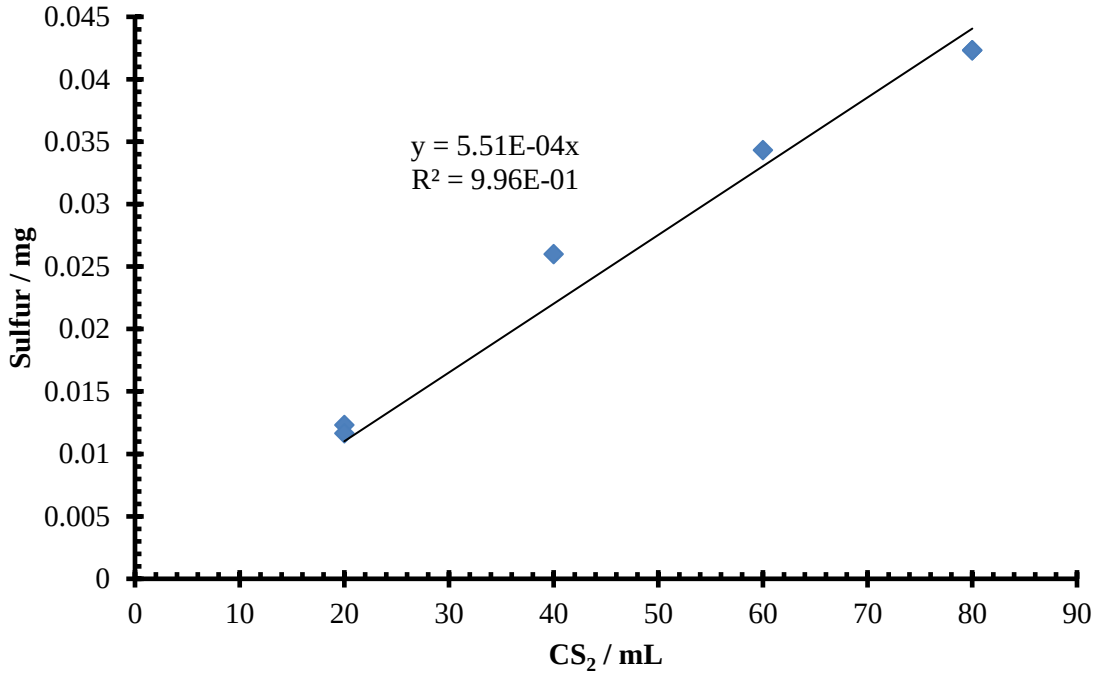

Figure A-3. The residual amount of sulfur from the evaporated CS_2.

For every mL CS_2 used and evaporated, there was 5 μg residual sulfur. While these are very small amounts, using a large quantity of CS_2 to dissolve and recovery all the sulfur can add a significant amount of extra sulfur to the solubility value. The amount of sulfur originated from CS_2 evaporation was subtracted from the sulfur solubility value in CO_2.

A.3 LabVIEW interface

Measurement and controlling of the custom-built systems were achieved by LabVIEW, which is a graphical programming language. LabVIEW enabled the integration of the experimental components into a single control panel and allowed the user to operate and read from multiple devices. Figure A-2 shows what the control panel displayed including the instrument controls and data collection from the platinum resistance thermometer, pressure transducer, and poppet valve.

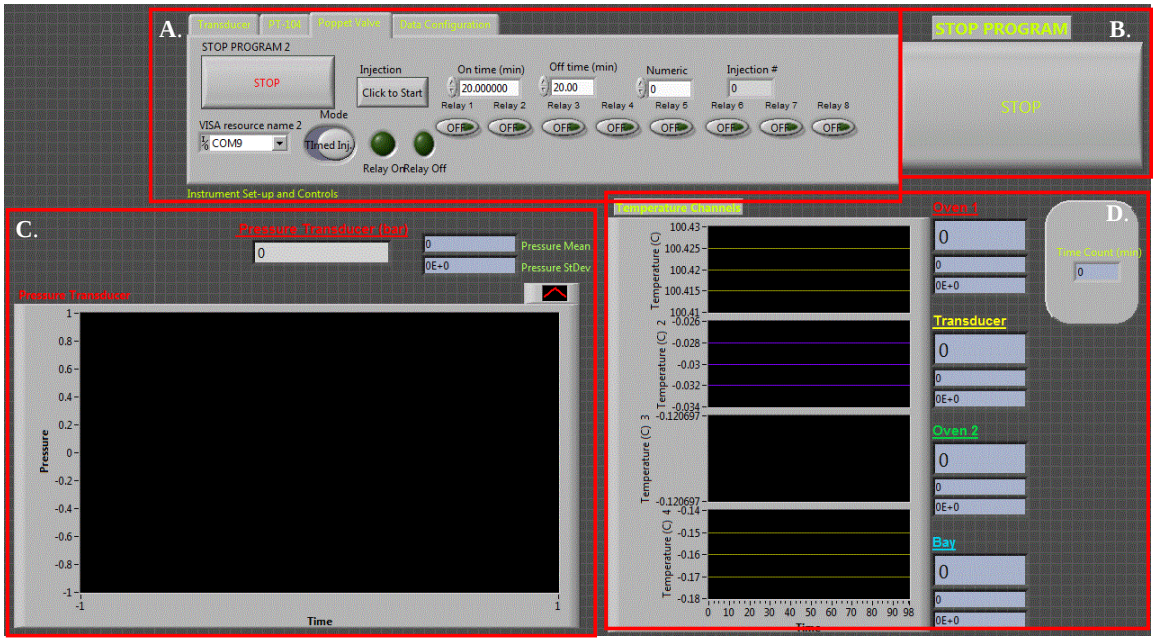

Figure A-2. LabVIEW front control panel for the custom-built sulfur saturation system: A. tabbed controls for device communication and data configuration. B. program shut-off. C. live-update plot of pressure measurement from the pressure transducer. D. live-update plot of temperature measurement from platinum resistance thermometer.

For the sulfur solubility experiments, the poppet valve was set to go on at intervals. For the heterogeneous catalysis, the poppet valve control was modified to trigger at a certain pressure.

A.4 GC calibration

The calibration for [H_2S] was initially done every 3-6 months to achieve the calibration curve shown in Figure A-1. However, following the initial calibration results, it was determined that there was a sulfur deposition issue in the valve that controlled the mixture flow towards the bypass in Figure 3-1. Since there was a good understanding in the [H_2S] of reaction effluents and its response factor after the catalytic reactor, the calibration was no longer necessary unless there was an observed anomaly in the response of H_2S during subsequent experiments.

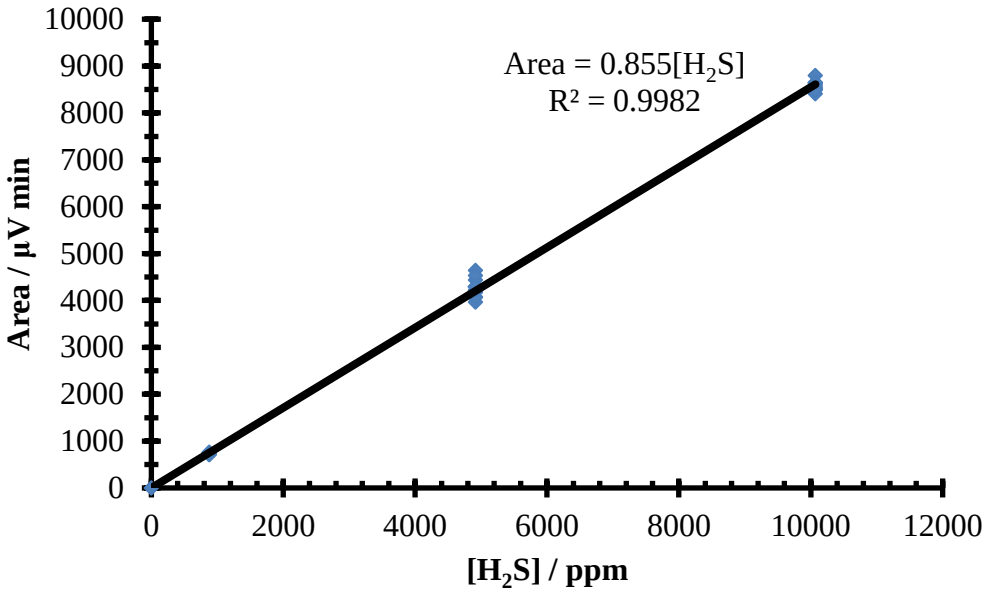

Figure A-1. Gas chromatography response area against H_2S concentrations.

Response factors of other species were found by a single point calibration, the response factors are being shown in Table A-1.

Table A-1. Gas Chromatography response factors for chemical species. Concentrations of species can be calculated by dividing the area with response factor.

Concentration / ppm	Response factor
O_2	Area/0.759
H_2S	Area/0.855
COS	Area/0.499
SO_2	Area/0.982

A.5 Copyright permission

Reprinted with permission from { Lee, S.; Deering, C. E.; Stashick, M. J.; Chou, N.; Marriott, R. A., Experimental high-pressure hydrogen sulfide partial oxidation and equilibrium calculation by Gibbs Energy Minimization. *Ind. Eng. Chem. Res.* **2020**, 59 (45), 19890-19896.}. Copyright {2020} American Chemical Society.

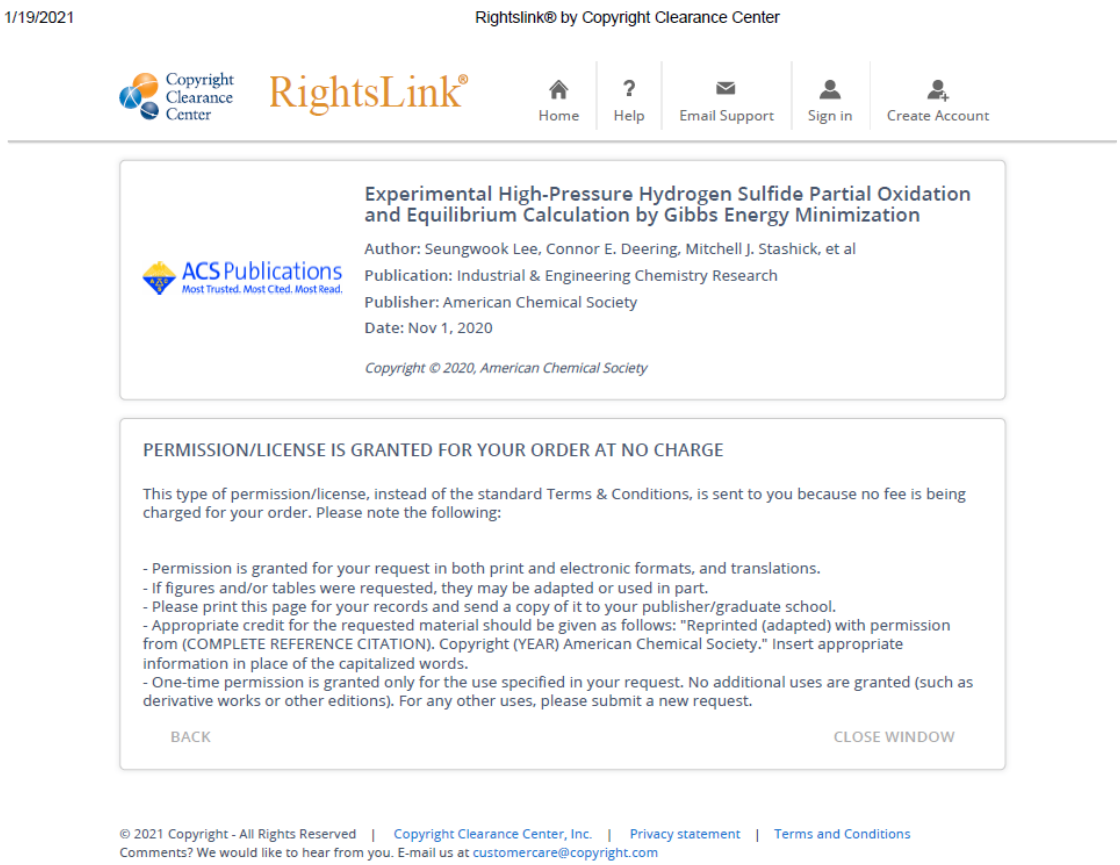

Bibliography

[1] BC Oil and Gas Commission. Hydrocarbon and By-Product Reserves Report January-December 2012. http://www.bcogc.ca/node/11111/download (accessed April 2, 2018).

[2] Marriott, R. A.; Pirzadeh, J. J.; Marrugo-Hernandez, J. J.; Raval, S, Hydrogen sulfide formation in oil and gas. *Can. J. Chem*. **2016**, 94, 406-413.

[3] Tyndall, K.; McIntush, K.; Lundeen, J.; Fisher, K.; Beitler, C., When is CO_2 more hazardous than H_2S. *Hydrocarb. Process* **2011,** *90* (1), 45-48.

[4] TransCanada, Gas Quality Specification TransCanada and other pipelines, 2010. http://www.tccustomerexpress.com/docs/Gas_Quality_Specifications_Fact_Sheet.pdf (accessed Aug 7, 2018).

[5] Malik, Q. M.; Islam, M. R., CO_2 Injection in the Weyburn Field of Canada: Optimization of Enhanced Oil Recovery and Greenhouse Gas Storage With Horizontal Wells. In Improved Oil Recovery Symposium, Society of Petroleum Engineers: Tulsa, Oklahoma, 2000.

[6] Thomas, S., Enhanced oil recovery - An overview. *Oil Gas Sci. Technol.* **2008**, 63 (1), 9-19.

[7] Beckman, E.J. Supercritical and near-critical CO_2 in green chemical synthesis and processing. *J. Supercrit. Fluids* **2004**, 28, 121-191.

[8] Dalrymple, D. A.; Trofe, T. W.; Evans, J. M., Liquid redox sulfur recovery options, costs, and environmental considerations. *Environmental Progress* **1989**, 8 (4), 217-222.

[9] Kelley, B. T.; Valencia, J. A.; Northrop, P. S.; Mart, C. J., Controlled Freeze Zone™ for developing sour gas reserves. *Energy Procedia* **2011**, 4, 824-829.

[10] Lallemand, F.; Lecomte, F.; Streicher, C., Highly Sour Gas Processing: H_2S Bulk Removal With the Sprex Process. International Petroleum Technology Conference, Doha, Qatar, 2005.

[11] Terrien, P.; Dubettier, R.; Leclerc, M.; Meunier, V. Engineering of air separation and Cryocap^{TM} units for large size plants, Oxyfuel Combustion Conference, Ponferrada, Spain, 9-13 Sept, 2013; Ponferrada, Spain, 2013.

[12] Lee, S.; Marriott, R. A., Solubility of Elemental Sulfur in Dense Phase Carbon Dioxide from T = 324 to 424 K and p = 10 and 20 MPa. *J. Natural Gas Eng.* **2018**, 3 (1), 62-73.

[13] Lee, S.; Deering, C. E.; Stashick, M. J.; Chou, N.; Marriott, R. A., Experimental high-pressure hydrogen sulfide partial oxidation and equilibrium calculation by Gibbs Energy Minimization. *Ind. Eng. Chem. Res*. **2020**, 59 (45), 19890-19896.

[14] Kohl, A. L.; Nielsen, R. B., In Gas Purification, 5th ed.; Gulf Professional Publishing: Houston, 1997.

[15] Bernardo, P.; Drioli, E.; Golemme, G., Membrane Gas Separation: A Review/State of the Art. *Ind. Eng. Chem. Res.* **2009**, 48 (10), 4638-4663.

[16] Tagliabue, M.; Farrusseng, D.; Valencia, S.; Aguado, S.; Ravon, U.; Rizzo, C.; Corma, A.; Mirodatos, C., Natural gas treating by selective adsorption: Material science and chemical engineering interplay. *Chem. Eng. J.* **2009**, 155 (3), 553-566.

[17] Faiz, R.; Al-Marzouqi, M., Insights on natural gas purification: Simultaneous absorption of CO_2 and H_2S using membrane contactors. *Sep. Purif. Technol.* **2011**, 76 (3), 351-361.

[18] Mandal, B. P.; Biswas, A. K.; Bandyopadhyay, S. S. Selective absorption of H_2S from gas streams containing H_2S and CO2 into aqueous solutions of N-methyldiethanolamine and 2-amimno-2-methyl-1-propanol. *Sep. Purif. Technol.* **2004**, 35 (3), 191-202.

[19] Office of FOSSIL ENERGY. Pre-Combustion Carbon Capture Research. https://www.energy.gov/fe/science-innovation/carbon-capture-and-storage-research/carbon-capture-rd/pre-combustion-carbon#:~:text=Today's%20commercially%20available%20pre%2Dcombustion,cycle%20(IGCC)%20power%20plant. (accessed January 18, 2021).

[20] Energy & Environmental Research Center. Estimating the Cost to Capture, Comress, and Transport CO_2 from Stationary Sources in the PCOR Partnership Region. https://undeerc.org/pcor/technicalpublications/pdf/TP-2010-Cost-Capture-Compress-Transport-CO2-Stationary-Sources-PCOR.pdf . (accessed January 18, 2021).

[21] Campbell, J. M., Gas conditioning and processing. Campbell Petroleum Series: 1982; Vol. 4.

[22] Linstrom, P. J.; Mallard, W. G., Eds., NIST Chemistry WebBook, NIST Standard Reference Database Number 69, National Institute of Standards and Technology, Gaithersburg MD, 20899, http://webbook.nist.gov, (retrieved May 19, 2016).

[23] Koytsoumpa, E. I.; Bergins, C.; Kakaras, E., The CO_2 economy: Review of CO_2 Capture and resue technologies. *J. Supercrit. Fluids*, **2018**, 132, 3-16.

[24] Guvelioglu, G. H.; Higginbotham, P.; Palamara, J. E.; Arora, G.; Mamorsh, D. L.; Fisher, K. S., H_2S Removal from CO_2 by Distillation. In Laurance Reid Gas Conditioning Conference, Norman, Oklahoma, 2015.

[25] Naber, J.; Wesselingh, J.; Groenendaal, W., Sulfur developments: new Shell process treats Claus off-gas. *Chem. Eng. Prog.* **1973**, 69, (12).

[26] van Nisselrooy, P. F. M. T. and Lagas, J. A. Superclaus reduces SO2 emission by the use of a new selective oxidation catalyst. *Catal. Today* **1993**, 16, 263-271.

[27] Lagas, J. A.; Borsboom, J.; Berben, P. H. "The Superclaus Process," 38th Annual Laurance Reid Gas Conditioning Conference, Proceedings Addendum, Univ. of Oklahoma, Norman, Oklahoma (Mar. 7-9, 1988), pp 41-59.

[28] Gamson, B.; Elkins, R., Sulfur from hydrogen sulfide. *Chem. Eng. Progress* **1953**, 49 (4), 203-215.

[29] Chase, M. W., NIST-JANAF Thermochemical Tables, 4th edition. *J. Phys. Chem. Ref. Data* **1998**, 9, 1-1951.

[30] Laidler, Keith J., and John H. Meiser. *Physical Chemistry*. Menlo Park, California, Benjamin/Cummings, 1982.

[31] White, W. B.; Johnson, S. M.; Dantzig, G. B., Chemical equilibrium in complex mixtures. *J. Chem. Phys.* **1958**, 28 (5), 751-755.

[32] Monnery, W. D. In Geothermal Steam Economic H_2S Abatement and Sulphur Recovery, Proceedings of the World Geothermal Congress, 2005.

[33] Savin, S.; Nougayrede, J. In 99.9% Sulphur Recovery with a New Version of Sulfreen Process, International Gas Research Conference, Government Institutes Inc.: 1995; 352-360.

[34] Goddin, C. S.; Hunt, E. B.; Palm, J. W., CBA process ups Claus recovery. [Amoco cold bed adsorption process]. *Hydrocarb. Process.* **1974**, 53 (10) 122-24.

[35] Heigold, R. L. and Berkeley, D. E., Pine River uses 4-converter as MCRC sub-dewpoint for sulphur recovery. *Oil Gas J.* **1983**, 81 (37), p. 1156.

[36] Nichol, R. J.; Sapiro, R. H. Purification of gases. 1965.

[37] Wermink, W. N. Development and design of the in-situ regeneration section of Vitrisol®, a novel, highly selective desulphurization process. PhD thesis, University of Groningen, The Netherlands, 2019.

[38] Greenwood, N. N.; & Earnshaw, A. *Chemistry of the Elements*, 2nd ed.; Oxford: Butterworth-Heinemann. 1997

[39] Chisholm, H. Brimstone. In *Encyclopedia Britannica*. 11th ed.; Cambridge University Press. 1911, 4, 571.

[40] Eow, J. S. Recovery of sulfur from sour acid gas: A review of the technology, *Environmental Progress* **2002**, 21 (3), 143–162.

[41] Marriott, R. A.; Wan, H. H., Standard values of fugacity for sulfur which are self-consistent with the low-pressure phase diagram. *J. Chem. Thermodyn.* **2011**, 43 (8), 1224-1228.

[42] Steudel, R.; Eckert, B., Solid Sulfur AllotropesSulfur Allotropes. In *Elemental Sulfur and Sulfur-Rich Compounds I*, Steudel, R., Ed. Springer Berlin Heidelberg: Berlin, Heidelberg, 2003; 1-80.

[43] Sofekun, G. O.; Evoy, E.; Lesage, K. L.; Chou, N.; Marriott, R. A., The rheology of liquid elemental sulfur across the λ-transition, *J. Rheology* **2018**, 62 (2), 469-476.

[44] Stashick, M. J. and Marriott, R. A. Viscoelastic behavior corresponding to reptative relation times across the λ-transition for liquid elemental sulfur, *J. Chem. Phys.* **2020**, 152, 044503.

[45] Stashick, M. J.; Sofekun, G. O. and Marriott R. A. Modifying effects of hydrogen sulfide on the rheometric properties of liquid elemental sulfur. *AIChE J*, **2020**, 66 (6), e16225.

[46] Marriott, R. A. and Fitzpatrick, E. Physical sulfur solevents I: the sulfur solubility in BTX and a general solubility equation for physical sulfur solvents, ASRL QB. XLV, 2008, No. 1, 1-24.

[47] Meyer, B. Elemental sulfur *Chem. Rev.* **1976**, 76 (3), 367-388.

[48] Apodaca, L. E. Sulfur, U.S. Geological Survey, Mineral Commodity Summaries, January 2020

[49] Nehb, W.; Vydra, K. Sulfur. In *Ullmann's Encyclopedia of Industrial Chemistry*, Weinheim: Wiley-VCH Verlag GmbH & Co. KGaA; 2006; vol. 1. 1-32.

[50] Lindenmann, J.; Matzi, V.; Neuboeck, N.; Ratzenhofer-Komenda, B.; Maier, A; Smolle-Juettner, F. M. Severe hydrogen sulphide poisoning treated with 4-dimethylaminophenol and hyperbaric oxygen. *Diving and Hyperbaric Medicine* **2010**, 40 (4), 213–217.

[51] Lewis, R.J. (1996). *Sax's Dangerous Properties of Industrial Materials*, 9th ed. NewYork; Van Nostrand Reinhold. 1996.

[52] Apodaca, L. E. Sulfur, U.S. Geological Survey, Minerals Yearbook. 2017

[53] King, M. J.; Davenport, W. G.; Moats, M. S. *Sulfuric Acid Manufacture: Analysis, Control and Optimization*, 2nd ed., Elsevier Ltd. 2013.

[54] Oae, S. *Organic Chemistry of Sulfur*, New York: Springer U.S. 1977.

[55] Qiancheng, M. In *Greenhouse Gases: Refining the Role of Carbon Dioxide*, NASA Science Briefs. March, 1998.

[56] Susan T. Carbon Dioxide. In *Ullmann's Encyclopedia of Industrial Chemistry*, Weinheim: Wiley-VCH Verlag GmbH & Co. KGaA 2005.

[57] Span, R.; Wagner, W., A new equation of state for carbon dioxide covering the fluid region from the triple-point temperature to 1100 K at Pressures up to 800 MPa. *J. Phys. Chem. Ref. Data* **1996**, 25 (6), 1509-1596.

[58] Lemmon, E. W.; Huber, M. L.; McLinden, M. O., NIST Standard Reference Database 23: Reference Fluid Thermodynamic and Transport Properties-REFPROP, Version 8.0, National Institute of Standards and Technology, Standard Reference Data Program. Gaithersburg, 2007.

[59] Minder, B.; Mallat, T.; Baiker, *A. Enantioselective hydrogenation in supercritical fluids. Limitations of the use of supercritical* CO_2. Proceedings of the Third International Symposium on High-pressure Chemical Engineering, Zurich, 1996, 139-144.

[60] Li, Z.; Mayer, R. J.; Ofial, A. R.; Mayr, H. From Carbodiimides to Carbon Dioxide: Quantification of the Electrophilic Reactivities of Heteroallenes. *J. Am. Chem. Soc.* **2020**, 142 (18), 8383–8402.

[61] Raventós, M.; Duarte, S.; Alarcón, R. Application and Possibilities of Supercritical CO_2 Extraction in Food Processing Industry: An Overview, *Food Sci. Tech. Int.* **2002**, 8 (5), 269-284

[62] Park, H.S.; Choi, H.; Lee, S.J.; Park, K.W.; Choi, S.; Kim, K.H. Effect of mass transfer on the removal of caffeine from green tea by supercritical carbon dioxide, *J. Supercrit. Fluids* **2007**, 42 (2), 205-211.

[63] Hazekamp, A.; Simmons, R.; Peltenburg-Looan, A.; Sengers, M.; van Zweden, R.; Verpoorte, R. Preparative isolation of Cannabinoids from Cannabis sativa by centrifugal partition chromatography. *J. Liq. Chromatogr. Relat. Technol.* **2004**, 27, 2421-2439.

[64] Mendes, R. L.; Reis, A. D.; Pereira, A. P.; Cardoso, M. T.; Palavra, A. F.; Coelho, J. P. Supercritical CO_2 extraction of alpha-linolenic acid (GLA) from the cyanobacterium Arthrospira (Spirulina) maxima: experiments and modeling, *Chem. Eng. J.* **2005**, 105, 147-152.

[65] Reverchon, E. Supercritical fluid extraction and fractionation of essential oils and related products, *J. Supercrit. Fluids* **1994**, 10, 1-37.

[66] Reverchon, E.; De Marco, I. Supercritical fluid extraction and fractionation of natural matter, *J. Supercrit. Fluids* **2006**, 38, 146-166.

[67] Sovova, H. Mathematical model for supercritical fluid extraction of natural products and extraction curve evaluation, *J. Supercrit. Fluids* **2005**, 33, 35-52.

[68] Sovova, H.; Sajfrtova, M.; Opletal, L. Near-critical extraction of pigments and oleoresin from stinging nettle leaves, *J. Supercrit. Fluids* **2004**, 30, 213-224.

[69] Zizovic, I.; Stamenic, M.; Orlovic, A.; Skala, D. Supercritical carbon dioxide extraction of essential oils from plants with secretory ducts: mathematical modeling on the micro-scale, *J. Supercrit. Fluids* **2007**, 39, 338-346.

[70] Perrotin-Brunel, H.; Cabeza Perez, P.; van Roosmalen, M. J. E.; van Spronsen, J.; Witkamp, G.-J.; Peters, C. J. Solubility of [Δ]9- tetrahydrocannabinol in supercritical carbon dioxide: Experiments and modeling. *J. Supercrit. Fluids* **2010**, 52, 6–10

[71] Gelbein, A. P. Thinking out of the box, *Chemtech*. **1998**, 28 (9), 1.

[72] Hancu, D., & Beckman, E.J. Generation of Hydrogen Peroxide in Liquid CO_2. I. Design, Synthesis and Phase Behavior of CO_2-philic Anthraquinones. *Ind. Eng. Chem. Res.*, **1999**, 38 (7), 2824-2932

[73] Zabetakis, M. G. Flammability and Characteristics of Combustible Gases and Vapors. Bureau of Mines Bulletin, 1965, 627.

[74] Hancu, D. and Beckman, E. J. Generation of hydrogen peroxide directly from H_2 and O_2 using CO_2 as the solvent, *Green Chem.* **2001**, 3, 80-86

[75] Pande, J. O. and Tonheim, J. Ammonia plant NII: Explosion of hydrogen in a pipeline for CO_2, *Process Safety Progress*, **2001**, 20 (1), 37–39.

[76] Holm L.W. Carbon dioxide Solvent Flooding for Increased Oil Recovery, *Trans. AIME* **1959**, 216, 225-231.

[77] Subramaniam, B. Enhancing the stability of porous catalysts with supercritical reaction media. *Appl. Catal. A*: *Gen.* **2001**, 212 (1-2) 199-213

[78] Rodriguez, F. *Principles of Polymer Systems*, 4th ed., McGraw-Hill: New York, 1996.

[79] Serin, J. P.; Jay, S.; Cezac, P.; Contamine, F.; Mercadier, J.; Arrabie, C.; Legros-Adrian, J. M., Experimental studies of solubility of elemental sulphur in supercritical carbon dioxide. *J. Supercrit. Fluid* **2010**, 53 (1-3), 12-16.

[80] Gu, M. X.; Li, Q.; Zhou, S. Y.; Chen, W. D.; Guo, T. M., Experimental and modeling studies on the phase-behavior of high-H_2S content natural gas mixtures. *Fluid Phase Equilibria* **1993**, 82, 173-182.

[81] Kennedy, H. T.; Wieland, D. R., Equilibrium in the methane - carbon dioxide - hydrogen sulfide - sulfur System. *Trans. Am. Inst. Min. Met. Eng.* **1960**, 219 (7), 166-169.

[82] Bartlett, P. D.; Meguerian, G., Reactions of elemental sulfur. 1. The uncatalyzed reaction of sulfur with triarylphosphines. *J. Am. Chem. Soc.* **1956**, 78 (15), 3710-3715.

[83] Clark, P. D.; Lesage, K. L., Quantitative-determination of elemental sulfur in hydrocarbons, soils, and other materials. *J. Chromatogr. Sci.* **1989**, 27 (5), 259-261.

[84] McGregor, D. E.; Dalla Lana, I. G.; Liu, C. L.; Cormode, A. E. *A Kinetic Study of the Catalytic Reaction of H_2S and SO_2 to Elemental Sulfur*, Proc. 4th Euro/2nd Int. Symp. Chem. React. Eng., Elsevier, Amsterdam, 1972, B2, 9-12.

[85] Dalla Lana, I. G.; Liu, C. L.; Cho, B. K. *The Development of a Kinetic Model for Rational Design of Catalytic Reactors in the Modified Claus Process*, Proc. 6th Euro/4th Int. Symp. Chem. React. Eng., Dechema. Frankfurt. 1976, V 196-205.

[86] George, Z. M. Kinetics of cobalt-molybdate-catalyzed reactions of SO_2 with H_2S and Cos and the hydrolysis of COS, *J. Catal.*, **1974**, 32 (2), 261-271.

[87] Liu, C.L. Ph.D. Dissertation, University of Alberta, Edmonton, Alberta, Canada, 1978.

[88] Quft, C.; Tellier, J.; Voirin, R. Poisoning of Claus Catalyes Sy Sulphation. *Stud. Surf. Sci. Catal.* **1980**, 6, 323-329.

[89] Razzaghi, M. and Dalla Lana, I. G. Calculation of effectiveness factor for multiple claus reactions with single-step rate-controlling. *Can. J. Chem. Eng.* **1984**, 62 (3) 413-418.

[90] Elmasry, H. A. The Claus reaction: Effect of forced feed composition cycling. *Appl. Catal.* **1985**, 16 (3), 301-313.

[91] Birkholz, R. K. O.; Behie, L. A. and Dalla Lana, I. G. Kinetic modelling of a fluidized bed claus plant. *Can. J. Chem. Eng.* **1987**, 65 (5), 778-784.

[92] Dowling, N. I.; Marriott, R. A.; Primak, A.; Manley, S., The kinetics of H_2S oxidation by trace O_2 and prediction of sulfur deposition in acid gas compression systems. *In Sour Gas and Related Technologies*, John Wiley & Sons, Inc.: 2012; 183-214.

[93] Mendioroz, S.; Munoz, V.; Alvarez, E.; Palacios, J. M. Kinetic study of the Claus reaction at low temperature using γ-alumina as catalyst. *Appl. Catal. Gen.* **1995**, 132, 111-126.

[94] Davydov, A. A.; Marshneva, V. I.; Shepotko, M. L. Metal oxides in hydrogen sulfide oxidation by oxygen and sulfur dioxide: I. The comparison study of the catalytic activity. Mechanism of the interactions between H_2S and SO_2 on some oxides. *Appl. Catal. A*: *Gen.* **2003**, 244 (1), 93-100.

[95] Bahman, Z. An investigation on the most important influencing parameters regarding the selection of the proper catalysts for Claus SRU converters. *J. Ind. Eng. Chem.* **2009**, 15, 143-147.

[96] Mora, R. L. Sulphur condensation influence in Claus catalyst performance. *J. Hazard Mater*. 2000, 79 (1), 103-115

[97] Maglio, A. and Schubert, P.F., New Claus catalyst tests accurately reflect process conditions, *Oil Gas J*. **1988**, 86 (37), 85–90.

[98] Bartholomew, C. H.; Farrauto, R. J., *Fundamentals of Industrial Catalytic Processes*, 2nd ed., John Wiley & Sons, Inc.; New Jersey, 2006.

[99] Satterfield, C. N. *Heterogeneous Catalysis in Industrial Practice*, 2nd ed., McGraw-Hill; New York, 1991.

[100] Mars, P. and van Krevelen, D. W. Oxidations carried out by means of vanadium oxide catalysts, *Chem. Eng. Sci.* **1954**, 3 (1), 41-59.

[101] Mars, P. and Maessen, J. G. H. The mechanism and the kinetics of sulfur dioxide oxidation on catalysts containing vanadium and alkali oxides, *J. Catal*. **1968**, 10 (1), 1-12.

[102] Clark, P.; Dowling, N.; Huang, M.; Okamona, O.; Butlin, G.; Hou, R.; Kijlstra, W., Studies on Sulfate Formation during the Conversion of H_2S and SO_2 to Sulfur Over Activated Alumina. *Appl. Catal. A*, **2002**, 235, 61-69.

[103] Ertl, G., Ammonia Synthesis-Heterogeneous, in *Encyclopedia of Catalysis*, Ed. I. T. Horvath. John Wiley & Sons, New Jersey, vol. 6, pp. 329-352. 2003

[104] Anderson, R. B. *The Fischer-Tropsch Synthesis*. Academic Press, Orlando, Florida, 1984.

[105] Compton A.; Bincaz I. and Bermel, C. *Comparative H_2S Economics for Shale Gas*. Ninety-First Annual Gas Processors Association Convention Tulsa, OK, 2012.

[106] Primack, H. S.; Reedy, D. E.; Kin, F. R., Method of stabilizing chelated polyvalent metal solutions. Google Patents: 1984.

[107] Prestonthomas, H., The International Temperature Scale of 1990 (ITS-90). Metrologia 1990, 27 (1), 3-10.

[108] LabVIEW Development System, v8.0, National Instruments, 2005.

[109] O'Connell, J. P.; Sharygin, A. V.; Wood, R. H., Infinite dilution partial molar volumes of aqueous solutes over wide range of conditions. *Ind. Eng. Chem. Res.* **1996**, 35 (8), 2808-2812.

[110] Quiram, D. J.; O'Conell, J. P.; Cochran, H. D., The solubility of solids in compressed gases. *J. Supercrit. Fluids* **1994**, 7 (3), 159-164.

[111] Prausnitz, J. M.; Lichtenthaler, R. N.; de Azevedo, E. G., Molecular Thermodynamics of Fluid-Phase Equilibria. Pearson Education: 1998.

[112] O'Connell, J. P.; Sharygin, A. V.; Wood, R. H., Infinite dilution partial molar volumes of aqueous solutes over wide range of conditions. *Ind. Eng. Chem. Res.* **1996**, 35 (8), 2808-2812.

[113] Deering, C. E.; Cairns, E. C.; McIsaac, J. D.; Read, A. S.; Marriott, R. A., The partial molar volumes for water dissolved in high-pressure carbon dioxide from T = (318.28 to 369.40) K and pressures to p = 35 MPa. *J. Chem. Thermodyn.* **2016**, 93, 337-346.

[114] Deering, C. E.; Saunders, M. J.; Commodore, J. A.; Marriott, R. A., The volumetric properties of carbonyl sulfide and carbon dioxide mixtures from T = 322 to 393 K and p = 2.5 to 35 MPa: application to COS hydrolysis in subsurface injectate streams, *J. Chem. Eng.* Data **2016**, 61, 1341-1347.

[115] Adeniyi, K. I.; Wan, H. H.; Deering, C. E.; Bernard, F.; Chisholm, M. A.; Marriott, R. A. High-pressure Hydrogen Sulfide Experiments: How did our Safety Measurements and Hazard Control Work During a Failure Event? *Safety* **2000**, 6, 15.

[116] Workplace Health and Safety Bulletin. Available online: (https://open.alberta.ca/dataset/91b7ed98-abc3-4267-a71b304e68d11f78/resource/689ff88d-54a2-4d65-9d69-7e3103b67e07/download/whs-pub-ch029.pdf)

[117] Dowling, N. I.; Bernard, F.; Leung, J.; Lesage, K. L. Analytical Procedure for the Determination of Trace Carbon Impurity in Elemental Sulfur, *J. Sulfur Chem*. **2008**, 29, 129–137.

[118] Sui, R.; Lavery, C. B.; Deering, C. E.; Prinsloo, R.; Li, D.; Chou, N.; Lesage, K. L.; Marriott, R. A. Improved Carbon Disulfide Conversion: Modification of an Alumina Claus Catalyst by Deposition of Transition Metal Oxides. *App. Cat. A.* **2020**, 604, 117773.

[119] Brunauer, S.; Emmett, P. H.; Teller, E. Adsorption of Gases in Multimolecular Layers. *J. Am. Chem. Soc.* **1938**, 60, 309.

[120] Barrett, E. P.; Joyner, L. G.; Halenda, P. P. The Determination of Pore Volume and Area Distributions in Porous Substances. I. Computations from Nitrogen Isotherms. *J. Am. Chem. Soc.* **1951**, 73, 373.

[121] Lemmon, E. W.; Span, R., Short Fundamental Equations of State for 20 Industrial Fluids. *J. Chem. Eng. Data* **2006**, 51 (3), 785-850.

[122] Wagner, W.; Pruß, A., The IAPWS Formulation 1995 for the Thermodynamic Properties of Ordinary Water Substance for General and Scientific Use. *J. Phys. Chem. Ref. Data* **2002**, 31 (2), 387-535.

[123] Kunz, O.; Wagner, W. The GERG-2008 Wide-Range Equation of State for Natural Gases and Other Mixtures: An Expansion of GERG2004. *J. Chem. Eng. Data* **2012**, 57, 3032−3091.

[124] Commodore, J. A.; Deering, C. E.; Marriott, R. A., Phase behaviour and reaction thermodynamics involving dense-phase CO2 impurities, In Carbon dioxide capture and acid gas injection, Wu, Y. and Carroll, J. Ed.; Wiley: 2017.

[125] Baiker, A. Supercritical fluids in heterogeneous catalysis, *Chem. Rev.* **1999**, 99, 453-474.

[126] Wynnyk, K. G.; Hojjati, B.; Marriott, R. A. High-pressure sour gas and water adsorption on zeolite 13X. *Ind. Eng. Chem. Res.* **2018**, 57, 15357– 15365.

[127] Espenson, J. H. *Chemical Kinetics and Reaction Mechanisms*. 2nd ed., University of California, McGraw-Hill, 1995.

[128] Seki, T.; Grunwaldt, J.; Baiker, A. Heterogeneous Catalytic Hydrogenation in Supercritical Fluids: Potential and Limitations. *Ind. Eng. Chem. Res.* **2008**, 47, 4561-4585.

[129] Banuti, D. T.; Raju, M.; Ihme, M. On the Characterization of transcritical fluid states; Annual Research Briefs; Center for Turbulence Research: 2017; p.165.

[130] Frank, J. and Rabinowitch, E. Some remarks about free radicals and the photochemisty of solutions. *Trans*. *Faraday Soc*., **1934**, 30, 120.

[131] Ryan, J.; Schaffert, F., CO_2 Recovery by the Ryan-Holmes Process. *Chem. Eng. Progress* **1984**, 80 (10), 53-56.